

# Kaon production in heavy ion reactions at intermediate energies

Christian Fuchs

Institut für Theoretische Physik der Universität Tübingen,  
Auf der Morgenstelle 14, D-72076 Tübingen, Germany

May 24, 2019

## Abstract

The article reviews the physics related to kaon and antikaon production in heavy ion reactions at intermediate energies. Chiral dynamics predicts substantial modifications of the kaon properties in a dense nuclear environment. The status of the theoretical predictions as well as experimental evidences for medium effects such as repulsive/attractive mass shifts for  $K^+/K^-$  are reviewed. In the vicinity of the thresholds, and even more pronounced below threshold, the production of strangeness is a highly collective process. Starting from elementary reaction channels the phenomenology of  $K^+$  and  $K^-$  production, i.e. freeze-out densities, time scales etc. as derived from experiment and theoretical transport calculations is presented. Below threshold kaon production shows a high sensitivity on the nuclear compression reached in heavy ion reactions. This allows to put constraints on the nuclear equation-of-state which are finally discussed.

*Keywords:* Kaons, strangeness production, heavy ion reactions, subthreshold particle production, ChPT, chiral symmetry restoration, transport models, QMD, collective flow, nuclear equation of state.

## Contents

<b>1</b>	<b>Introduction</b>	<b>2</b>
<b>2</b>	<b>Kaons in dense matter</b>	<b>6</b>
2.1	Chiral SU(3) Lagrangian . . . . .	6
2.2	Effective chiral Lagrangian . . . . .	7
2.2.1	Mean field dynamics . . . . .	9
2.2.2	Higher order corrections . . . . .	11
2.3	Non-perturbative coupled channel dynamics . . . . .	13
2.3.1	In-medium potentials . . . . .	15
2.3.2	In-medium cross sections . . . . .	16
2.4	Kaons in pion matter . . . . .	17
2.5	Chiral symmetry restoration? . . . . .	19
<b>3</b>	<b>Phenomenology of strangeness production</b>	<b>21</b>
3.1	Elementary reaction channels . . . . .	21
3.2	Hidden strangeness production . . . . .	23

3.3	Densities and time scales . . . . .	24
3.3.1	Conditions for strangeness production . . . . .	24
3.3.2	Energy and mass dependence . . . . .	26
3.3.3	Chemical freeze-out . . . . .	29
3.3.4	Thermal freeze-out . . . . .	33
<b>4</b>	<b>Strangeness production in transport models</b>	<b>34</b>
4.1	Mean field dynamics for strange particles . . . . .	34
4.1.1	Transport equation for kaons . . . . .	35
4.1.2	Equations of motion . . . . .	37
4.2	Off-shell transport . . . . .	39
4.3	Collisions . . . . .	41
4.3.1	Elementary cross sections . . . . .	42
4.3.2	Shift of thresholds . . . . .	44
4.3.3	Angular distributions . . . . .	46
4.4	Comparison of different transport models . . . . .	47
<b>5</b>	<b>Probing in-medium kaon potentials</b>	<b>52</b>
5.1	Total Yields . . . . .	52
5.2	Dynamical Observables . . . . .	57
5.2.1	In-plane flow . . . . .	57
5.2.2	Out-of-plane flow . . . . .	59
5.3	Consistency of the results . . . . .	62
5.3.1	Consistency between transport predictions . . . . .	62
5.3.2	$p + A$ reactions . . . . .	65
<b>6</b>	<b>Probing the nuclear equation of state</b>	<b>66</b>
6.1	Modeling the nuclear EOS . . . . .	66
6.1.1	Predictions for the nuclear EOS . . . . .	66
6.1.2	Skyrme forces in QMD . . . . .	68
6.2	Particle production and the compression phase in HICs . . . . .	70
6.2.1	Pions . . . . .	70
6.2.2	Kaons - historical overview . . . . .	72
6.3	The ratio Au+Au/C+C . . . . .	73
6.3.1	Phase space dependence . . . . .	75
6.3.2	Stability of the EOS dependence . . . . .	76
6.4	Constraints from other sources . . . . .	79
6.4.1	Nucleon flow . . . . .	79
6.4.2	Neutron stars and symmetry energy . . . . .	81
<b>7</b>	<b>Summary and outlook</b>	<b>82</b>

## 1 Introduction

For more than two decades strangeness production has been one of the major research topics of heavy ion physics at intermediate energies. First experiments on strangeness production were already performed in the early 80ties at the LBL in Berkeley [1]. These were, however, restricted to collisions of light nuclei. In the middle of the 90ties the whole field obtained a significant push when the KaoS [2] and the FOPI [3] Collaborations at the Gesellschaft für Schwerionenforschung (GSI) in Darmstadt/Germany

started to deliver high precision data for kaon and antikaon production in heavy systems. The kaon spectrometer KaoS has stopped data acquisition in 2004 and will be dismantled at the GSI. Hence it is a proper time to draw some resume on what has been achieved during the last twenty years and which problems still have to be settled. The present article tries to summarize the status of the field and to draw conclusions from the various experimental and theoretical efforts.

Strangeness production in heavy ion reactions at intermediate energies is of high interest since it opens the possibility to attack several fundamental questions of nuclear and hadron physics which are not only interesting by themselves but have also astrophysical implications and/or are related to fundamental aspects of Quantum Chromo Dynamics (QCD).

What makes the production of strange hadrons special is the fact that strangeness is exactly conserved in hadronic reactions. Open strangeness can be produced by the creation of kaon ( $K^+(\bar{u}s)$ ,  $K^0(\bar{d}s)$ ) - antikaon ( $K^-(u\bar{s})$ ,  $\bar{K}^0(d\bar{s})$ ) pairs or by kaon-hyperon pairs. The hyperons carrying one strange quark are  $\Lambda(u\bar{d}s)$  and  $\Sigma$  ( $\Sigma^-(d\bar{d}s)$ ,  $\Sigma^0(u\bar{d}s)$ ,  $\Sigma^+(u\bar{u}s)$ ) hyperons. The production of hidden strangeness through  $\phi(s\bar{s})$  mesons is possible but suppressed according to the Okubo-Zweig-Iizuka selection rule [4]. Since data on  $\phi$  production are extremely scarce at intermediate energies, the present article will mainly focus on kaon and antikaon production.

A first consequence of strangeness conservation is the fact that  $K^+$  mesons, once produced, cannot be absorbed by the surrounding nucleons. This results in a rather long mean free path of about 7 fm of  $K^+$  mesons in nuclear matter and makes them a suitable 'penetrating' probe for the dense fireball produced in heavy ion reactions. Final state interactions such as elastic kaon-nucleon scattering or the propagation in potentials influence the dynamics but do not change the total yields. A second consequence of strangeness conservation are the high production thresholds. The cheapest way to produce an  $s\bar{s}$  pair is the reaction  $NN \rightarrow N\Lambda K^+$  which has a threshold of  $E_{\text{lab}} = 1.58$  GeV for the incident nucleon. When the incident energy per nucleon in a heavy ion reaction is below this value one speaks about *subthreshold* kaon production. Subthreshold kaon production is in particular interesting since it ensures that the kaons originate from the high density phase of the reaction. The missing energy has to be provided either by the Fermi motion of the nucleons or by energy accumulating multi-step reactions. Both processes exclude significant distortions from surface effects if one goes sufficiently far below threshold. In combination with the long mean free path subthreshold  $K^+$  production is an ideal tool to probe compressed nuclear matter in relativistic heavy ion reactions. Indeed, one of the major motivations to start the kaon project at the GSI was to explore the nuclear equation-of-state (EOS) at supra-normal densities, i.e. significantly above nuclear saturation density  $\rho_0 \simeq 0.16 \text{ fm}^{-3}$ . A better knowledge of the high density behavior of the nuclear EOS is relevant for astrophysical purposes, e.g. for the understanding of neutron stars and supernovae explosions. Heavy ion reactions provide the only possibility to attack this question experimentally and to constrain theoretical models above saturation density. After a more than thirty years quest for the nuclear EOS it seems that by studying subthreshold  $K^+$  production substantial progress could be achieved in the recent years.

A second push of more theoretical nature was given to the field when chiral models became more and more popular in the late 80ties and early 90ties. Chiral symmetry is an exact symmetry of QCD in the limit of massless quarks. Since the up and down current quark masses are small, i.e. of the order of 5-10 MeV, this symmetry is still approximately fulfilled. In nature it is, however, spontaneously broken by the non-vanishing – and large – expectation value of the scalar chiral quark condensate  $\langle\bar{q}q\rangle$  of the QCD vacuum (for a pedagogical review see e.g. [5]). The spontaneous symmetry breaking, similar to the spontaneous magnetization of a ferromagnet which breaks the symmetry of the underlying Hamiltonian, implies the existence of massless Goldstone bosons which are the pions. The small pion mass of 140 MeV ensures that the concept of chiral symmetry is a fundamental feature of low energy hadron physics. By the extension to the full SU(3) sector the pseudoscalar meson octet of  $\pi, \eta, K$  and  $\bar{K}$  mesons plays now the role of the Goldstone bosons. With a strange quark mass of about 150 MeV the explicit symmetry breaking is much larger in the strange sector than in the SU(2) sector but the

general concepts of chiral symmetry and its spontaneous breaking are believed to be still valid. They do not only allow to understand the origin of the pseudoscalar meson masses. Chiral perturbation theory (ChPT) is also considered as the *exact*, QCD based, theory of the pion-nucleon interaction at low energies [6].

Hence it was a natural step to extend ChPT to the SU(3) flavor sector [7]. However, the situation turned out to be more complicated than in pure SU(2). While the  $\pi N$  and the  $KN$  interactions can be treated perturbatively, the  $\bar{K}N$  interaction is already around threshold dominated by the presence of resonances. This makes a perturbative treatment of the antikaon-nucleon interaction impossible. Instead, non-perturbative approaches are required, which can be achieved within chiral dynamics, however, by the price of loosing of a well defined expansion scheme. This essential difference between kaons and antikaons will be reflected at many points in the following discussions. It is the main reason why conclusions on in-medium modifications of kaon properties are much firmer than those for antikaons.

Such medium modifications are closely connected to the conjecture of a partial restoration of chiral symmetry in dense matter. The chiral condensate  $\langle \bar{q}q \rangle$  is expected to be reduced at finite density and/or temperature [8, 9, 10] which should be reflected, e.g., in shifts of the corresponding meson masses. Heavy ion reactions open thus the possibility to test fundamental concepts of hadron physics and QCD. A strong reduction of the  $K^-$  mass, as also supported by the investigation of kaonic atoms [11], will have severe astrophysical consequences. It can lead to  $K^-$  condensation in neutron stars [7, 12, 13, 14] which, due to additional negative charge, increases the proton fraction and softens thus the equation-of-state for the neutron star. The onset of  $K^-$  condensation is reached when the electron chemical potential starts to exceed that of the kaons  $\mu_e \geq m_{K^-}^*$  which might happen at around 4-5 times nuclear saturation density. This lowers the maximal neutron star mass to about 1.5 solar masses and the core of a supernova, if heavier than this value, will collapse into a black hole. This, on the other hand will lead to a large number of low mass black holes in the universe [15] (for a recent review see [16]).

In the late 80ties/ early 90ties first mean field calculations [7, 17] predicted already a moderately repulsive  $K^+$  potential ( $V \sim +(20 \div 30)$  MeV) and a strongly attractive  $K^-$  potential ( $V \sim -(100 \div 200)$  MeV) at nuclear saturation density. Such a value of the  $K^+$  potential is in accordance with the  $K^+N$  scattering length and theoretical estimates for the potential remained fairly stable over the years. For antikaons the situation is more complex. The resonant character of the  $K^-N$  interaction makes the mean field picture highly questionable and the size of the in-medium  $K^-$  potential is even not yet completely settled from the theoretical side.

A major challenge studying strangeness production in heavy ion reactions is to verify (or falsify) the conjecture of the existence of these two potentials, to determine their size from experiment and to put constraints on theoretical models. However, heavy ion reactions are highly dynamical processes. At intermediate energies the phase space distributions of the colliding nuclei are far from global and even local equilibrium over most of the duration of the reaction [18]. Since observables are not snapshots but the results of space-time integrals over the entire reaction dynamics it is unavoidable to account for this dynamical evolution. This means that the link between experiment and the underlying physics has to be provided by dynamical transport models. Semi-classical transport equations of a Boltzmann type can be derived from non-equilibrium quantum field theory [19, 20]. Corresponding Boltzmann-Uehling-Uhlenbeck (BUU) [21, 22] models or, alternatively, the Quantum-Molecular-Dynamics (QMD) approach [23] are well established transport models and explain successfully a large variety of hadronic observables in heavy ion reactions, such as e.g. collective flow pattern or spectra and abundances of newly produced particles [24, 25]. Most of the results presented in this review are based on the QMD approach. Details of the Tübingen QMD model can be found in [26, 27].

Such hadronic transport models propagate one-body phase space distributions in self-consistent potentials and account for elastic and inelastic two-body scattering processes. They contain basic quantum features such as final state Pauli-blocking for fermions. As soon as particle production comes

into play the transport approach becomes a coupled-channel problem. The various hadron species are coupled via production and absorption processes and by their mean fields. Transport models are generally mean field approaches which rely on the quasi-particle approximation (QPA) for stable particles and narrow resonances.  $K^+$  mesons can safely be treated within such a framework since they retain good quasi-particle properties also in a dense environment. Antikaons, in contrast, seem to develop complex structures in their spectral functions which would require to account for off-shell effects beyond the quasi-particle approximation. There exist first attempts to go in this direction [28] but most available calculations on  $K^-$  production are based on the QPA.

The review is now organized as follows: Chapter 2 gives an overview of the theoretical predictions for the in-medium modifications which the kaons should experience in a dense nuclear environment. Since chiral perturbation theory is considered as the most suitable tool to study the interactions of pseudoscalar mesons with nucleons at low energies the chapter starts with a short outline of the derivation of effective kaon-nucleon models based on chiral dynamics. Mean field models as well as more elaborated coupled channel dynamics which are required by the resonant structure of the antikaon-nucleon interactions, are briefly discussed. For completeness also the expected scenario in the complementary case, i.e. in a high temperature, baryon dilute but pion dominated, environment is mentioned. Chapter 3 summarizes the phenomenology of strangeness production in heavy ion collisions around threshold energies. Starting from elementary processes, i.e. strangeness production and exchange reactions, the presently accepted scenarios for kaon and antikaon production are developed as they can be deduced from experiments and corresponding dynamical simulations. This concerns the questions of system size dependences, freeze-out densities, time scales etc.. An important question is in this context the degree of equilibration which the  $K^\pm$  mesons reach or do not reach in the expanding system. This question is intimately connected with the possibility to probe the early high density phase of a heavy ion reaction. If the kaons would have time to equilibrate they would loose their memory on the early reaction stages. Chapter 4 turns then to the treatment of strangeness production within dynamical transport models. Here we focus on the  $K^+$  production and discuss exemplarily the realization within the Tübingen QMD approach. The treatments within transport models used by other groups are similar in principle, but can differ in details. Finally a comparison of the predictions from various transport models for selected pion and kaon observables is given. The search for signatures of in-medium mass shifts, or more generally, in-medium potentials is discussed in Chapter 5. Mass shifts lead first of all to shifts of the production threshold which are reflected in the total particle yields. Since conclusions are only possible relative to a free mass scenario they have to be based on transport simulations. The data situation strongly supports the in-medium mass scenario, at least concerning the  $K^+$  mesons. These observations are complemented by the study of dynamical observables such as the collective in-plane and out-of-plane pattern. Finally Chapter 6 turns to the original issue which motivated the kaon program at the GSI, namely to extract information on the nuclear equation-of-state. The measurement of  $K^+$  excitation functions down to energies far below threshold can be considered as a breakthrough. Before coming to the interpretation of the data a brief summary on the present status of the theoretical prediction for the nuclear EOS is given. The dependence of the kaon production on the compression achieved in heavy ion reactions puts constraints on the EOS which are discussed in detail. Finally the consistency with information from other sources such as nucleon and neutron stars is outlined.

The review closes with a summary of the major results.

## 2 Kaons in dense matter

### 2.1 Chiral $SU(3)$ Lagrangian

The natural framework to study the interaction between pseudoscalar mesons and baryons at low energies is chiral perturbation theory (ChPT). Kaplan and Nelson were the first to apply the chiral Lagrangian to the properties of kaons in nuclear matter [7]. Later on this framework has been used by many other authors [8, 12, 29, 30, 31, 32, 33, 34, 35, 36, 37, 38]. The corresponding chiral  $SU(3)_L \times SU(3)_R$  Lagrangian used by Kaplan and Nelson reads

$$\begin{aligned} \mathcal{L} = & \frac{1}{4} f^2 \text{Tr} \partial^\mu \Sigma \partial_\mu \Sigma^+ + \frac{1}{2} f^2 \Lambda [\text{Tr} M_q (\Sigma - 1) + \text{h.c.}] + \text{Tr} \bar{B} (i \gamma^\mu \partial_\mu - m_B) B \\ & + i \text{Tr} \bar{B} \gamma^\mu [V_\mu, B] + D \text{Tr} \bar{B} \gamma^\mu \gamma^5 \{A_\mu, B\} + F \text{Tr} \bar{B} \gamma^\mu \gamma^5 [A_\mu, B] \\ & + a_1 \text{Tr} \bar{B} (\xi M_q \xi + \text{h.c.}) B + a_2 \text{Tr} \bar{B} B (\xi M_q \xi + \text{h.c.}) \\ & + a_3 [\text{Tr} M_q \Sigma + \text{h.c.}] \text{Tr} \bar{B} B. \end{aligned} \quad (1)$$

The degrees of freedom in the Lagrangian (1) are the baryon octet  $B$

$$B = \begin{pmatrix} \frac{\Lambda}{\sqrt{6}} + \frac{\Sigma^0}{\sqrt{2}} & \Sigma^+ & p \\ \Sigma^- & \frac{\Lambda}{\sqrt{6}} - \frac{\Sigma^0}{\sqrt{2}} & n \\ \Xi^- & \Xi^0 & -\frac{2}{\sqrt{6}} \Lambda \end{pmatrix} \quad (2)$$

with a degenerate mass  $m_B$ , and the pseudoscalar meson octet  $\phi$

$$\phi = \sqrt{2} \begin{pmatrix} \frac{\eta_8}{\sqrt{6}} + \frac{\pi^0}{\sqrt{2}} & \pi^+ & K^+ \\ \pi^- & \frac{\eta_8}{\sqrt{6}} - \frac{\pi^0}{\sqrt{2}} & K^0 \\ K^- & \overline{K^0} & -\frac{2}{\sqrt{6}} \eta_8 \end{pmatrix} \quad (3)$$

entering into the chiral pseudoscalar meson fields

$$\Sigma = \exp(2i\phi/f_\pi) \quad \text{and} \quad \xi = \sqrt{\Sigma} = \exp(i\phi/f_\pi) . \quad (4)$$

The pseudoscalar meson decay constants are equal in the  $SU(3)_V$  limit and given by the weak pion decay constant  $f_\pi \simeq 93$  MeV. The current quark mass matrix which is responsible for explicit chiral symmetry breaking is given by

$$M_q = \begin{pmatrix} m_q & 0 & 0 \\ 0 & m_q & 0 \\ 0 & 0 & m_s \end{pmatrix} \quad (5)$$

if one neglects the small difference between the up and down quark masses ( $m_u \simeq m_d \equiv m_q \simeq 5.5$  MeV). The constants  $F$  and  $D$  are the  $SU(3)$  axial vector couplings with  $F + D = g_A$  which determine the pseudo-vector meson-baryon coupling strengths through corresponding Goldberger-Treiman relations.

Chiral symmetry of QCD is explicitly broken by the finite, but small quark masses (5). However, compared to the chiral symmetry breaking scale  $\Lambda_\chi \simeq 4\pi f_\pi \sim 1$  GeV the up and down quark masses and also the strange quark mass ( $m_s \simeq 150$  MeV) are small and the QCD Lagrangian is still approximately chirally invariant. The same holds for the mesonic sector of the chiral Lagrangian (1). This allows a systematic expansion in powers of hadron momenta and light quark masses over  $\Lambda_\chi$ , i.e. chiral perturbation theory [6]. In the baryonic sector chiral symmetry is broken due to the baryon mass  $m_B$ . In the Lagrangian  $m_B$  is degenerate for the baryon octet and the mass spectrum has to be fixed through the expansion coefficients.

The mesonic vector  $V_\mu$  and axial vector  $A_\mu$  currents are defined as

$$V_\mu = \frac{1}{2}(\xi^+ \partial_\mu \xi + \xi \partial_\mu \xi^+) \text{ and } A_\mu = \frac{i}{2}(\xi^+ \partial_\mu \xi - \xi \partial_\mu \xi^+), \quad (6)$$

respectively.

The treatment of the full Lagrangian (1) is complicated since it leads automatically to a coupled channel problem. This approach has been pursued by several authors [30, 32, 33, 34, 35, 36, 37, 38]. However, for many applications, in particular studying kaon properties at the mean field level, an effective chiral Lagrangian based on kaon and nucleon degrees of freedom can be used. We discuss the effective  $KN$  Lagrangian approach first and turn then to the more involved coupled channel problem.

## 2.2 Effective chiral Lagrangian

The Lagrangian (1) can be reduced to an effective Lagrangian by the steps outlined below [7, 39]. One should, however, be aware that the following expansion is not chiral perturbation theory since it mixes contributions of different order in ChPT.

First the pseudoscalar meson field  $\Sigma$  is expanded up to order  $1/f_\pi^2$  and only the kaon field  $K$  is kept. The terms involving the axial vector current do not contribute to the kaon mass and can be ignored. The first two terms in Eq. (1) are the kinetic and the mass term

$$\partial^\mu \bar{K} \partial_\mu K - \Lambda(m_q + m_s) \bar{K} K \quad , \quad (7)$$

from where one can identify the kaon mass

$$m_K^2 = \Lambda(m_q + m_s) \quad . \quad (8)$$

The kaon field is given by

$$K = \begin{pmatrix} K^+ \\ K^0 \end{pmatrix} \text{ and } \bar{K} = (K^- \bar{K}^0) \quad . \quad (9)$$

Keeping explicitly only nucleon and kaon degrees of freedom, the third and fourth terms in Eq. (1) lead to the Dirac equation for the nucleon field

$$N = \begin{pmatrix} p \\ n \end{pmatrix} \text{ and } \bar{N} = (\bar{p} \bar{n}), \quad (10)$$

and the Weinberg-Tomozawa  $KN$  interaction term [40]

$$\bar{N}(i\gamma^\mu \partial_\mu - m_B)N - \frac{3i}{8f_\pi^2} \bar{N} \gamma^\mu N \bar{K} \overset{\leftrightarrow}{\partial}_\mu \quad . \quad (11)$$

The last three terms in Eq. (1) can be similarly worked out and lead to a scalar  $KN$  interaction, the so-called Kaplan-Nelson term [7]

$$\begin{aligned} \text{Tr} \bar{B}(\xi M_q \xi + \text{h.c.})B &= 2m_q \bar{N}N - \frac{\bar{N}N}{2f_\pi^2}(m_q + m_s) \bar{K}K \\ \text{Tr} \bar{B}B(\xi M_q \xi + \text{h.c.}) &= 2m_s \bar{N}N - \frac{\bar{N}N}{f_\pi^2}(m_q + m_s) \bar{K}K \\ [\text{Tr} M_q \Sigma + \text{h.c.}] \text{Tr} \bar{B}B &= 2(2m_q + m_s) \bar{N}N - \frac{2\bar{N}N}{f_\pi^2}(m_q + m_s) \bar{K}K \quad . \end{aligned} \quad (12)$$

Combining these expressions, the full Lagrangian reads

$$\begin{aligned}
\mathcal{L} = & \bar{N}(i\gamma^\mu\partial_\mu - m_B)N + \partial^\mu\bar{K}\partial_\mu K - \Lambda(m_q + m_s)\bar{K}K \\
& - \frac{3i}{8f_\pi^2}\bar{N}\gamma^\mu N\bar{K} \overset{\leftrightarrow}{\partial}_\mu K + [2m_qa_1 + 2m_sa_2 + 2(2m_q + m_s)a_3]\bar{N}N \\
& - \frac{\bar{N}N\bar{K}K}{2f_\pi^2}(m_q + m_s)(a_1 + 2a_2 + 4a_3) .
\end{aligned} \tag{13}$$

Now one can fix the remaining free parameters  $a_1$ ,  $a_2$ , and  $a_3$  from the nucleon mass

$$m_N = m_B - 2[a_1m_q + a_2m_s + a_3(2m_q + m_s)] \tag{14}$$

and the kaon-nucleon sigma term  $\Sigma_{KN}$  can be identified

$$\Sigma_{KN} = -\frac{1}{2}(m_q + m_s)(a_1 + 2a_2 + 4a_3) . \tag{15}$$

Eq. (15) is obtained using eq. (14) for the nucleon mass and the definition of the sigma term

$$\Sigma_{KN} = \frac{1}{2}(m_q + m_s)\left[\frac{1}{2}\frac{\partial m_N}{\partial m_q} + \frac{\partial m_N}{\partial m_s}\right] \tag{16}$$

The effective chiral kaon-nucleon Lagrangian reads now up to order  $(1/f_\pi^2)$

$$\begin{aligned}
\mathcal{L} = & \bar{N}(i\gamma^\mu\partial_\mu - m_N)N + \partial^\mu\bar{K}\partial_\mu K - (m_K^2 - \frac{\Sigma_{KN}}{f_\pi^2})\bar{N}N\bar{K}K \\
& - \frac{3i}{8f_\pi^2}\bar{N}\gamma^\mu N\bar{K} \overset{\leftrightarrow}{\partial}_\mu K .
\end{aligned} \tag{17}$$

It contains a vector interaction, the Weinberg-Tomozawa term, which is repulsive for kaons and attractive for antikaons due to  $g$ -parity. The attractive scalar interaction, the Kaplan-Nelson term, is equal for kaons and antikaons. The strength of the Kaplan-Nelson term depends thereby on the magnitude of the kaon-nucleon sigma term  $\Sigma_{KN}$ . The Weinberg-Tomozawa term is current algebra while the Kaplan-Nelson interaction is next to leading order in ChPT.

In contrast to the pion-nucleon-sigma term which is experimentally well determined from pion-nucleon scattering ( $\Sigma_{\pi N} \simeq 45$  MeV), the kaon-nucleon-sigma term is a relatively uncertain quantity since it is related to the strangeness content of the nucleon. In addition to the explicit breaking from the quark masses (5) chiral symmetry is spontaneously broken by the large expectation values of the scalar quark condensate  $\langle\bar{q}q\rangle \simeq ((230 \pm 25) \text{ MeV})^3$  of the QCD vacuum. The pion, respectively the complete pseudoscalar meson octet assuming  $SU(3)_V$  symmetry, plays the role of the Goldstone boson of chiral symmetry breaking. Thus, like for the pion, the kaon mass  $m_K$  can be related to the vacuum quark condensates  $\langle\bar{q}q\rangle$  by the Gell-Mann-Oakes-Renner (GOR) relation [41]

$$m_K^2 = \frac{1}{2}(m_u + m_s)\langle\bar{u}u + \bar{s}s\rangle . \tag{18}$$

$m_u$  in eq. (18) is the up-quark current mass and  $m_s$  is the strange quark mass. In the nucleon the right hand side of eq. (18) defines the kaon-nucleon sigma term

$$\Sigma_{KN} = \frac{1}{2}(m_u + m_s)\langle N|\bar{u}u + \bar{s}s|N\rangle . \tag{19}$$

Kaon-nucleon scattering yields values for the isospin averaged sigma term of about  $\Sigma_{KN} \simeq 400$  MeV whereas lattice QCD predicts values between 300-450 MeV [8, 42, 43], heavy baryon ChPT [44]  $\Sigma_{KN} = 380 \pm 40$  MeV (I=1) and chiral quark model calculations [45]  $\Sigma_{KN} = 386$  MeV. Thus  $\Sigma_{KN}$  can range from  $2m_\pi$  up to 450 MeV, however, with the tendency of a value around 400 MeV to establish.

### 2.2.1 Mean field dynamics

For estimates of kaon mass shifts in nuclear matter and kaon dynamics in heavy ion reactions the above Lagrangian (17) is usually applied in mean field approximation. Already in the early 90ties mean field calculations were carried out in the Nambu-Jona-Lasinio (NJL) model [17]. In the context of chiral SU(3) dynamics the mean field approximation means to treat the  $KN$  interaction at the tree level. The in-medium Klein-Gordon equation for the kaons follows from (17) via the Euler-Lagrange equations

$$\left[ \partial_\mu \partial^\mu \pm \frac{3i}{4f_\pi^2} j_\mu \partial^\mu + \left( m_K^2 - \frac{\Sigma_{KN}}{f_\pi^2} \rho_s \right) \right] \phi_{K^\pm}(x) = 0 \quad . \quad (20)$$

Here  $j_\mu = \langle \bar{N} \gamma_\mu N \rangle$  is the nucleon four-vector current and  $\rho_s = \langle \bar{N} N \rangle$  the scalar baryon density. With the vector potential

$$V_\mu = \frac{3}{8f_\pi^2} j_\mu \quad (21)$$

and an effective kaon mass  $m_K^*$  defined as [46]

$$m_K^* = \sqrt{m_K^2 - \frac{\Sigma_{KN}}{f_\pi^2} \rho_s + V_\mu V^\mu} \quad (22)$$

the Klein-Gordon Eq. (20) can be written as

$$[(\partial_\mu \pm iV_\mu)^2 + m_K^{*2}] \phi_{K^\pm}(x) = 0 \quad . \quad (23)$$

Thus the vector field is introduced by minimal coupling into the Klein-Gordon with opposite signs for  $K^+$  and  $K^-$  while the effective mass  $m_K^*$  is equal for both. Introducing effective momenta ( $k_\mu^* = (E^*, \mathbf{k}^*)$ ) as well

$$k_\mu^* = k_\mu \mp V_\mu \quad (24)$$

the Klein-Gordon equation (20,23) reads in momentum space

$$[k^{*2} - m_K^{*2}] \phi_K(k) = 0 \quad . \quad (25)$$

Eq. (25) is just the mass-shell constraint for quasi-particles inside the nuclear medium. There exists now a complete analogy to the quasi-particle picture for the nucleons in relativistic mean field theory, e.g. in the Walecka model of Quantum Hadron Dynamics (QHD) [47] where the nucleon obeys an effective Dirac equation

$$[\not{k}^* - m^*] u(k) = 0$$

for the in-medium nucleon spinors  $u$ . From Eqs. (25) the dispersion relation follows

$$E(\mathbf{k}) = k_0 = \sqrt{\mathbf{k}^{*2} + m_K^{*2}} \pm V_0 \quad . \quad (26)$$

In nuclear matter at rest where the space-like components of the vector potential vanish, i.e.  $\mathbf{V} = 0$  and  $\mathbf{k}^* = \mathbf{k}$ , Eq. (26) reduces to

$$E(\mathbf{k}) = \sqrt{\mathbf{k}^2 + m_K^2 - \frac{\Sigma_{KN}}{f_\pi^2} \rho_s + V_0^2} \pm V_0 \quad . \quad (27)$$

Eq. (26) accounts for the full Lorentz structure, a fact which comes into play when heavy ion collisions are considered where one has to transform between different reference frames, e.g. the center-of-mass

frame of the colliding nuclei and the frame where a kaon is created. Like in electrodynamics the spatial components of the vector field give rise to a Lorentz force [46] as discussed in detail in Chap. 4.

Now one can also introduce the kaon optical potential through the in-medium dispersion relation

$$0 = k_\mu^{*2} - m_K^{*2} = k_\mu^2 - m_K^2 - 2m_K U_{\text{opt}} \quad . \quad (28)$$

In mean field approximation the difference between the mass shell conditions for kinetic and canonical quantities is simply given by the optical or Schroedinger equivalent potential

$$U_{\text{opt}}(\rho, \mathbf{k}) = -\Sigma_S \pm \frac{k_\mu V^\mu}{m_K} + \frac{\Sigma_S^2 - V_\mu^2}{2m_K} = \pm \frac{k_\mu V^\mu}{m_K} - \frac{\Sigma_{\text{KN}}}{f_\pi^2} \rho_s \quad . \quad (29)$$

Here we introduced the total scalar kaon self-energy

$$\Sigma_S \equiv m_K - m_K^* \approx \frac{1}{2m_K} \left( \frac{\Sigma_{\text{KN}}}{f_\pi^2} \rho_s - V_\mu^2 \right) \quad . \quad (30)$$

From Eq. (28) follows

$$\frac{\mathbf{k}^2}{2m_K} + U_{\text{opt}} = \frac{\mathbf{k}_\infty^2}{2m_K} \quad (31)$$

where  $|\mathbf{k}_\infty|$  is the asymptotic momentum  $\mathbf{k}_\infty^2 = k_0^2 - m_K^2$  of the incoming particle in the Schroedinger equation. Thus  $U_{\text{opt}}$  of Eq. (29) corresponds to the potential in the non-relativistic Schroedinger equation. Again the optical potential is of identical structure as the central part of the optical potential for nucleons [47]. However, in the latter case an additional spin-dependent part of the interaction can be obtained from a Fouldy-Wouthousen transformation of the Dirac equation.

In this context it should be mentioned that in the literature it is often not distinguished between in-medium 'mass' and in-medium energy shifts, i.e. the energy (27) at zero momentum is identified as an in-medium mass  $m_K^* \equiv E(\mathbf{k} = 0)$ . In order to strengthen the analogy with the relativistic mean field picture for baryons and to distinguish clearly between the different Lorentz properties -  $m_K^*$  given by Eq. (22) is by definition a Lorentz scalar - we will distinguish between these two quantities in the discussion of medium effects.

To call  $m_K^*$  the in-medium mass is also consistent with the general picture of a reduction of meson masses in dense and hot hadronic matter. From the Hellmann-Feynman theorem follows a reduction of the non-strange quark condensate  $\langle \bar{u}u + \bar{d}d \rangle$  which is linear to first order in the nuclear density\*  $\rho$  [48, 8]

$$\frac{\langle \rho | \bar{u}u + \bar{d}d | \rho \rangle}{\langle \bar{u}u + \bar{d}d \rangle} \simeq 1 - \frac{\Sigma_{\pi N}}{f_\pi^2 m_\pi^2} \rho + \dots \quad . \quad (32)$$

Model calculations [17, 9, 10], e.g. within the NJL model, predicted a similar reduction of the chiral condensate. Assuming an analogous behavior of the strange condensate yields

$$\frac{\langle \rho | \bar{u}u + \bar{s}s | \rho \rangle}{\langle \bar{u}u + \bar{s}s \rangle} \simeq 1 - \frac{\Sigma_{\text{KN}}}{f_\pi^2 m_K^2} \rho + \dots \quad . \quad (33)$$

Combining now the GOR relation (18) with (33), the effective kaon mass scales with density as

$$m_K^{*2} = m_K^2 - \frac{\Sigma_{\text{KN}}}{f_\pi^2} \rho + \mathcal{O}(k_F^4) \quad (34)$$

which is exactly the form of eq. (22) and consistent with the picture of partial restoration of chiral symmetry.

---

\*In isospin symmetric nuclear matter the density is related to the Fermi momentum by  $\rho = 2 k_F^3 / (3 \pi^2)$

## 2.2.2 Higher order corrections

The importance of higher order contributions beyond tree level can be estimated from the empirical kaon-nucleon scattering lengths. Such a comparison gives also a feeling how far the mean field model complies with kaon-nucleon scattering.

To lowest order in density the mass or energy shift of a meson is generally given by the forward scattering length, in the case of kaons

$$\Delta E_K^2(\mathbf{k} = 0) = E_K^2 - m_K^2 = -\pi \left( 1 + \frac{m_K}{m_N} \right) \left( a_{KN}^{(I=0)} + 3 a_{KN}^{(I=1)} \right) \rho + \mathcal{O}(k_F^4) . \quad (35)$$

The empirical values of the isospin  $I = 0$  and  $I = 1$   $K^+$ -nucleon scattering lengths are  $a_{K^+N}^{(I=0)} \simeq 0.02$  fm and  $a_{K^+N}^{(I=1)} \simeq -0.32$  fm [49] which leads to a repulsive mass shift of about 28 MeV at nuclear saturation density ( $k_F \simeq 265$  MeV). Higher order corrections in the density expansion of (35) were found to be small for  $K^+$ . The  $k_F^4$  correction was found to increase the repulsive  $K^+$ -mass shift only by about 20% [35] compared to expression (35). This fact makes the density expansion useful in the  $K^+$  sector. The empirical scattering lengths can now be compared to the tree level Weinberg-Tomozawa interaction which yields  $a_{K^+N}^{(I=0)} = 0$  fm and  $a_{K^+N}^{(I=1)} \simeq -0.585$  fm [30]. Thus current algebra and the corresponding effective  $KN$  Lagrangian (17) is in rough qualitative agreement with the constraints from low energy  $K^+$  nucleon scattering. In the effective model the too large vector repulsion (21) is compensated by the attractive scalar Kaplan-Nelson potential (34). Compared to the empirical values, the repulsion is now, however, overcompensated [39].

One way to overcome this problem at the mean field level has been suggested by Brown and Rho [31]. They subsumed higher correlations of chiral order  $Q^3$  and above into a medium dependence of the pion decay constant which should scale in matter similar as the chiral condensate: Assuming the Gell-Mann-Oakes-Renner relation (18) to be still valid in the medium, one obtains the following relation for the in-medium pion decay constant  $f_\pi^*$

$$\frac{f_\pi^{*2}}{f_\pi^2} = \frac{m_\pi^2}{m_\pi^{*2}} \frac{\langle \rho | \bar{q}q | \rho \rangle}{\langle \bar{q}q \rangle} . \quad (36)$$

From ChPT [50] and  $\pi$ -mesonic atoms [51] the (s-wave) pion mass is known to change only slightly with density. Using the empirical values of  $m_\pi^*(\rho_0)/m_\pi \approx 1.05$ , one obtains

$$f_\pi^{*2}(\rho_0)/f_\pi^2 \approx 0.6 \quad (37)$$

at nuclear saturation density  $\rho_0 \simeq 0.16$  fm $^{-3}$ . A dropping pion decay constant enhances both, the vector repulsion and the scalar attraction. However, as found in one-loop ChPT the additional attraction is counterbalanced by the range term which is of the same order as the Kaplan-Nelson term. Similar results have been found for pions [52]. Moreover, such a dropping of the pion decay constant seems to be supported by the potentials extracted from pionic atoms [53]. At the mean field level these results can be incorporated by replacing  $f_\pi^2 \mapsto f_\pi^{*2}$  only in the vector potential (21).

Fig. 1 shows the in-medium energy shift of  $K^+$  and  $K^-$  and the in-medium mass defined by (22) in nuclear matter. MFT denotes thereby the Lagrangian (17) with a value of  $\Sigma_{KN} = 350$  MeV which has originally been used by Li and Ko [39]. MFT+corr. denotes the mean field model proposed by Brown et al. [31] including the above mentioned higher order corrections with a value of  $\Sigma_{KN} = 450$  MeV. The MFT and MFT+corr. curves shown in Fig. 1 are obtained by Eqs. (22,27) with the corresponding values for  $\Sigma_{KN}$ , however in the MFT+corr. case with the additional replacement of  $f_\pi^2$  by  $f_\pi^{*2}$  in the vector field (21). The empirical energy shifts are shown as well in Fig. 1. For  $K^+$  the value is obtained by Eq. (35) from the empirical  $K^+N$  scattering length. The  $K^-$  band corresponds to the empirical iso-spin averaged  $K^-N$  scattering length of  $\bar{a}_{K^-N} = 0.62 \pm 0.5$  fm extracted from kaonic atom data [54].

The strength of the empirical  $K^-$ -nucleus potential is in the analysis of Batty et al. [54] quite robust against a variation of the nuclear wave functions and the inclusion of  $p$ -wave interactions. The  $s$ -wave potential shown in Fig. 1 gives therefore a good impression of the values determined from kaonic atoms.

Similar results have been obtained with slightly modified versions of the effective chiral Lagrangian [36], in the quark-meson-coupling model [55] shown in Fig. 1, and in relativistic mean field calculations where kaons are coupled to static  $\sigma, \omega, \rho$  and  $\delta$  meson background fields [56].

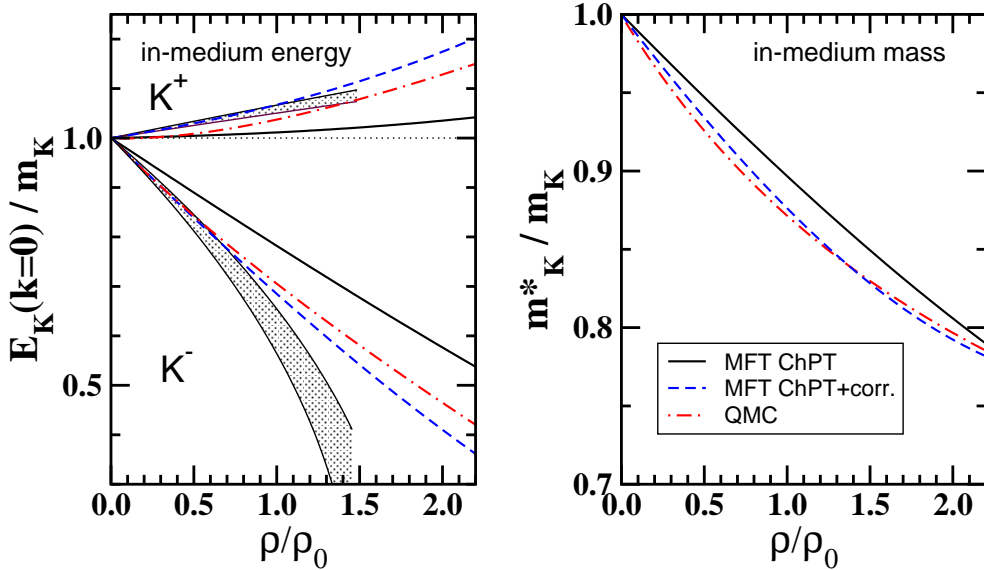


Figure 1: In-medium kaon energy (left) and quasi-particle mass (right) in the chiral mean field theory (MFT ChPT) and including higher order corrections (MFT ChPT+corr.) [31]. Results from the mean field quark-meson-coupling (QMC) model [55] are shown as well. The bands represent the values extracted from empirical  $K^+N$  scattering and  $K^-$  atoms [54].

In this context it is worth to mention that the philosophy behind the  $KN$  mean field model is similar to that of effective relativistic nucleon-meson Lagrangians of QHD [47, 57]. Both are designed to describe in-medium properties, in the latter case nuclear matter and finite nuclei. In both cases the structure of the interaction complies with the knowledge from free scattering, however, the models do not pretend to give a quantitative description of free scattering data. In the present case this is true for the  $K^+$  sector. The situation becomes, however, much less satisfying turning to the  $K^-$  sector.

Again one can use the low density theorem to estimate the medium effects to leading order in density. The empirical scattering lengths  $a_{K^-N}^{(I=0)} \simeq (-1.70 + i 0.68) \text{ fm}$  and  $a_{K^-N}^{(I=1)} \simeq (0.37 + i 0.60) \text{ fm}$  [49, 58] imply according to (35) a repulsive mass shift of 23 MeV and a width of  $\Gamma_{K^-} \simeq 147 \text{ MeV}$  at saturation density. In contrast to  $K^+$ , the next order correction to the density expansion of Eq. (35) is large, resulting in a total repulsive mass shift of 55 MeV and a width of  $\Gamma_{K^-} \simeq 195 \text{ MeV}$  [35]. First of all, this questions the convergence of a density expansion for the  $K^-$ -mode. Moreover, the leading terms suggest a repulsive  $K^-$  potential which stands in clear contradiction to the empirical knowledge from kaonic atom data ( $\bar{a}_{K^-N} = 0.62 \pm 0.5 \text{ fm}$ ) [54] suggesting sizable attraction at small density. Finally the empirical  $K^-N$  scattering lengths are in disagreement with the Weinberg-Tomozawa term which predicts an attractive mass shift. These facts imply that perturbation theory is not applicable in the  $K^-$  sector. The reason lies in the existence of a resonance, the  $\Lambda(1405)$  close the  $K^-p$  threshold which makes the  $K^-p$  interaction repulsive at threshold. The appearance of resonances requires generally a non-perturbative treatment of two-body scattering processes.

## 2.3 Non-perturbative coupled channel dynamics

A non-perturbative calculation of the full two-body scattering amplitude  $T$  requires to solve the Lippmann-Schwinger equation, respectively its relativistic counterpart, the Bethe-Salpeter equation. For kaon-nucleon scattering the Bethe-Salpeter equation reads schematically

$$T_{KN \rightarrow KN} = V_{KN \rightarrow KN} - i \int V_{KN \rightarrow MB} G_B D_M T_{MB \rightarrow KN} \quad (38)$$

where  $G_B$  and  $D_M$  are baryon and meson propagators, respectively

$$G_B(p) = \frac{1}{\not{p} - m_B + i\epsilon} , \quad D_M(k) = \frac{1}{k^2 - m_M^2 + i\epsilon} . \quad (39)$$

The Bethe-Salpeter equation (38) iterates the  $KN$  interaction kernel  $V$  to infinite order. It is a coupled channel equation since it contains not only kaon and nucleon degrees of freedom but involves the complete baryon ( $B = N, \Lambda, \Sigma$ ) and pseudoscalar meson ( $M = \pi, K$ ) octet (2) and (3) of the chiral Lagrangian. The coupling to  $\Xi$ 's and  $\eta$ 's can be neglected. The  $\Lambda$ ,  $\Sigma$  and  $\pi$  degrees of freedom are, however, essential for  $KN$  scattering.

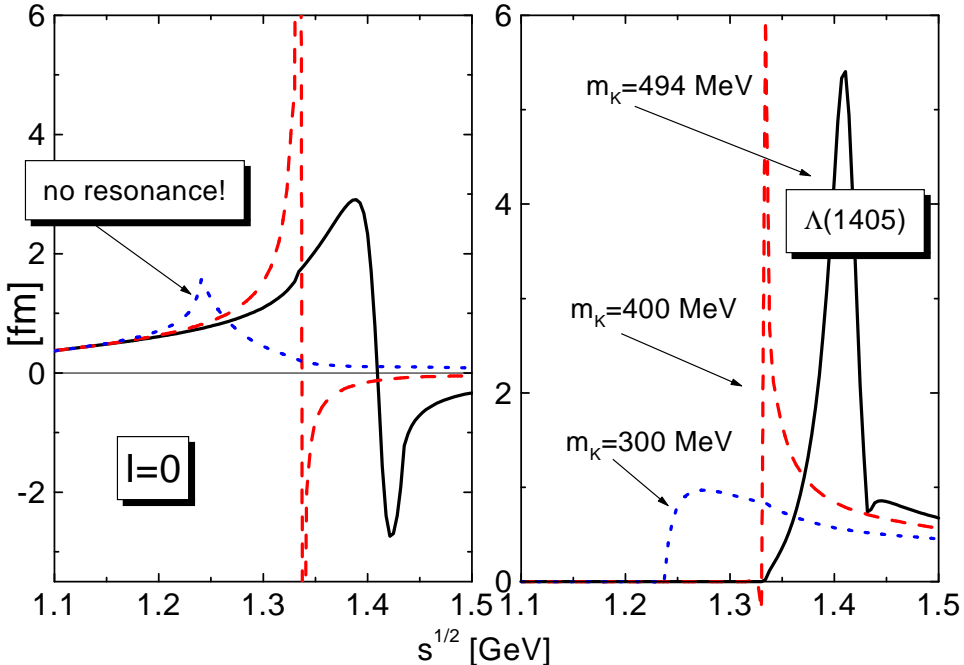


Figure 2: Real (left) and imaginary (right) part of the isospin zero s-wave  $K^-$ -nucleon scattering amplitude from the iterated Weinberg-Tomozawa interaction in a coupled channel calculation. The figure is taken from [38].

Hence the strategy is different to the  $\pi N$  sector where a perturbative expansion of the  $SU(2)$  chiral Lagrangian has been demonstrated to be very successful [59]. In the  $SU(3)_V$  sector the interaction kernel  $V$  rather than directly the scattering amplitude has to be expanded. This kernel is then iterated to all orders in the Bethe-Salpeter equation. The leading order in the expansion of the  $KN$  interaction is current algebra, i.e. the Weinberg-Tomozawa term (11) which is of chiral order  $Q$ . Fig. 2 shows the real and imaginary part of the isospin zero s-wave  $K^-$ -nucleon scattering amplitude from the iterated Weinberg-Tomozawa interaction in a coupled channel calculation from Ref. [38]. It is nicely demonstrated that using the physical kaon mass the  $\Lambda(1405)$  is dynamically generated as a pole in the

$K^-$ -proton scattering amplitude. A decrease of the  $K^-$  mass leads to a disappearance of the  $\Lambda(1405)$  which will be crucial for the discussion of in-medium effects.

Expanding  $V$  beyond current algebra the corresponding coefficients have to be fixed by  $KN$  scattering data. Coupled channel calculations for  $s$ -wave scattering with the interaction kernel truncated at chiral order  $Q^2$  were first carried out by Kaiser et al. [30].  $p$ -wave contributions have been taken into account at the one-loop level by Kolomeitsev et al. [60] and in coupled channel calculations by Lutz et al. [38]. Higher partial waves have been taken into account in the G-Matrix calculations of Ramos and Oset [61] and by Tolos et al. [62, 63], in the latter case with an interaction kernel  $V$  based on the Jülich meson-exchange potential [64].

After fixing the model parameters from free  $NK$  scattering one is now able to systematically incorporate medium effects and to determine thus in-medium scattering amplitudes, mass shifts and spectral functions. Medium modifications of the Bethe-Salpeter-equation (38) are the following ones:

- **Pauli-blocking** of intermediate nucleon states: The Pauli principle is of course not active for hyperons and suppresses  $NK$  excitations compared to  $Y\pi$  excitations.
- **Self-consistency:** This means a self-consistent dressing of the  $K^-$  propagator

$$D_{K^-}(k) \mapsto D_{K^-}^*(k) = \frac{1}{k^2 - m_K^2 - \Pi_{K^-}} \quad (40)$$

by the in-medium kaon self-energy  $\Pi_{K^-}$ . Since  $K^-$  mesons receive a substantial width in the medium  $\Pi_{K^-}$  is generally complex

$$\Re \Pi_{K^-}(k) = 2E(\mathbf{k}) \Re U_{\text{opt}}(E, \mathbf{k}) , \quad \Im \Pi_{K^-}(k) = -2E(\mathbf{k}) \Gamma_{K^-}(E, \mathbf{k}) \quad (41)$$

- **Dressing of the nucleon propagator:** At finite nuclear density the nucleon propagator is dressed by the nucleon self-energy  $\Sigma_N$  due to the interaction with the surrounding nucleons

$$G_N^*(p) = \frac{1}{p - m_N + \Sigma_N + i\epsilon} . \quad (42)$$

Nucleons are still good quasi-particles and thus  $\Sigma_N = \Sigma_S + \gamma_\mu \Sigma_V^\mu$  is real. Scalar and vector contributions of  $\Sigma_N$  can e.g. be taken from the Walecka model of nuclear matter [47]. The same holds for the other baryons of the baryon octet (2) where self-energy contributions can e.g. be derived from simple counting of non-strange quarks, e.g.  $\Sigma_\Lambda = 2/3 \Sigma_N$ .

- **Dressing of the pion propagator:** Analogous to the kaons the intermediate pion propagator  $D_\pi \mapsto D_\pi^*$  is dressed by a pion self-energy  $\Pi_\pi$  due to  $\Delta$ -hole or  $N$ -hole excitations in the nuclear medium.

The effect of Pauli blocking was first pointed out by Koch [65] and later on studied in detail by Waas, Kaiser, Rho and Weise [33, 34]. Pauli blocking effects were found to play a dominant role since the attractive  $K^-N$  interaction is reduced at finite densities. This acts effectively as a repulsive force which shifts the  $\Lambda(1405)$  resonance above the  $K^-p$  threshold and leads to a dissolution of this resonance at densities above  $2 - 3\rho_0$ . Since the existence of the  $\Lambda(1405)$  was, on the other hand, the origin of the repulsive  $K^-N$  scattering length at threshold, a shift or a dissolution of this resonance causes an in-medium  $K^-$  potential which is now close to the tree-level result predicted by the attractive Weinberg-Tomozawa term. However, self-consistency, i.e. the dressing of the  $K^-$  propagator by the attractive potential counteracts the Pauli effect. As pointed out by Lutz [35] a decreasing  $K^-$  mass results in a negative shift of the  $\Lambda(1405)$ , regarded as a bound  $K^-p$  state, and compensates the positive Pauli shift to large extent. The position of the  $\Lambda(1405)$  pole stays now fairly constant but the resonance is still substantially broadened and dissolves at high densities (as can be seen from the schematic calculation shown in Fig. 2.) The influence of dressing of nucleon and hyperon propagator due to short-range  $NN$  and  $NY$  correlations has been investigated in [66].

### 2.3.1 In-medium potentials

The dressing of nucleon and hyperon propagators is generally included in such type of calculations but the effects are of minor importance. A strong influence has, however, a dressing of the pion propagator by an attractive pion potential which arises due to nucleon- and  $\Delta$ -hole excitations in the medium. As shown by Ramos and Oset [61] and also found by Tolos et al. [62] the thresholds of the  $\pi\Lambda$  and  $\pi\Sigma$  channels are lowered resulting in less attraction for the in-medium  $K^-$  potential.

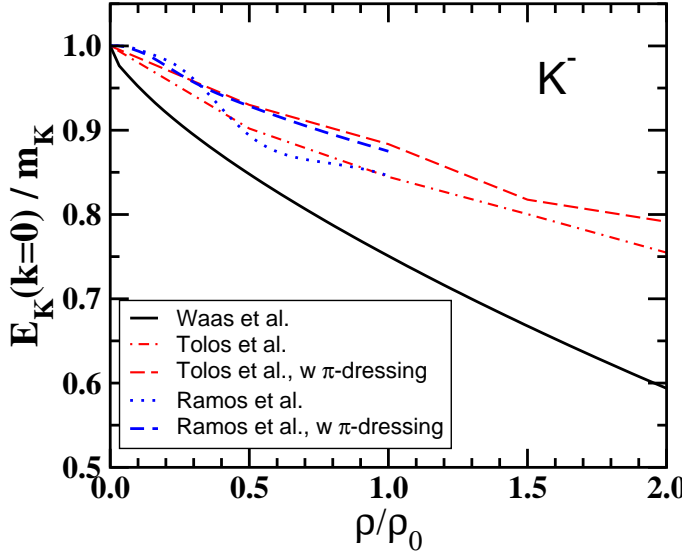


Figure 3: In-medium  $K^-$  energy obtained in coupled channel calculations which includes Pauli-blocking (Waas et al., [33]), kaon dressing (Ramos et al., [61]) and pion dressing (Ramos et al., [61], Tolos et al. [62]).

Fig. 3 shows the single particle energy or 'in-medium mass shift'  $E(\mathbf{k} = 0) = m_K + \Re U_{\text{opt}}(E, \mathbf{k} = 0)$  for antikaons obtained in various coupled channel calculations. This quantity can be compared to the mean field picture although such a comparison has to be taken with care. At finite densities the antikaons acquire a substantial in-medium width and do no more behave like good quasi-particles, as assumed in a mean field picture. In particular at low momenta the spectral functions can be of complex structure without a well defined quasi-particle pole which makes the interpretation of the in-medium self-energy  $\Pi_K$  in terms of on-shell potentials questionable. However, transport models are usually formulated in terms of quasi-particles. Hence, we do not want to refrain from this comparison. The microscopic coupled channel calculations deliver an attractive in-medium potential which is significantly smaller than in the mean field approaches, in particular when a self-consistent dressing of the kaon propagator is taken into account, and even smaller when pion dressing is included. This fact is also reflected in the optical potential (real part) shown in Fig. 4. We compare the momentum dependence of  $\Re U_{\text{opt}}$  at saturation density obtained in various approaches. Results are taken from the chiral mean field approach [31], denoted in Fig. 1 as MFT ChPT+corr., the coupled channel calculations of Tolos et al. [62], with and without pion dressing, and a dispersion analysis of  $K^+N$  and  $K^-N$  scattering amplitudes by Sibirtsev and Cassing [67]. Since the definition used to extract the optical potential from the self-energy  $\Pi$  varies in the literature, this comparison is based on relation (41) which has been used in [62] instead of Eq. (28). For  $K^+$  the magnitudes of the potential are consistent, i.e. the dispersion analysis agrees with the mean field approach at zero momentum. It predicts an almost momentum independent potential while  $U_{\text{opt}}$  is slightly rising as a function of momentum in mean field models. For  $K^-$  all models predict a considerably reduced attraction at high kaon momenta, however, the potential depths strongly deviate. The self-consistent coupled channel calculations from Schaffner et al. [68] predict an

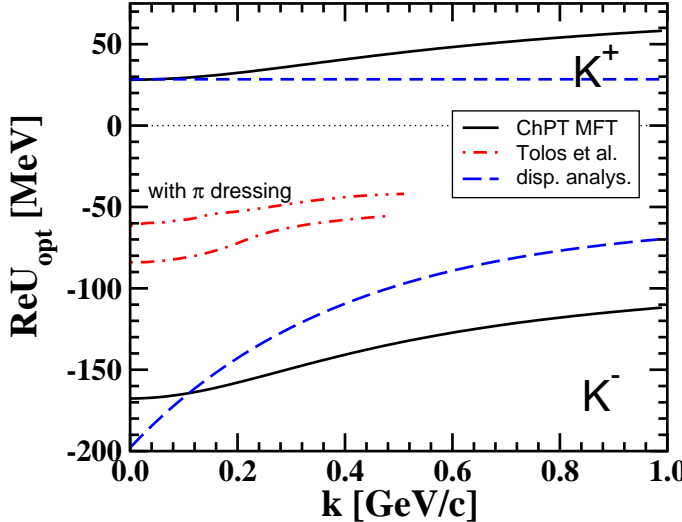


Figure 4: Optical kaon potentials at nuclear saturation density. Results from the chiral mean field approach (ChPT MFT), from coupled channel calculations (Tolos et al. [62]) and from the dispersion analysis of [67]) are compared.

even smaller potential which is of the size of -32 MeV at saturation density.

The dispersion analysis of Ref. [67] comes close to the mean field result which is, however, not astonishing since the authors disregarded the repulsive contributions from the  $\Sigma(1385)$  and  $\Lambda(1405)$  resonances according to the argument that these resonances should dissolve at finite density. They found their parameterization of the  $K^-$  potential consistent with data from  $p + A$  reactions [67].

All the microscopic approaches predict  $K^-$  potentials of only moderate attraction and are thus in stark contrast to the mean field picture and the standard analysis of kaonic atoms [11]. The latter suggests a strongly attractive on-shell  $K^-$  potential of about 200 MeV at  $\rho_0$ . It is not yet fully clear if the microscopic approaches which comply with kaon-nucleon scattering data, can explain kaonic atoms as well. However, there are indications that kaonic atoms explore the antikaon potential only at the nuclear surface [69, 70] and weak  $K^-$  potentials describe the available data as well [71]. A final answer would require to account for the full off-shell behavior of self-energy and spectral properties of a bound  $K^-$  state. However, such calculations have not yet been performed.

Figure 5 demonstrates finally the validity of the quasi-particle picture. It shows the kaon and antikaon spectral functions at saturation density obtained from coupled channel calculations from Ref. [72] (including pion dressing) for different momenta. The kaons have still a clear quasi-particle peak which in the medium acquires a finite width. The latter is, however, quite small (less than 5 MeV) for small momenta and increases up to 15 MeV at a momentum above 400 MeV which is still moderate. Hence the quasi-particle picture and the mean field approximation are well justified. As already stressed several times, the situation for  $K^-$  mesons is quite different. In particular at low momenta the spectral functions are broad and of complex structure. At larger momenta a quasi-particle peak may still be visible but also here substantial strength is shifted to lower momenta. Thus the mean field approximation is questionable for the antikaons.

### 2.3.2 In-medium cross sections

Coupled channel calculations may predict sizeable in-medium modifications of the pion-induced  $K^-$  production cross sections and the corresponding absorption cross sections  $\pi Y \longleftrightarrow NK^-$ . The fact that the s-wave  $\Lambda(1405)$  resonance lies only 27 MeV below the  $K^- p$  threshold implies a strong coupling to this state and requires a non-perturbative treatment. The melting of the  $\Lambda(1405)$  and  $\Sigma(1385)$  bound

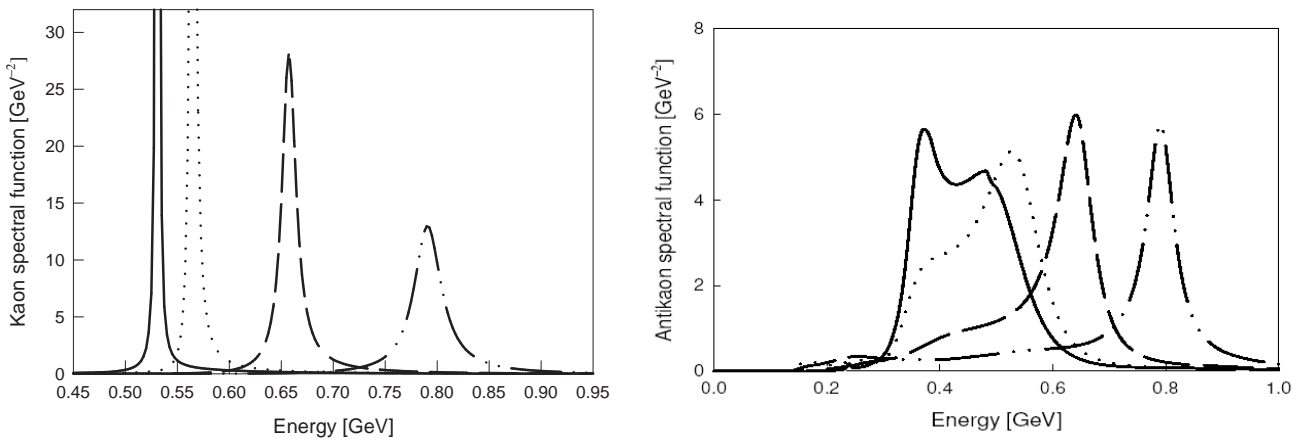


Figure 5: In-medium kaon (left) and antikaon (right) spectral functions from coupled channel calculations of [72] at saturation density. Results are shown for different kaon momenta:  $p_K = 0$  (solid line), 200 MeV (dotted line), 400 MeV (dashed line), and 600 MeV (dash-dot-dot line).

states due to Pauli blocking of the intermediate states in the BS-equation (38) leads to a dramatic increase in particular of the  $\pi\Sigma \rightarrow NK^-$  cross section at threshold. In [68] the enhancement factor was found to be more than one order of magnitude at  $\rho_0$ . However, self-consistency shifts the  $K^-$  mass below threshold and decreases the available phase space which counteracts the enhancement due to a melting  $\Lambda(1405)$ . In the calculations of Schaffner et al. [68] the  $\pi\Sigma \rightarrow NK^-$  is then only enhanced by a factor of two and the  $\pi\Lambda \rightarrow NK^-$  is hardly affected at all. In the self-consistent calculations of Lutz and Korpa [37] the predicted in-medium modifications of these cross sections are practically opposite. They account in addition for the full in-medium modifications of the  $K^-$  spectral distributions and obtain a strong enhancement of the  $\pi\Lambda \rightarrow NK^-$  cross section due to the coupling to the  $\Sigma(1385)$  but almost no changes for the  $\pi\Sigma \rightarrow NK^-$  channel. The G-matrix calculations of Tolos et al. [62] came to opposite conclusions, namely an almost complete suppression of the pion induced reactions in the nuclear environment. Such strong modifications of the  $K^-$  production cross sections and the corresponding absorption cross sections would have severe consequences for the  $K^-$  dynamics in heavy ion reactions.

## 2.4 Kaons in pion matter

In heavy ion reactions at intermediate energies the matter is baryon dominated, at ultra-relativistic energies at CERN-SPS or at RHIC the matter is, however, pion dominated. For completeness it is thus instructive to consider this case as well. The problem of medium modifications experienced by kaons in a hot pion gas has been dressed in the early 90ties in Refs. [73] and [74] where the authors came, however, to opposite conclusions concerning the kaon mass shifts. Recently this problem has been picked up by Martemyanov et al. [75]. In Ref. [75] the kaon self-energy has been determined in a model independent way to leading order in pion density, based on ChPT at low temperatures and experimental phase shifts at high temperatures.

Analogous to nuclear matter (35) the kaon self-energy  $\Pi_K(k^2, E)$  can be expressed in terms of the  $\pi K$  forward scattering amplitudes for on-shell pions and off-shell kaons. The necessary on-shell  $\pi K$  amplitudes have been evaluated in ChPT to order  $p^4$  by several authors (see e.g. [76] and references therein). Near the threshold, the isospin-even (+) and odd (-)  $\pi K$  scattering amplitudes can be

expressed in terms of scattering lengths and effective ranges  $a_\ell^{(\pm)}$  and  $b_\ell^{(\pm)}$

$$A^{(\pm)}(s, t, k^2) = 8\pi\sqrt{s} \left[ a_0^{(\pm)} + p^{*2} (b_0^{(\pm)} + 3a_1^{(\pm)}) + \frac{3}{2} t a_1^{(\pm)} \right] + c^{(\pm)}(k^2 - m_K^2) \quad (43)$$

with  $p^* = p^*(\sqrt{s}, m_\pi, m_K)$  the c.m. momentum of the  $\pi K$  system [75]. The  $K$ -meson self-energy is then obtained by integration over the corresponding pionic Bose distributions

$$d\rho_\pi = \frac{d^3 k_\pi}{(2\pi)^3} \left( \exp\left(\frac{E_\pi - \mu_\pi}{T}\right) - 1 \right)^{-1} \quad (44)$$

with the scalar pion density  $d\rho_{s\pi} = d\rho_\pi/(2E_\pi)$

$$-\Pi_K(k^2, E) = \int A^{(+)}(s, 0, k^2) (d\rho_{s\pi^+} + d\rho_{s\pi^0} + d\rho_{s\pi^-}) + \int A^{(-)}(s, 0, k^2) (-d\rho_{s\pi^+} + d\rho_{s\pi^-}) . \quad (45)$$

To lowest order ChPT isospin symmetric pion matter does not change the kaon dispersion law. The leading order effect appears at the one loop level. The mean field, i.e. the scalar mass shift  $\delta m_K$  and the vector potential  $V_K$  follow from the self-energy at the on-shell point which can be expressed in terms of  $s$ - and  $p$ -wave scattering lengths and  $s$ -wave effective ranges:

$$\Pi_K(m_K^2, m_K) = -4\pi\rho_\pi \frac{m_\pi + m_K}{m_\pi} a_0^{(+)} . \quad (46)$$

With  $\delta m_K + V_K = \Pi_K(m_K^2, m_K)/2m_K$ . From (46) follows also the vector potential

$$V_K = -\frac{2\pi\rho_\pi}{m_\pi + m_K} \left[ a_0^{(+)} + 2m_\pi m_K (b_0^{(+)} + 3a_1^{(+)}) \right] . \quad (47)$$

Since ChPT is only valid at temperatures well below the pion mass in Ref. [75] the high temperature behavior has been based on a more phenomenological approach which parameterizes the experimental phase shifts and matches smoothly with the one-loop ChPT low-temperature limit. The corresponding kaon self-energy at threshold, the mass shift and the vector potential are shown in Fig. 6 as a function of temperature. At  $T = 170$  MeV one obtains a negative mass shift  $\delta M_K = -33$  MeV and a repulsive vector potential of  $V_K = 21$  MeV. There exists a remarkable analogy to the nuclear matter case: the kaon mass shift at high temperatures is large and negative, the vector potential is large and positive, their sum is relatively small and negative. Kaons are therefore bound in pion matter similar to nucleons or antikaons in nuclear matter. The vector potential is, however,  $C$ -even, distinct from the case of nuclear matter. In addition both, kaons and antikaons acquire a substantial in medium width  $\Gamma_K^*$  at finite temperature [75].

In-medium modifications of the kaons have direct implications on the  $\phi$  meson properties. At ultra-relativistic energies an inconsistency has been observed between the  $\phi$  yields measured through the dilepton and  $K\bar{K}$  channels. In Pb+Pb collisions at CERN/SPS energies ( $E_{\text{lab}} = 158$  AGeV) the  $\mu^+\mu^-$  yield from  $\phi$  decays was measured by the NA50 Collaboration [77] and the  $K\bar{K}$  channel by the NA49 [78]. The leptonic channel was found to be enhanced by a factor of two to four compared to the mesonic channel. A similar observation has been made in Au+Au collisions at RHIC ( $\sqrt{s_{NN}} = 200$  GeV) by PHENIX [79, 80] which measured simultaneously the  $\phi \rightarrow e^+e^-$  and  $K\bar{K}$  channels. At RHIC energies this apparent enhancement of the leptonic channel can qualitatively be understood by an enhanced in-medium  $\phi$  width  $\Gamma_\phi^{\text{med}} \sim 2 \div 3 \Gamma_\phi^{\text{vac}}$  and the final state interaction of the corresponding kaons inside the fireball [75, 81].

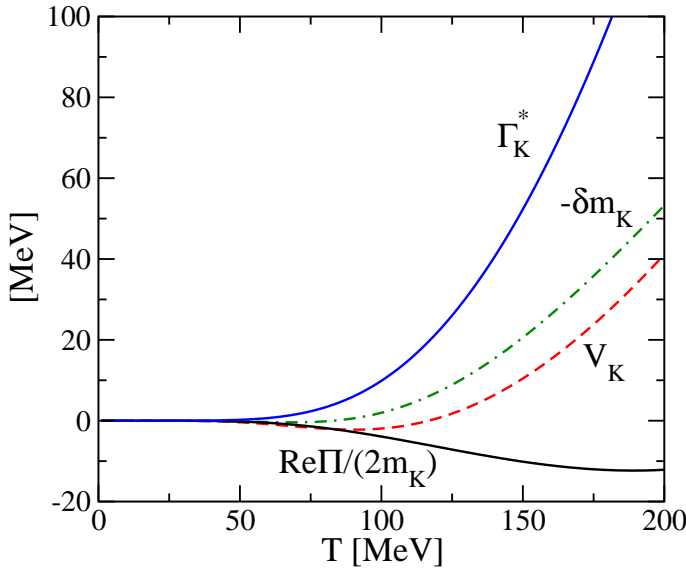


Figure 6: Medium modifications of kaons in an isospin-symmetric hot pion gas: self-energy  $\Re\Pi_K/(2m_K)$ , mass shift  $-\delta m_K$ , vector potential  $V_K$ , and kaon collision width  $\Gamma_K^*$  versus temperature  $T$ . Results are taken from [75].

## 2.5 Chiral symmetry restoration?

At the end of this chapter I want to shortly address the question of chiral symmetry restoration. The spontaneously broken chiral symmetry of QCD manifests itself in the large expectation value of the scalar quark condensate  $\langle\bar{q}q\rangle$  of the QCD vacuum while the small but finite current quark masses are responsible for the explicit chiral symmetry breaking of QCD. In the chiral limit of vanishing current quark masses, the Goldstone bosons of spontaneous chiral symmetry breaking, i.e. the pion, respectively the full pseudo-scalar octet, become massless. This fact is guaranteed by the Gell-Mann-Oakes-Renner relation. However, through the GOR relation the pseudoscalar meson masses are also directly proportional to the scalar condensates. The GOR relation is of leading order in the quark masses. By in-medium chiral symmetry restoration one understands now the fact that dropping pseudoscalar meson masses are caused by a reduction of the condensate at finite nuclear density and/or temperature. The meson masses approach the chiral limit although the explicit symmetry breaking is still valid.

How such a scenario is connected with the medium properties obtained from chiral dynamics is, however, a non-trivial question. The leading term in the chiral pseudoscalar meson-nucleon interaction is the Weinberg-Tomozawa term. At finite nuclear density it is responsible for the splitting of the energy levels between the degenerate flavor eigenstates  $K^+(u\bar{s})$  and  $K^-(\bar{u}s)$  due to SU(3) flavor symmetry breaking. As indicated in Fig. 7, SU(3) flavor symmetry is broken by the non-vanishing up and down quark densities  $\rho_{u/d}$  while the strange quark density  $\rho_s$  is still zero. Isospin symmetric pion matter, in contrast, is flavor symmetric and there occurs no mass splitting between kaons and antikaons. Charge symmetry breaking which occurs in isospin asymmetric nuclear matter leads to an additional mass splitting of the different isospin states  $K^+$  and  $K^0(d\bar{s})$ , respectively  $K^-$  and  $\bar{K}^0(\bar{d}s)$ .

In chiral coupled channel dynamics the leading order Weinberg-Tomozawa kaon-nucleon interaction is iterated to infinite order. The kaons obtain medium modifications, i.e. mass shifts and changes of their spectral distributions. However, in this framework their origin can not easily be traced back to a restoration of chiral symmetry. Such an interpretation is to some extent possible when the Kaplan-Nelson term in the KN-interaction is taken into account. The Kaplan-Nelson term is of order  $\langle\bar{q}q\rangle$  and therefore directly related to the in-medium condensates via the GOR relation. In the mean field picture the two effects, mass splitting (Weinberg-Tomozawa) and dropping mass (Kaplan-Nelson) are clearly

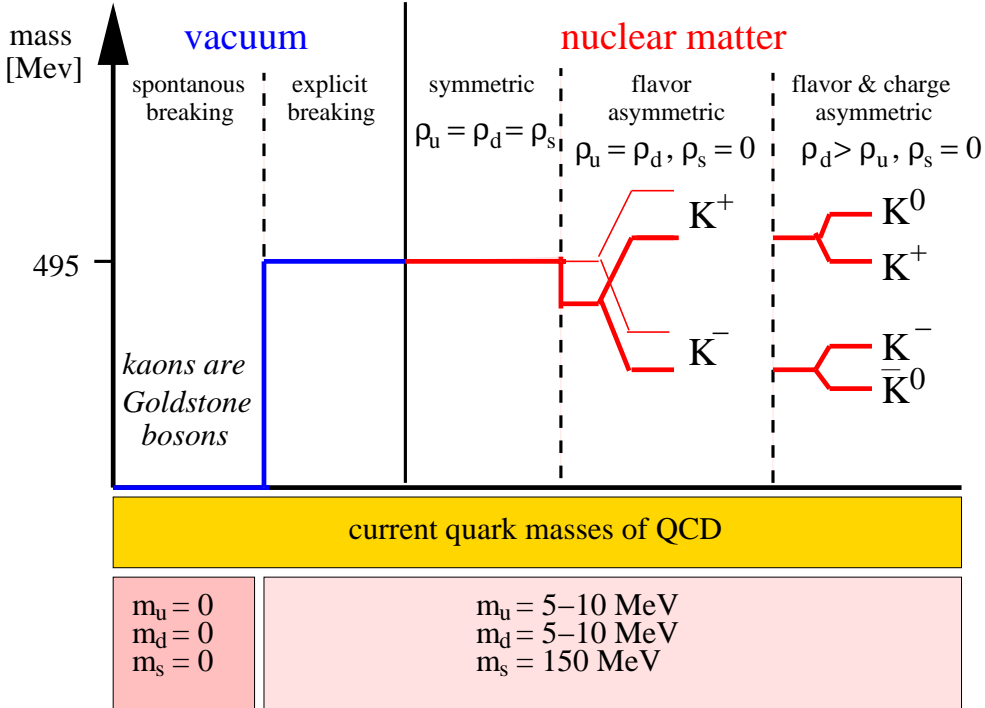


Figure 7: Schematic representation of kaon and antikaon energy shifts in dense nuclear matter due to  $SU(3)$  symmetry breaking ( $\rho_u = \rho_d, \rho_s = 0$ ). The Weinberg-Tomozawa term leads to the  $K^+/K^-$  mass splitting (thin line) while the Kaplan-Nelson term is responsible for the common mass shift (thick line).

separated and the latter one can be interpreted in terms of a partial chiral symmetry restoration. Fig. 7 illustrates this scenario schematically.

In coupled channel chiral dynamics it is no more straightforward to disentangle *ordinary* hadronic many-body effects from a change of the QCD vacuum. The principle connection of hadronic many-body effects with basic QCD quantities such as the chiral condensate is provided by the Hellman-Feynman theorem which relates  $\langle \bar{q}q \rangle$  with the derivative of the QCD-Hamiltonian with respect to the current quark masses. In nuclear matter the condensate is in the same way obtained from the total energy density  $\mathcal{E}$

$$\langle \rho | \bar{q}q | \rho \rangle = \langle \bar{q}q \rangle + \frac{1}{2} \frac{d\mathcal{E}}{dm_q} . \quad (48)$$

Eq. (48) implies that many-body correlations, albeit based on hadronic degrees of freedom, provide contributions to the in-medium quark condensate. The practical use of this type of quark-hadron duality is, however, rather limited. While there exist sophisticated models for the treatment of hadronic many-body correlations, such as e.g. Brueckner theory, one would have in addition to know the dependence of these correlations on the current quark masses. For pionic correlations, lets call them  $\mathcal{C}_\pi$ , such a procedure may in principle be possible making use of the GOR relation, i.e.  $\partial \mathcal{C}_\pi / \partial m_q = \partial \mathcal{C}_\pi / \partial m_\pi m_\pi / 2m_q$ . The derivative of the nucleon mass is given by the pion-nucleon  $\Sigma$  term  $dm_N / dm_q = \Sigma_{\pi N} / m_q$  and analogous relations exist for the strange quark. However, these derivatives are only valid to leading order in ChPT which restricts their applications to the mean field level. Attempts to proceed in such a direction have been performed, e.g., by Cohen et al. [48] and more recently by Chanfray and Ericson [82].

$K^+$	$K^-$	type
$BB \rightarrow BYK^+$	$BB \rightarrow BBK^+K^-$	strangeness production primary/secondary
$\pi B \rightarrow YK^+$	$\pi B \rightarrow BK^+K^-$	strangeness production secondary
	$BY \rightarrow BBK^-$	strangeness exchange
	$\pi Y \leftrightarrow BK^-$	strangeness exchange
$YK^+ \rightarrow \pi B$		strangeness absorption
$BK^+ \leftrightarrow BK^{+0}$	$BK^- \leftrightarrow BK^-(\bar{K}^0)$	elastic/charge exchange

Table 1: Elementary hadronic reactions which are relevant for kaon dynamics at intermediate energies.  $B$  stands for nucleons or nucleon resonances ( $N, \Delta, N^*$ ) and  $Y$  for hyperons ( $\Lambda, \Sigma$ ).

### 3 Phenomenology of strangeness production

#### 3.1 Elementary reaction channels

We start with a short discussion of the various reaction channels which determine the kaon and antikaon production at intermediate energies, the role these channels play in the complex reaction dynamics and their experimental and theoretical knowledge. The various processes are summarized in Tab. 1. They

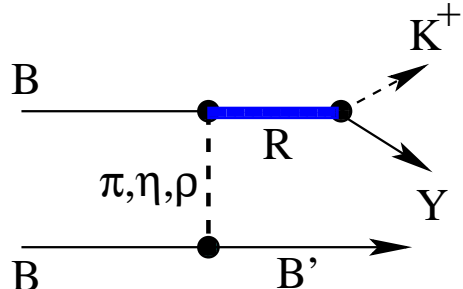


Figure 8: Diagrammatic representation of the reaction  $BB \rightarrow BYK^+$  within the one-boson-exchange + resonance model.

can be classified in primary and secondary strangeness production reactions, strangeness and charge exchange reactions and strangeness absorption reactions. Strangeness production can be subdivided into two classes, namely baryon induced ( $BB \rightarrow BYK^+$ ,  $BB \rightarrow BBK^+K^-$ ) and pion induced ( $\pi B \rightarrow YK^+$ ,  $\pi B \rightarrow BK^+K^-$ ) reactions.  $B$  stands here for a baryon which can be either a nucleon or a nucleon resonance ( $N, \Delta, N^*$ ) and  $Y$  for hyperons ( $\Lambda, \Sigma$ ). The first class falls into two subclasses: primary reactions with two nucleons in the entrance channel and secondary reactions with at least one nucleon resonance in the entrance channel. Meson induced reactions are by definition of secondary type. Both involve at least a two step process with first the production of the intermediate resonance or meson. Primary reactions play the dominant role for kaon and antikaon production at higher energies and contribute dominantly to the high momentum part of the spectra. However, at subthreshold energies the production rates are dominated by the secondary type reaction mechanism. The same feature appears already in proton-nucleus collisions [83, 84, 67, 85]. Other processes like the production of multi-strange baryons ( $\Xi, \Omega$ ) or hidden strangeness ( $\phi$ ) are subdominant and will be discussed separately.

### $BB \rightarrow BYK^+$ :

The reaction  $pp \rightarrow p\Lambda K^+$  sets the threshold for  $K^+$  production in free space ( $T_p = 1.58$  GeV). Historically this cross section was overestimated for a long time [86], in particular close to threshold. The situation improved when the COSY-11 Collaboration delivered data for  $pp \rightarrow p\Lambda K^+$  close to threshold [87]. An open question is still the isospin dependence of this channel. Isotopic relations predict  $(pn \rightarrow n\Lambda K^+) = 2(pp \rightarrow p\Lambda K^+)$  while recent proton-deuteron data indicate that the  $pn$  cross section might be even larger [88]. Already rather early it was noticed that secondary reactions ( $N\Delta \rightarrow NYK^+$ ), where the  $\Delta$  resonance plays the role of an energy storage, contribute essentially to the subthreshold kaon yield in HIC's [89, 90, 91, 92, 93, 94] while multi-step processes of higher order with two  $\Delta$  resonances in the entrance channel are suppressed [91, 95, 96]. Reactions with a  $\Delta$  in the exit channel are energetically suppressed. Since no experimental data exist for cross sections involving nucleon resonances one has here to rely on model calculations. Commonly used parameterizations are based on one-boson-exchange models [97, 98] or on more microscopic one-boson-exchange + resonance models [99, 100, 101, 102]. Both models are usually applied at the tree level. The resonance model assumes thereby that the heavy meson production process runs over the excitation of an intermediate nucleon resonance  $R = N^*, \Delta$  as depicted in Fig. 8. The model parameters, i.e. coupling constants can be fixed from data on  $\pi N \rightarrow YK^+$  reactions. As already shown in [99] the resonant s-channel is dominant in  $pp \rightarrow p\Lambda K^+$ , non-resonant t-channel contributions can be parameterized through  $K^*$  exchange. This type of resonance models are popular and generally quite successful in the description of heavy meson production ( $\rho, \omega, \phi$ ) close to threshold [103, 104, 105, 106, 107, 108].

### $\pi B \rightarrow YK^+$ :

The importance of this channel for HIC's was first pointed out by Fuchs et al. [109] and confirmed by the Giessen group [94]. Depending on energy and system size the pion-induced reactions  $\pi N \rightarrow YK^+, \pi\Delta \rightarrow YK^+$  can contribute up to about 50% of the total kaon yield. Naturally the contribution is largest in heavy systems. The corresponding cross sections are relatively well constrained by pion-proton scattering data. The parameterizations of Tsushima et al. [110] obtained within an one-boson-exchange + resonance model are presently used in most transport calculations.

### $YK^+ \rightarrow \pi B$ :

At subthreshold energies strangeness absorption plays no significant role. That the probability for such an event is, however, not complete vanishing has been demonstrated in [111]. Since strangeness absorption would be the only possibility to drive kaons towards chemical equilibrium the chemical kaon freeze-out occurs already at a non-equilibrium stage [112].

### $BB \rightarrow BBK^+K^-$ :

The reaction  $pp \rightarrow ppK^+K^-$  sets the threshold for  $K^-$  production in free space ( $T_p = 2.50$  GeV). The history of this reaction is similar to that of  $pp \rightarrow p\Lambda K^+$ . Also here early predictions [113] overestimated this cross section in the vicinity of the threshold by about two orders of magnitude, as it turned out when COSY-11 provided the first data point close to threshold [114]. Tree level OBE calculations based on pion and kaon exchange are able to reproduce the near threshold behavior [115]. In contrast to  $pp \rightarrow p\Lambda K^+$  this reaction seems to be dominated by t-channel exchange. Hence the resonance model which is based on resonant s-channel exchange has not been applied. Reactions which involve nuclear resonances in the initial and/or final state have not been investigated theoretically and are neglected in corresponding transport calculations.

### $\pi B \rightarrow BK^+K^-$ :

The  $\pi N \rightarrow NK^+K^-$  and  $\pi N \rightarrow N\pi K^+K^-$  cross sections are experimentally well constrained. Calculations based on tree level one-boson-exchange have been performed in [115]. Transport calculations [116, 96] estimate this channel of about equal importance as baryon induced primary  $K^-$  production.

### $BY \longleftrightarrow BBK^-$ :

As first pointed out by Ko [117], strangeness exchange is the dominant mechanism for  $K^-$  production at subthreshold energies. The relative importance of the two possibilities, through nucleon-hyperon

scattering or pion absorption are not yet completely settled. More than 20 years ago Ko [117] estimated the contribution of this channel to about 10%. The  $NY \rightarrow NNK^-$  can in principle easily be determined in a OBE picture since the cross section factorizes in the pion exchange and the experimentally known  $\pi Y \longleftrightarrow NK^-$  part. The importance of this channels is, however, still controversial. In [116] it was found to contribute only a few percent to the total antikaon yield in heavy ion reactions whereas a recent reanalysis of this channel by Barz et al. [118] stresses its importance (about 25%) for  $p + A$  reactions.

$\pi Y \longleftrightarrow BK^-$ :

This channel is experimentally well known from  $K^-$ -proton scattering (for a recent partial wave analysis see [119]). The cross sections are large, e.g. 40-70 mb for  $NK^- \rightarrow \pi Y$  depending on relative momentum. Strangeness exchange reactions are essential for the  $K^-$  dynamics in heavy ion collisions. The cross sections are generally large, i.e. of the order of mbarn, whereas the strangeness production is of the order of  $\mu$ barn. In the standard scenarios strangeness exchange through pion absorption is one of the major sources for the  $K^-$  yield at subthreshold energies [94, 120]. The reason lies in the fact that the threshold for strangeness production through hyperons in association with  $K^+$  mesons is about 1 GeV below the direct  $K^+K^-$  production threshold and these strange quarks can be transferred to antikaons by pion absorption. This drives the  $Y - K^-$  system towards chemical equilibrium whereas for anti-strangeness no comparable process exists. Hence, antikaons freeze out later than kaons [111, 120]. However, due to the strong coupling of the  $K^-$ -nucleon system to the  $\Lambda(1405)$  large medium effects have to be expected for the  $\pi\Sigma \longleftrightarrow NK^-$  cross section and this reaction has theoretically been studied in great detail [68, 37, 61, 62, 121]. The medium dependence of the cross sections is, however, still controversial and ranges from moderate enhancement close to threshold to a strong suppression (see discussion in chapter 5). This, of course would change the complete scenario of  $K^-$  production and absorption.

$BK \longleftrightarrow BK, B\bar{K} \longleftrightarrow B\bar{K}$ :

Because of strangeness conservation the kaon final state interaction is at low energies dominated by elastic kaon-nucleon scattering. This does in principle not affect the total yields. However, elastic scattering changes the shape of the momentum spectra significantly. Rescattering makes the spectra harder and changes the angular distributions [122, 123, 124]. In systems with large isospin asymmetry charge exchange  $pK^+ \longleftrightarrow nK^0$  may also slightly affect the final yields. The elastic antikaon cross section is large ( $\sim 20 - 100$  mb), in particular at low momenta, which is the result of the strong coupling to the  $\Lambda(1405)$  resonance. It competes, however, with  $K^-$  absorption. The corresponding charge exchange cross section  $pK^- \longleftrightarrow n\bar{K}^0$  is comparatively small and does not significantly influence the  $K^-$  dynamics.

### 3.2 Hidden strangeness production

In addition to open strangeness production through  $K\bar{K}$  pairs or kaon-hyperon pairs hidden strangeness can be produced through  $\phi(s\bar{s})$  mesons. The  $\phi$  is a  $0^-(1^{--})$  vector meson with the same quantum numbers as the  $\omega$  and has a mass of 1020 MeV. However, compared to the  $\omega$  the production of  $\phi$  mesons is strongly suppressed due to the Okubo-Zweig-Iizuka (OZI) [4] selection rule which forbids the appearance of disconnected quark line diagrams. According to the OZI estimate  $\phi$  mesons can only be produced due to a small admixture of non-strange light quarks in their wave function. The corresponding mixing angle  $\theta_{mix}$  is equal to  $\theta_{mix} \approx 3.7^\circ$  [125]. According to this mixing angle the ratio of  $\phi$  and  $\omega$  mesons cross sections should at comparable energies naively be equal to

$$R_{\phi/\omega} = \tan^2 \theta_{mix} \cdot F \approx 4.2 \times 10^{-3} \cdot F, \quad (49)$$

where  $F$  is a correction due to the different phase space factors for  $\phi$  and  $\omega$  mesons. Experimentally, the ratio  $R_{\phi/\omega}$  is in  $pp \rightarrow pp\phi(\omega)$  reactions, however, known to be one order of magnitude larger than

the naive expectation [126]. Elementary  $\phi$  production has been calculated within several approaches, mostly within meson exchange models [127, 128, 129]. In Refs. [107] and [108] the cross section for  $\omega$  and  $\phi$  meson production in  $pp$  collision have been calculated within the resonance model. The experimental data are well reproduced and the large violation of the OZI prediction for the  $\phi$  over  $\omega$  production, observed experimentally, could be explained in [108] without the introduction of additional parameters. The reactions of the type  $NN \rightarrow NN\phi$  and  $\pi N \rightarrow N\phi$  should be OZI suppressed compared to open strangeness production as well, whereas the DISTO results [126] show that almost 50% of the  $pp \rightarrow ppK^+K^-$  cross section is resonant, i.e. running over an intermediate  $\phi$ . When parameterizations of the  $NN \rightarrow NNK^+K^-$  are used in transport calculations the resonant parts of these cross sections are usually implicitly included.

The FOPI Collaboration measured the  $\phi$  production in Ni+Ni reactions at 1.93 AGeV and came to the conclusion that at least about 20% of the observed  $K^-$  mesons originate from  $\phi$  decays [130]. Due to the large coupling to the  $K\bar{K}$  channel (the partial  $\Gamma(\phi \rightarrow K^+K^-)$  decay width is about 50%) one can expect that the  $\phi$  reacts sensitive on medium modifications of the kaons which will mainly result in a broadening of the  $\phi$  width in hadronic matter (see e.g. [75] and refs. therein). The  $\phi$  production in heavy ion reactions has been studied in [127, 131]. However, also with the inclusion of medium effects the corresponding  $\phi$  yields are underestimated by a factor two to three by these transport calculations which indicates that  $\phi$  production in heavy ion reactions is not yet fully understood. The situation will probably be improved when the HADES Collaboration will be able to measure the  $\phi$  production through the  $e^+e^-$  decay channel. The dilepton spectra should provide a very clear access to a broadening of the  $\phi$  and the underlying in-medium modifications of the kaons.

### 3.3 Densities and time scales

Since the conjecture that the early and dense phase of heavy ion reactions can be probed by  $K^+$  production has been put forward by Aichelin and Ko about two decades ago [132] strong efforts were undertaken to settle this question, both from the experimental and the theoretical side. The original motivation was to study the nuclear equation of state at supra-normal densities. This point will be addressed in detail in Chap. 6. The prerequisite for such an enterprise is of course the fact that  $K^+$  mesons originate indeed from the early phase *and* from supra-normal densities. Both features were predicted by transport calculations in the early 90ties [132, 91, 90, 92, 133]. At that time experimental data on subthreshold kaon production were scarce and the same was true for the elementary cross sections which serve as input for the transport calculations. Hence these calculations were burdened with large uncertainties but the predictions on densities and time scales turned out to be stable. A more recent analysis is e.g. given in [111].

#### 3.3.1 Conditions for strangeness production

$K^+$  mesons are produced in the early and dense phase of a heavy ion reaction. E.g. at an incident energy of 1 AGeV they reach their chemical freeze-out values already after 15 fm/c which is the phase where maximal compression is reached. One should, however, keep in mind that at such time scales the surrounding nuclear environment is still in a pronounced non-equilibrium state [111, 18]. The same is in principle also true for  $K^-$  mesons. However, due to high absorption rates through strangeness exchange reactions  $K^-N \leftrightarrow Y\pi$  they have the tendency to reach chemical equilibrium much faster. We will come back to this point in subsection 3.4.

Experimental evidence for an early  $K^+$  freeze-out is provided by the fact that  $K^+$  mesons and high-energy pions behave qualitatively similar. This fact is demonstrated by Fig. 9 where the experimentally extracted inverse slope parameters for kaons and high-energy pions ( $E_{\text{cm}}^{\text{kin}} > 300$  MeV) are compared. Also rapidity distributions of  $K^+$  and high  $p_T$  pions are similar and clearly distinct from low  $p_T$  pions

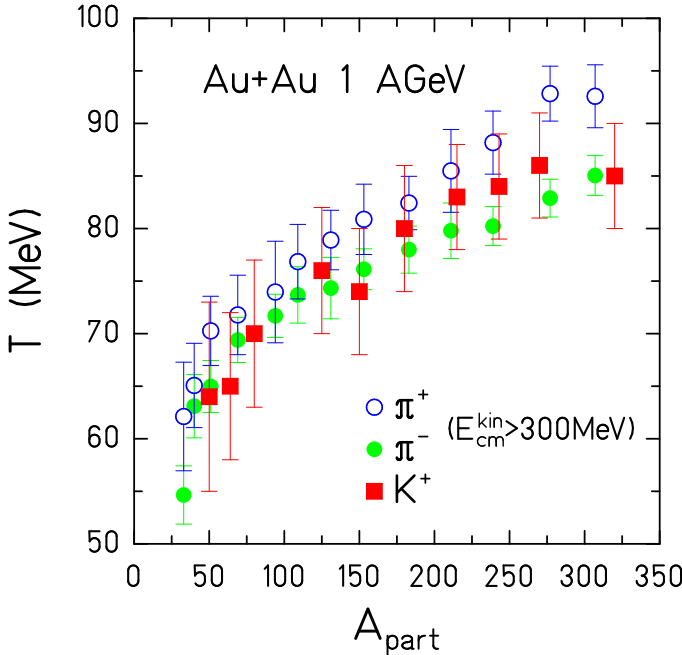


Figure 9: Measured inverse slope parameters for high-energy pions and  $K^+$  mesons in Au+Au reactions at 1 AGeV. The figure is taken from [134].

[135]. At SIS energies both, kaons and pions with  $p_T \gtrsim 0.5$  GeV are produced at equivalent “subthreshold” energies and identical slopes of the spectra imply that these particles freeze out under similar conditions. High- $p_T$  particles probe in general the early stage of a heavy ion reactions and this feature is independent of the considered energy range. For pions at SIS energies this behavior was predicted by transport models [136, 137, 27] and experimentally verified by the simultaneous measurement of pion in-plane and out-of-plane flow [138, 139]. The energy dependence of the pion flow is caused by spectator matter shadowing which can be used as a time clock for the reaction [138, 134]. To obtain a quantitative picture of the density range probed by  $K^+$  production, in Fig. 10 baryon densities are shown at the space-time coordinates where  $K^+$  mesons are created. The figure shows the densities in central collisions ( $b=0$  fm) for three typical mass systems, Au+Au, Ni+Ni and C+C at 1.0 AGeV. The density distribution  $dM_{K^+}/d\rho$  is defined as

$$dM_{K^+}/d\rho = \sum_i^{N_{K^+}} \frac{dP_i}{d\rho_B(\mathbf{x}_i, t_i)} \quad (50)$$

where  $\rho_B$  is the baryon density at which the kaon  $i$  was created and  $P_i$  is the corresponding production probability. For a better comparison of the different reaction systems the curves are normalized to the corresponding mass numbers. Fig. 10 illustrates the fact that nuclear compression is probed by  $K^+$  production. Most kaons are produced at supra-normal densities between one and three times  $\rho_0$ . The maximal densities are, on the other hand, correlated with the system size. A dependence on the nuclear EOS will therefore be most pronounced in large systems as discussed in detail in chapter 6. Closely connected to the densities is the average number of collisions  $N_C$  which particles encountered prior to the production of a  $K^+$  meson. The distributions shown in Fig. 11 are obtained in analogous way as the density distributions, i.e.  $dM/dN_C = \sum_i dP_i/dN_C^i$  with  $N_C^i = \frac{1}{2}(N_{C1}^i + N_{C2}^i)$  the average number of collisions which two hadrons ( $1, 2 = N, \Delta, \pi$ ) experienced before they produced kaon  $i$  with production probability  $P_i$ . As before the curves are normalized to the mass numbers of the different

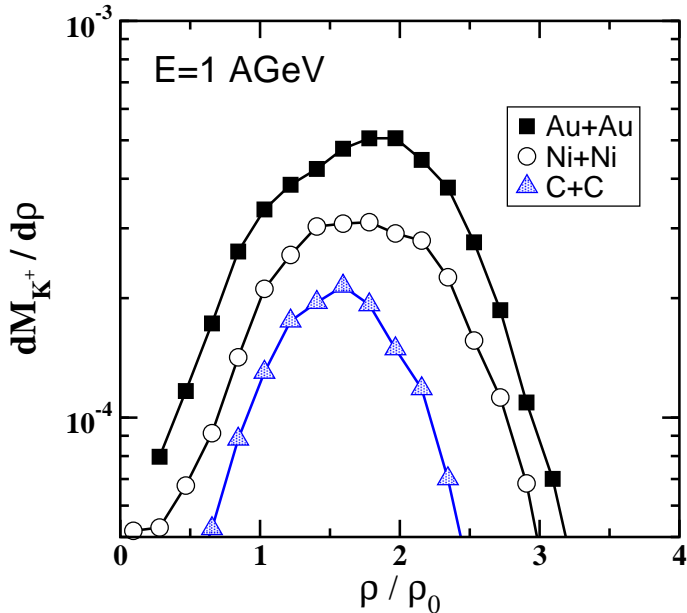


Figure 10: Nuclear density at the production of a  $K^+$  meson. Results from transport calculations for central C+C, Ni+Ni and Au+Au collisions at 1 AGeV, normalized to the mass numbers, are shown.

	C+C	Ni+Ni	Au+Au
$K^+$ (1.0 AGeV)	$58 \pm 6$	$75 \pm 6$	$85 \pm 6$
$K^-$ (1.8 AGeV)	$55 \pm 6$	$90 \pm 5$	–

Table 2: Experimental inverse slope parameters for  $K^+$  and  $K^-$  at comparable energies above threshold for different mass systems (from [134, 140, 141]).

reaction systems. This quantity is a suitable measure for the collectivity probed by  $K^+$  production. Fig. 11 (left panel) demonstrates that subthreshold kaon production is indeed a multi-step process. At 1 AGeV the average number of hadron-hadron collisions prior to the production of a kaon is larger than one and increases with the system size. This feature is also reflected in the  $A_{\text{part}}$  dependence of the experimentally extracted inverse slope parameters of the kaon spectra shown in Fig. 9. In more central reactions kaons seem to originate from an environment with apparently higher temperature which must, however, not be thermally equilibrated. The inverse slope parameters rise also with system size, Tab. 2, which is consistent with the collision history shown in Fig. 11. The inverse slope parameters can also simply be considered as a measure of the collectivity experienced by the kaons. The question if equilibrium has been reached or not is a subtle one and cannot be decided exclusively from experiment. With increasing energy the number of multi-step processes involved in the kaon production decreases which can be seen from the right panel of Fig. 11. There the number of collisions are shown at different energies 1 and 1.5 AGeV. For better comparison the curves are normalized to each other. In the light C+C system the decrease is more pronounced than in Au+Au and similar to p+A reactions most kaons are now produced in primary reactions.

### 3.3.2 Energy and mass dependence

The fact that subthreshold kaon production is a collective phenomenon is clearly reflected in the dependence of the kaon yield on the number of participating nucleons.  $A_{\text{part}}$  is defined as the number of nucleons contained in the overlapping region of the two colliding nuclei. For a given impact parameter

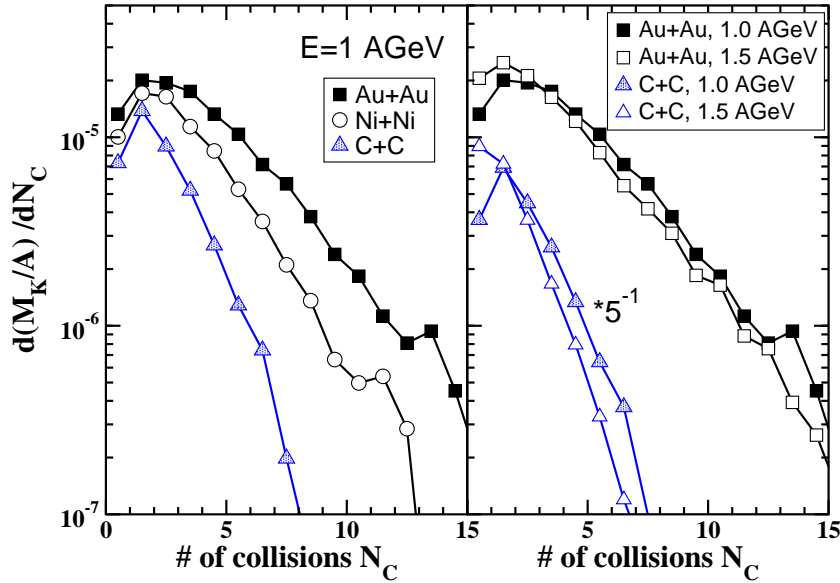


Figure 11: System size and energy dependence of the number of binary collisions which particles encountered prior to the production of a  $K^+$  meson. Left: results from transport calculations for central Au+Au, Ni+Ni and C+C reactions at 1 AGeV. Right: Same for Au+Au and C+C at 1 and 1.5 AGeV (arbitrary normalization of the curves).

the overlap in a geometrical model is that of two hard spheres with radius  $r_0 A^{\frac{1}{3}}$  ( $r_0 = 1.2$  fm). In symmetric A+A collisions the mean  $A_{\text{part}}$  is given by  $\langle A_{\text{part}} \rangle = A/2$ , in exclusive reactions  $A_{\text{part}}$  is directly related to the centrality.

However, before turning to heavy ions it is useful to consider proton-nucleus reactions. A survey on the experimental situation of the mass dependence of  $K^+$  production in p+A can be found in [143]. If the kaons were dominantly produced through primary reactions the scaling law of the  $\sigma^{p+A \rightarrow K^+ X}$  cross section should follow that of the inelastic proton-nucleus cross section. For proton energies  $T_p \leq 2$  GeV the inelastic cross section is given by  $\sigma_{\text{inel}} \sim A^{0.69 \pm 0.03}$  which is close to that of an opaque nucleus ( $\sigma \sim A^{\frac{2}{3}}$ ). At  $T_p = 1.5$  GeV, i.e. close to threshold, a scaling law  $\sigma_{K^+} \sim A^\alpha$  with  $\alpha = 0.73 \pm 0.04$  has been extracted at SATURNE [144] which supports the primary reaction mechanism. Deep below threshold the missing mass of the kaons has to be provided by the Fermi motion inside the nucleus or the high momentum tails of the nucleon spectral functions. Such collective effects are not supposed to depend strongly on the system size. On the other hand, deep subthreshold energies favor the secondary production mechanism since, e.g., the Fermi motion can be utilized several times in multi-step processes. This would lead to a proportionality  $\sigma_{K^+} \sim A$ . Indeed, at PNPI a coefficient  $\alpha = 1.04 \pm 0.01$  has been extracted at  $T_p = 0.8 \div 1.0$  GeV [145]. Such an exponent is in line with the predictions from transport models which indicate that subthreshold kaon production in p+A is governed by secondary reactions [85]. More recently ANKE extracted values of  $\alpha = 0.74 \pm 0.05$  at  $T_p = 1.0$  GeV [146, 143] in line with SATURNE. The scaling depends, however, strongly on the experimental acceptance and thus experimental situation is not fully conclusive.

In summary, p+A reactions reveal a scaling law of the kaon multiplicity  $N_{K^+} = \sigma_{K^+}/\sigma_{\text{inel}} \sim A^\alpha$  with  $1.05 \leq \alpha \leq 1.48$ . In a Glauber picture an A+A collision can be understood as the superposition of independent NN collisions or as A  $\times$  (N+A). Assuming the Glauber picture to hold, the kaon multiplicity

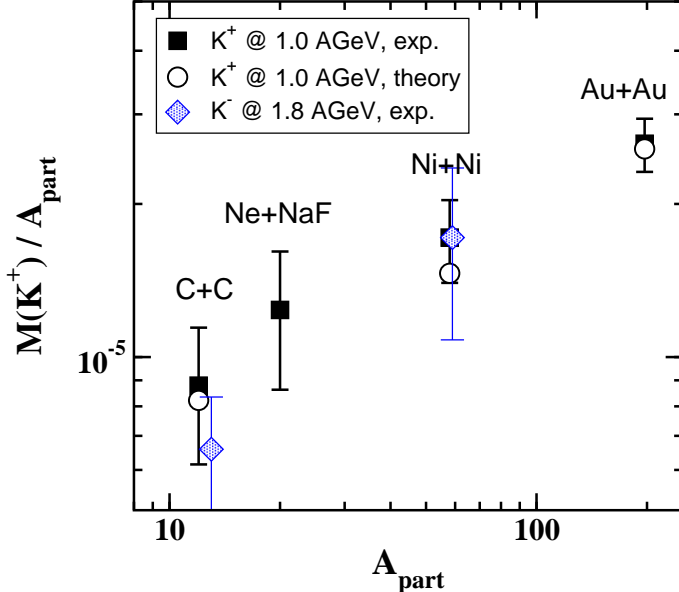


Figure 12:  $K^+$  multiplicities per  $A_{\text{part}}$  for different colliding mass systems at 1 AGeV. Data from KaoS [141, 142] are compared to theoretical QMD transport calculations. For C+C and Ni+Ni also  $K^-$  data [141, 140] at equivalent energy above threshold (1.8 AGeV) are shown.

$N_{K^+}$  should be linear proportional to  $A_{\text{part}}$ . This is evidently not the case. Fig. 12<sup>†</sup> shows KaoS data [134, 142] for different mass systems at 1 AGeV which can be fitted by  $N_{K^+} \propto A^\alpha$  with  $\alpha = 1.36$ . The observed non-linear increase as a function of system size is thus a clear indication for a collective production mechanism through multi-step scattering processes. The system size dependence of the measured multiplicities can be reproduced by theoretical transport calculations. In Fig. 12 we show results from QMD calculations which include a repulsive in-medium potential (see also chapters 4 and 5). The same non-linear scaling with  $A_{\text{part}}$  occurs as a function of centrality, i.e. the  $K^+$  yield in central reactions is strongly enhanced relative to peripheral reactions. The scaling of  $N_{K^+} \propto A_{\text{part}}^\alpha$  with  $\alpha = 1.8 \pm 0.15$  [2] is even more pronounced than the average  $A$  dependence of the kaon multiplicity of different A+A systems (Fig. 12). Since the bulk of kaons originates from semi-central collisions (e.g. in Au+Au from  $b \sim 5$  fm which corresponds to  $A_{\text{part}}/A_{\text{max}} \sim 0.7$  in Fig. 13) the pronounced centrality dependence is to some extent washed out in minimal bias reactions. As a function of centrality  $\alpha$  is significantly larger than the value of  $\alpha = 1.48$  which can maximally be deduced from p+A within a Glauber picture. This demonstrates that heavy ion collisions show qualitatively novel aspects compared to p+A. Fig. 13 compares the experimental  $A_{\text{part}}$  dependence in Ni+Ni and Au+Au reactions at 1 AGeV [141, 134] to QMD calculations. In both cases the data are well reproduced. The contributions of the different production mechanisms can be seen from Fig. 14. As expected, the primary  $NN \rightarrow NYK^+$  channels show a linear  $A_{\text{part}}$  dependence while the strong non-linear increase of the total yield is caused by secondary type reaction mechanisms. Here the processes  $N\Delta \rightarrow NYK^+$  and  $\pi N \rightarrow YK^+$  dominate while the higher order multi-step processes  $\Delta\Delta \rightarrow NYK^+$  and  $\pi\Delta \rightarrow YK^+$  are of minor importance.

For Ni+Ni the scaling parameter  $\alpha$  has also been measured as a function of the beam energy [141]. A slight decrease of  $\alpha = 1.9 \pm 0.25$  at 0.8 AGeV to  $\alpha = 1.65 \pm 0.05$  at 1.8 AGeV indicates the decreasing importance of collective effects with rising beam energy. The experimental facts are consistent with the theoretical findings discussed above, namely that the average number of collisions

<sup>†</sup>Although in minimal bias reactions the mean  $A_{\text{part}}$  is given by  $A/2$ , we scale the yields by  $\langle A_{\text{part}} \rangle = A/2$  which accounts for the fact that kaons are dominantly produced in central and semi-central reactions.

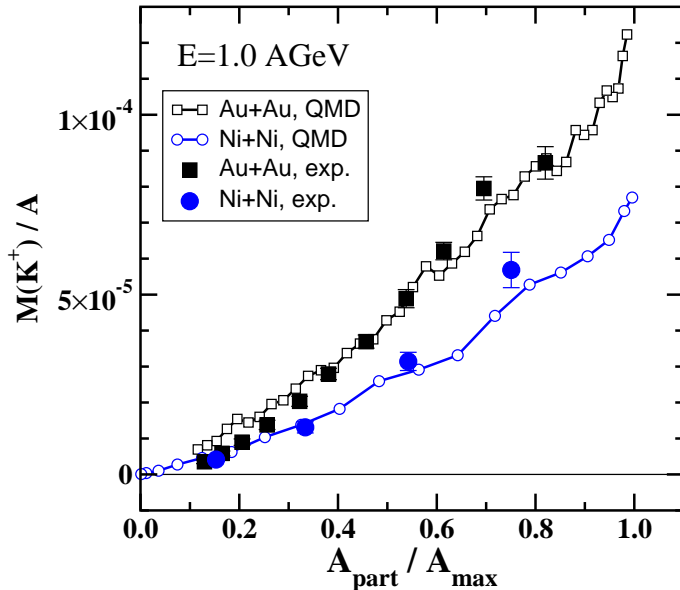


Figure 13:  $K^+$  multiplicities as a function of  $A_{\text{part}}$  in Au+Au and Ni+Ni reactions at 1 AGeV. Data from KaoS [134, 141] are compared to QMD transport calculations.

which the nucleons encountered prior to the production of a  $K^+$  meson increases a) with system size and b) going deeper below threshold. The particles have to accumulate the necessary energy by multiple scattering which is easier to achieve in central reactions and/or larger systems where higher densities are reached. The conditions are optimal in the early phase of the reaction where baryon as well as energy density are maximal. Corresponding data for antikaons are rare. However, existing  $K^-$  data indicate that the behavior of antikaons follows closely that of the kaons. In Ni+Ni at 1.8 AGeV a scaling law of  $N_{K^-} \propto A_{\text{part}}^\alpha$  with  $\alpha = 1.8 \pm 0.3$  has been observed [140, 141]. At a first glance this may be astonishing since one could expect that the strong  $K^-$  absorption leads to a weaker  $A_{\text{part}}$  dependence than for  $K^+$ . On the other hand, strangeness exchange is the dominant source for  $K^-$  production at subthreshold energies and primary hyperons are produced in association with the  $K^+$ 's. Since these primary hyperons have the same  $A_{\text{part}}$  as the  $K^+$ 's the  $K^-$ 's are forced to follow them.

### 3.3.3 Chemical freeze-out

The question of strangeness equilibration has a long history. Already in the classic paper by Koch, Müller and Rafelski [147] it was argued that at CERN energies strangeness saturation requires equilibration times  $\tau_{eq} \sim 80$  fm/c much longer than the reaction time and that the fact that particle spectra can nonetheless be described by a common Boltzmann factor  $T \sim 170$  MeV hints towards a sudden hadronization where the system crosses the phase boundary from the quark-gluon plasma to the hadronic phase. At SIS energies there is of course no such phase transition but the question remains whether the observed particle abundances have purely dynamical origin or can be understood by means of statistical concepts.

Transport calculations indicate that kaons as well as antikaons are dominantly produced in the early and dense non-equilibrium phase. Since kaons interact with the surrounding medium almost exclusively by elastic reactions  $KN \rightarrow NK$  (here we consider charge exchange as elastic) they have a long mean free path  $\sim 7$  fm and chemical freeze-out occurs early. This picture is supported by the fact that subthreshold kaons show similar features like high energy pions, see Fig. 9. High energy pions were experimentally proven to originate from the early phase [135, 138, 139]. The influence of strangeness

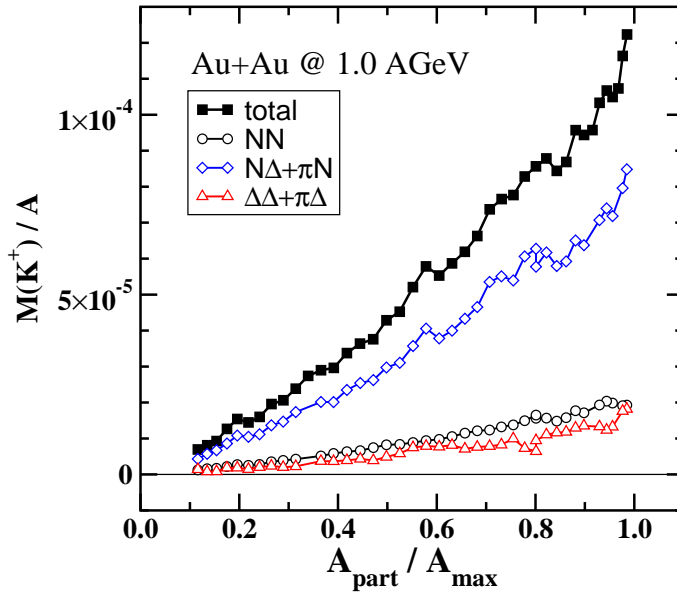


Figure 14:  $K^+$  multiplicities as a function of  $A_{\text{part}}$  in Au+Au at 1 AGeV for the different production channels  $NN$  (primary),  $N\Delta + \pi N$  (secondary) and  $\Delta\Delta + \pi\Delta$  (secondary).

absorption which might drive kaons to equilibrium has been studied in [111]. This process has extremely low probability since at subthreshold energies no more than one  $YK^+$  pair per nucleus-nucleus collision is created. This means that the same pair of particles has to meet again in the course of the reaction for the kaon to get annihilated. As long as kaon production is active the annihilation (loss) rate  $dN_L/dt$  is about one to two orders of magnitude smaller [111] and can be safely neglected in corresponding transport calculations. Hence the kaon yield freezes out early *and* at supra-normal nuclear density [111]. The conditions are not much different from those where the kaons are produced, see Fig. 10. The same conclusion can be drawn from the investigations of Bratkovskaya et al. [112] where chemical equilibration times in “infinite” hadron matter, i.e. a box with periodic boundary conditions, were studied using a BUU cascade model. The resulting equilibration times for pions and kaons as functions of the baryon density and the energy density  $\epsilon$  are shown in Fig. 15. In contrast to pions, kaons need at least  $\tau_{eq} \gtrsim 40$  fm/c to reach chemical equilibrium. Equilibration takes even longer at lower baryon and/or energy density. At SIS conditions, corresponding to the lower limit of  $\epsilon$  in Fig. 10,  $\tau_{eq}$  is above 100 fm/c which is at SIS energies about twice the duration of an heavy ion reaction like Au+Au.

For antikaons the situation is more complex. Though primary antikaon production takes also place in the initial and dense phase, strangeness can be redistributed between hyperons and antikaons. Strangeness exchange leads to annihilation rates which exceed the production rates in the expansion phase of a heavy ion collision [111, 120]. When the fireball becomes dilute the endothermic production  $K^-$  process dies out while the exothermic inverse reaction can still continue. Due to such a cross over there exists a situation where the equilibrium condition, namely production rate = annihilation rate, is formally fulfilled. However, this is not a stationary state since the system is expanding. The situation is illustrated by Fig. 16 where kaon and antikaon production (gain) rates  $dN_G/dt$  and annihilation (loss) rates  $dN_L/dt$  in a central ( $b=0$  fm) Ni+Ni reaction at 1.0 AGeV are shown. The results were obtained by Pal et al. [111]. Though closer, also  $K^-$ ’s seem not to reach chemical equilibrium in a thermodynamical sense. In thermal equilibrium the yields do exclusively depend on the chemical potentials and the temperature. As has been demonstrated by Hartnack et al. [120] this is not the case even when the equilibrium condition  $dN_G/dt = dN_L/dt$  is fulfilled: In the expanding system an artificial scaling of the strangeness exchange cross section  $\pi Y \leftrightarrow NK^-$  is directly reflected in the total yield.

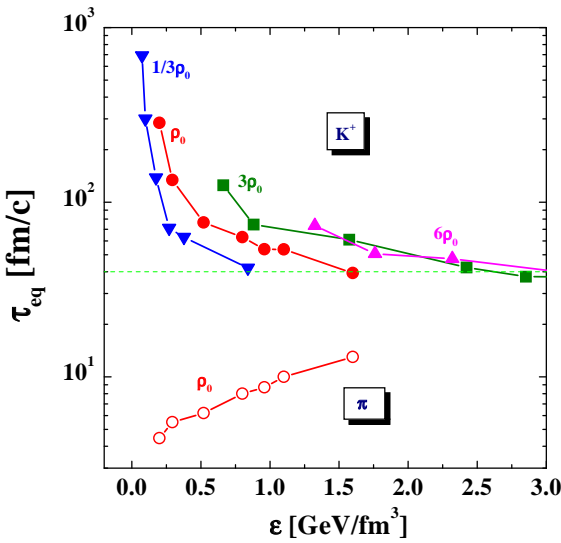


Figure 15: Chemical equilibration time  $\tau_{eq}$  for pions and kaons in infinite hadronic matter as a function of baryon density and energy density  $\epsilon$ . Results from a BUU cascade are shown. The figure is taken from [112].

In view of these facts it is astonishing that many features can also be understood by means of purely statistical concepts. The statistical model of an ideal hadron gas assumes that particles are emitted from a thermalized, eventually radially expanding fireball. It turned out to describe hadron yields and ratios successfully from AGS to RHIC energies (for a recent review see [148]).

In the framework of a grand canonical ensemble the particle number density  $n_i$  of species  $i$  is given by a Boltzmann distribution <sup>†</sup>

$$n_i = \frac{N_i}{V} = g_i \int_0^\infty \frac{d^3 k}{(2\pi)^3} e^{-(E_i - \mu_B B_i - \mu_S S_i)/T} . \quad (51)$$

$E_i = \sqrt{\mathbf{k}^2 + m_i^2}$  is the single particle energy of hadron species  $i$ ,  $T$  is the temperature,  $\mu_B$  and  $\mu_S$  are the baryon chemical potential and strangeness chemical potential.  $B_i$  and  $S_i$  are the baryon charge and strange charge and  $g_i$  the degeneracy factor of hadron  $i$ .  $V$  is the volume of the system. The characteristics of the fireball can be described by means of four independent parameters, such as volume  $V$ , total energy  $E$ , net baryon density  $\rho_B$  and net strangeness density  $\rho_S$ . These determine the fireball temperature  $T$ , the strangeness and baryon chemical potentials  $\mu_S$  and  $\mu_B$ . Since the total strangeness is zero the number of free parameters reduces to three, namely,  $V$ ,  $E$  and  $\rho_B = N_B/V$ . If one is only interested in particle ratios instead of total yields the volume dependence drops out and the number of parameters is reduced to two. They are usually chosen as the temperature and the baryon chemical potential and are determined by fitting experimental hadron yields.

Such a grand canonical description fails at SIS energies. However, as shown by Cleymans et al. [149] the statistical model works also at SIS if one accounts for exact strangeness conservation which leads to the following modification of Eq. (51) for kaons and antikaons

$$n_{K^+} = g_{K^+} \int_0^\infty \frac{d^3 k}{(2\pi)^3} e^{-E_{K^+}/T} \left[ g_{K^-} V \int_0^\infty \frac{d^3 k}{(2\pi)^3} e^{-E_{K^-}/T} + g_\Lambda V \int_0^\infty \frac{d^3 k}{(2\pi)^3} e^{-(E_\Lambda - \mu_B)/T} \right] \quad (52)$$

$$n_{K^-} = g_{K^-} \int_0^\infty \frac{d^3 k}{(2\pi)^3} e^{-E_{K^-}/T} \left[ g_{K^+} V \int_0^\infty \frac{d^3 k}{(2\pi)^3} e^{-E_{K^+}/T} \right] . \quad (53)$$

<sup>†</sup>In most actual calculations the more accurate Fermi and Bose distributions are used. The usage of Boltzmann distributions makes the present discussion, however, more transparent.

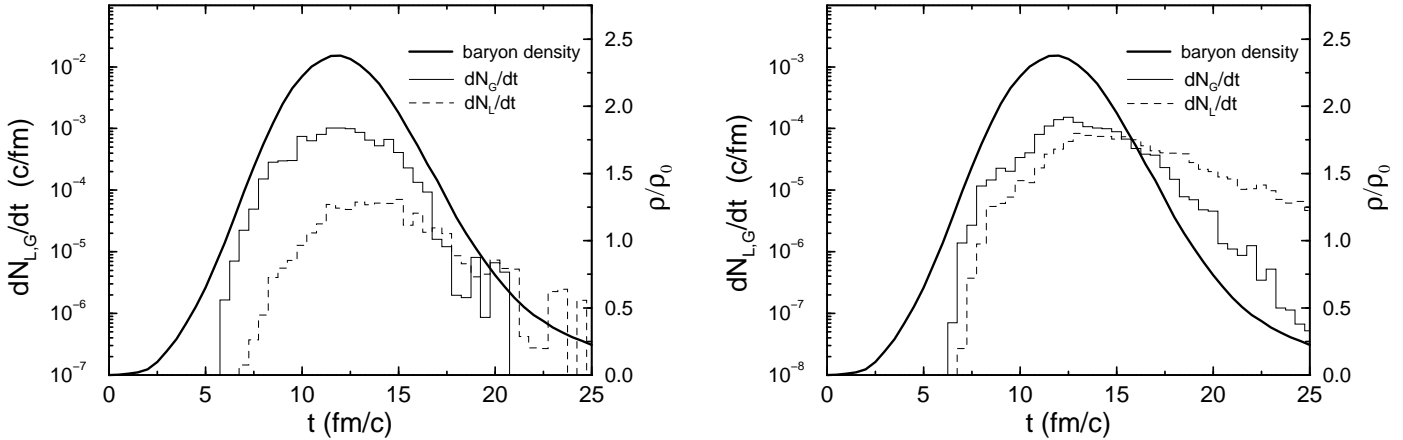


Figure 16: Kaon (left) and antikaon (right) production  $dN_G/dt$  and annihilation  $dN_L/dt$  rates in a central Ni+Ni reaction at 1.0 AGeV. The solid line shows the time evolution of the central density. The figure is taken from [111].

With this modification the statistical model delivers an accurate description of particle yields and ratios also at SIS energies (except of the  $\eta$  yield which is systematically underestimated) [149, 150]. The assumption of common freeze-out parameters for all hadron species stands, however, in clear contradiction to the dynamical transport calculations. In particular a freeze-out density of about  $\rho_0/4$  [149, 150] as obtained by the statistical model fit to the hadron multiplicities is much lower than the corresponding  $K^+$  freeze-out density obtained from the dynamical models.

The statistical model reproduces nonetheless several basic experimental features of the strangeness production at SIS. The canonical treatment leads to a quadratic  $A_{\text{part}}$  dependence of the kaon multiplicities  $N_{K^+} \sim V^2 \sim A_{\text{part}}^2$  which is close to the observed  $A_{\text{part}}$  dependence [2, 141]. Since pions are treated grand-canonical they scale linearly with  $V$  and  $A_{\text{part}}$ . Hence, the observed centrality dependence of the  $K^+/\pi^+$  ratio [2] is obtained for free. The same holds for the  $A_{\text{part}}$  dependence of the  $K^-/K^+$  ratio which is predicted to be flat in agreement with the Ni+Ni data. A fine tuning can be achieved by a variation of the temperature as a function of centrality [151]. This enforces, however, in a slight decrease of  $T$  for central reactions which contradicts the intuition of a larger energy deposit and a hotter fireball. In the larger Au+Au system the  $K^-/K^+$  ratio has even been found to slightly decrease with centrality [152] which is at variance with a statistical interpretation but easy to understand from a microscopic point of view due to the large  $K^-$  absorption cross section.

However, here appears another contradiction to the dynamical approaches: In contrast to the statistical model based on bare hadron masses, the transport models need to introduce in-medium kaon masses in order to reproduce the experimental  $K^-/K^+$  ratio [154, 155]. This apparent contradiction between dynamical and statistical approaches has been addressed by Brown et al. [156]. From eqs. (52) and (53) the  $K^+/K^-$  ratio is approximately given by

$$\frac{N_{K^+}}{N_{K^-}} \sim \left( \frac{m_\Lambda}{m_K} \right)^{\frac{2}{3}} \frac{e^{-(E_\Lambda - \mu_B)/T}}{e^{-E_{K^-}/T}}. \quad (54)$$

The experimental value <sup>§</sup> of  $N_{K^+}/N_{K^-} = 30$  in Ni+Ni at 1.8 AGeV [157] enforces a chemical potential which is significantly smaller than the  $\Lambda$  mass in order to punish hyperon production relative to that of  $K^-$ 's. A dropping  $K^-$  mass  $m_{K^-}^* = m_K - \alpha \rho_B$  compensates the  $\mu_B$  dependence in (54) to large

<sup>§</sup>In Refs. [150, 151] the earlier and smaller ratio  $N_{K^+}/N_{K^-} = 21 \pm 9$  from [141] has been used.

extent [156] and enables one to reproduce the experimental ratio with much larger freeze-out densities  $\rho \sim 1 \div 2\rho_0$ , depending on the strength of the mass reduction. Such values for the freeze-out density are now in agreement with the estimates from transport models.

However, the problem is not completely resolved since a more recent analysis [158] comes to the conclusion that the usage of in-medium masses obtained from coupled channel G-matrix calculations requires extremely low values for  $\rho$  and  $T$ , i.e.  $T \leq 34$  MeV and  $\rho \leq 0.02\rho_0$ . Such freeze-out parameters seem, however, to be far from reality. When the same in-medium potentials are, on the other hand, applied within dynamical transport calculations [121] the  $K^-/K^+$  ratio is fairly well reproduced. From this analysis one has to conclude that the statistical approach is at SIS energies not applicable to this observable, at least if one accounts also for in-medium effects.

### 3.3.4 Thermal freeze-out

In contrast to the chemical kaon freeze-out which takes place early, the kaon momentum distributions are strongly influenced by final state interactions. Both, elastic  $KN$  scattering as well as the propagation in a repulsive mean field from Coulomb and strong interactions makes the spectra harder [122, 124] and influences the collective in-plane [39, 46, 94, 159, 160] and out-of-plane flow [123, 161]. In the case of the  $K^-$ 's thermal and chemical freeze-out are not clearly separated since elastic and strangeness exchange cross sections are of the same order of magnitude. Propagation in an attractive mean field tends here to make the spectra softer.

The influence of the mean field on the shape of the spectra has e.g. been studied in Refs. [116, 121, 124]. Both, a repulsive  $K^+$  potential as well as an attractive  $K^-$  potential lead to deviations from a thermal spectrum which can be characterized by a radial flow component. In [124] the transverse mass ( $m_T = \sqrt{p_T^2 + m_K^2}$ ) spectra from QMD transport calculations were fitted by a radially expanding thermal source

$$\frac{d^3N}{d\phi dy dm_T} \sim e^{-(\frac{\gamma E}{T} - \alpha)} \left\{ \gamma^2 E - \gamma \alpha T \left( \frac{E^2}{p^2} + 1 \right) + (\alpha T)^2 \frac{E^2}{p^2} \right\} \frac{\sqrt{(\gamma E + \alpha T)^2 - m^2}}{p} \quad (55)$$

with a common radial kaon velocity  $\beta = v/c$ . In (55)  $E = m_T \cosh y$ ,  $p = \sqrt{p_T^2 + m_T^2 \sinh^2 y}$ ,  $\alpha = \gamma \beta p/T$  and  $\gamma$  is the Lorentz factor. The repulsive potential leads to a depletion of the low mass  $m_T$  spectrum and creates a characteristic 'shoulder-arm' shape which gives rise to a radial flow component. E.g. in typical Au+Au reactions at 1 AGeV the collective motion of the kaons due to the mean field has been found to be about 20% of the thermal motion ( $\beta_{\text{coll.}} \simeq 0.1$ ) [124].  $K^-$  mesons exhibit an analogous collective motion in the radial direction. However, the attractive potential leads here to a characteristic 'concave' structure in the transverse mass spectrum [124, 121] which was attributed to a 'virtual' radial flow in [124]. Thus a collective motion could in principle be distinguished from the thermal motion which would, however, require to measure low mass spectra with high precision.

Experimental evidence for different kinetic freeze-out of kaons and antikaons has been reported in [152] where in the same reaction (Au+Au at 1.5 AGeV)  $K^-$  spectra were found to be systematically softer than those of the  $K^+$ 's (see Fig. 17). Also the angular distributions are qualitatively different, i.e. strongly forward-backward peaked for  $K^+$  and much more isotropic for  $K^-$  [152]. Both facts indicate that kaons decouple early from the reactions dynamics while antikaons suffer strong final state interactions.

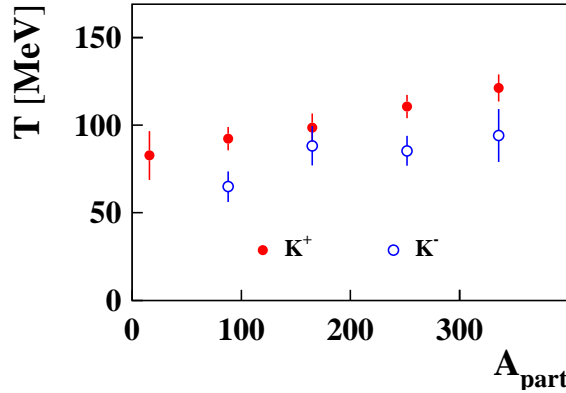


Figure 17: Inverse slope parameters  $T$  of  $K^\pm$  spectra in Au+Au reactions at 1.5 AGeV measured by KaoS [152]. The Figure is taken from [153].

## 4 Strangeness production in transport models

### 4.1 Mean field dynamics for strange particles

Semi-classical transport equations of a Boltzmann type can be derived from first principle quantum field theory. The starting point is the non-equilibrium real time Green's functions formalism [162] which leads after truncation of the Green's functions hierarchy at the two-body level, to the famous Kadanoff-Baym equations [163] for the one-body Green function. After a gradient expansion of Wigner transforms one arrives finally at the semi-classical kinetic equation. The kinetic equation is composed by a drift term, the Vlasov part, which propagates the one-body density and a collision term which accounts for two-body scattering. Derivations of the complete kinetic equation in full beauty and complexity are involved and can be found in the literature [20, 28, 163, 164, 165, 166] for both, fermions and bosons. To set the context the relevant steps are briefly reviewed:

Starting from the real time Schwinger–Keldysh formalism one obtains a matrix  $\underline{G}$  of Green functions, (anti-) chronologically ordered Green functions and correlation functions  $G^{>,<}$ . The correlation functions are defined as  $G^>(1, 1') = -i < \Psi(1) \bar{\Psi}(1') >$  and  $G^<(1, 1') = i < \bar{\Psi}(1) \Psi(1') >$  using the notation  $1 = (t_1, \mathbf{x}_1)$ . The quantity of interest is  $G^<$  because in the limit  $t_1 = t'_1$  it corresponds to a density. The Dyson equation in non-equilibrium is given as a matrix equation

$$D(1, 1') \underline{G}(1, 1') = \underline{\delta}(1 - 1') + \int d2 \underline{\Sigma}(1, 2) \underline{G}(2, 1') \quad , \quad (56)$$

with  $D(1, 1') \equiv \underline{\delta}(1 - 1')(i\gamma_\mu \partial_1^\mu - m)$  for spin-1/2 fermions and  $D(1, 1') \equiv -\underline{\delta}(1 - 1')(\partial_{1\mu} \partial_1^\mu + m)$  for bosons. The matrix of self-energies  $\underline{\Sigma}$ <sup>¶</sup> in Eq. (56) contains all higher order correlations originating from the higher order Green functions of the Schwinger–Keldysh hierarchy. When the hierarchy is truncated at the two-body level this leads to the T-matrix approximation summing all two-body ladder correlations. The kinetic equation for the correlation function  $G^<$  is obtained by subtracting from the Dyson equation (56) its adjoint. A Wigner transformation then allows to represent the kinetic equation in phase space, i.e.  $x - k$ -space, rather than in coordinate space. An essential step is the truncation of the gradient expansion of the Wigner transform of products retaining only terms of first order in  $\hbar$ , which neglect memory terms. The self-energy, Eq. (56), is decomposed into scalar and vector parts

$$\Sigma^+ = \Sigma_s^+ - \gamma^\mu \Sigma_\mu^+ \quad (57)$$

<sup>¶</sup>In this subsection fermions or bosons are not distinguished in the notation for their self-energy. Otherwise a bosonic self-energy is denoted by  $\Pi$ .

and the real part of  $\Sigma$  is used to define effective masses and kinetic momenta

$$m^* = M + \text{Re}\Sigma_s^+(x, k) \quad , \quad k_\mu^* = k_\mu + \text{Re}\Sigma_\mu^+(x, k) \quad (58)$$

of the dressed particles in the nuclear medium.  $\Sigma^+$  is the retarded self-energy constructed by the difference of the corresponding correlation functions  $G^\pm(1, 1') = \theta(\pm(t_1 - t_{1'})) [G^>(1, 1') - G^<(1, 1')]$  [167]. The Dirac structure of the correlation functions  $G^>,<$  can be separated off by a decomposition into a scalar spectral function  $a$ , a scalar distribution function  $f$  and the projector onto positive energy states  $\Lambda^+$

$$G^<(x, k) \propto i\Lambda^+ a(x, k) f(x, k) \quad (59)$$

$$G^>(x, k) \propto -i\Lambda^+ a(x, k) [1 \mp f(x, k)] \quad . \quad (60)$$

The  $\mp$  sign in Eq. (60) stands for fermions or bosons, respectively. In the case of nucleons the projector is given by  $\Lambda^+ = (k^* + m^*)/2m^*$ . In an essential approximation which concerns the the spectral properties of the hadrons is the quasiparticle approximation. It is valid in the limit of a small imaginary part of the self energy ( $\text{Im}\Sigma^+ \ll \text{Re}\Sigma^+$ ). The spectral function then reduces to the mass shell constraint  $a(x, k) = 2\pi\delta(k^{*2} - m^{*2}) 2\Theta(k_0^*)$  which sets the energy on the mass shell  $k_0^* = E^*(x, \mathbf{k}) = \sqrt{\mathbf{k}^{*2} + m^{*2}}$ . Thus, the number of variables of the distribution function  $f(x, k)$  is reduced from eight to seven

$$a(x, k) f(x, k) = 2\pi\delta(k^{*2} - m^{*2}) 2\Theta(k_0^*) f(x, \mathbf{k}) \quad (61)$$

which simplifies considerably practical implementations. As can be seen from Fig. 5 the quasiparticle approximation is well justified for kaons but less applicable to antikaons.

In many cases the kinetic equation is further treated in the Hartree approximation which implies to neglect the explicit momentum dependence of the mean field, i.e.  $\text{Re}\Sigma^+ = \text{Re}\Sigma_H^+(x)$ . Then the resulting kinetic equation can completely be formulated in terms of kinetic momenta instead of canonical momenta [167]

$$\begin{aligned} & [k^{*\mu} \partial_\mu^x + (k_\nu^* F^{\mu\nu} + m^* \partial_x^\mu m^*) \partial_\mu^{k^*}] (af)(x, k^*) \\ &= \frac{1}{2} \int \frac{d^4 k_2}{(2\pi)^4} \frac{d^4 k_3}{(2\pi)^4} \frac{d^4 k_4}{(2\pi)^4} a(x, k) a(x, k_2) a(x, k_3) a(x, k_4) W(kk_2|k_3 k_4) \\ & \times (2\pi)^4 \delta^4(k + k_2 - k_3 - k_4) [f(x, k_3) f(x, k_4) (1 \mp f(x, k)) (1 \mp f(x, k_2)) \\ & - f(x, k) f(x, k_2) (1 \mp f(x, k_3)) (1 \mp f(x, k_4))] \quad . \quad (62) \end{aligned}$$

Eq. (62) resembles the well known transport equation of a Boltzmann–Uehling–Uhlenbeck type. The left hand side is a drift term driven by the mean field via the kinetic momenta  $k^*$ , the field strength tensor  $F^{\mu\nu}(x) = \partial_x^\nu \text{Re}\Sigma_H^{+\mu}(x) - \partial_x^\mu \text{Re}\Sigma_H^{+\nu}(x)$ , and the effective mass  $m^*$ . The right hand side is a collision integral which contains the transition rate  $W$  or equally the in–medium cross section given by  $(k^* + k_2^*)^2 d\sigma/d\Omega(k, k_2) = W(kk_2|k_3 k_4)$ . The collision term contains Pauli-blocking, respectively Bose enhancement factors  $(1 \mp f)$  for the final states.

As soon as one has to deal with different particle species which are interacting, e.g. via production and absorption processes, the transport problem becomes a coupled channel problem. This means that one has to solve a separate transport equation for each degree of freedom, but these are coupled to each other by their collisions intergrals and the mean fields.

#### 4.1.1 Transport equation for kaons

A full transport equation for kaons can in principle be derived as outlined above. However, since we are only interested in the structure of the relativistic equations of motion, we restrict the discussion in the

following to the mean field level and the left hand side of the transport equation (62), i.e. the Vlasov equation.

The Vlasov equation can easily be derived from the Klein-Gordon equation for the kaon field. For simplicity we restrict the discussion to  $K^+$  mesons since the derivation for  $K^-$ 's is fully analogous. Starting from the Klein-Gordon equation (23) the field equations for the kaon field and its adjoint read

$$[(\partial_\mu + iV_\mu)^2 + m_K^{*2}] \phi_K(x_1) = 0 \quad (63)$$

$$[(\partial_\mu - iV_\mu)^2 + m_K^{*2}] \phi_K^*(x_2) = 0 \quad . \quad (64)$$

In mean field approximation to the chiral  $SU(3)$  Lagrangian as discussed in Chap. 2 a vector potential with alternating sign for kaons and antikaons, i.e.  $V_\mu = \pm \frac{3}{8f_\pi^2} j_\mu$  for  $K^\pm$  and an attractive scalar part occur. The latter can be absorbed into the effective mass  $m_K^* = \sqrt{m_K^2 - \frac{\Sigma_{KN}}{f_\pi^2} \rho_s + V_\mu V^\mu}$  which is equal for kaons and antikaons. Here one has already made use of the quasiparticle approximation since Eqs. (63,64) contain only the real part of the kaon self-energy  $\Pi_K$  (41). Multiplying equations (63) and (64) by the respective adjoint field and subtracting them, yields

$$\begin{aligned} & [\partial_\mu^{x_1} \partial_{x_1}^\mu - \partial_\mu^{x_2} \partial_{x_2}^\mu + 2i (V_\mu(x_1) \partial_{x_1}^\mu + V_\mu(x_2) \partial_{x_2}^\mu) - V_\mu(x_1) V^\mu(x_1) \\ & + V_\mu(x_2) V^\mu(x_2) + m_K^{*2}(x_1) - m_K^{*2}(x_2)] \phi(x_1) \phi^*(x_2) = 0 \quad . \end{aligned} \quad (65)$$

Introducing center-of-mass and relative coordinates

$$x = \frac{1}{2} (x_1 + x_2) \quad , \quad r = x_1 - x_2$$

one has

$$\partial_\mu^{x_1} \partial_{x_1}^\mu - \partial_\mu^{x_2} \partial_{x_2}^\mu = 2\partial_\mu^x \partial_r^\mu \quad .$$

The fields are now expanded to first order in gradients

$$\begin{aligned} V_\mu(x_1) \partial_{x_1}^\mu + V_\mu(x_2) \partial_{x_2}^\mu &= \cosh\left(\frac{r}{2} \cdot \partial_x\right) V_\mu(x) \partial_x^\mu + 2 \sinh\left(\frac{r}{2} \cdot \partial_x\right) V_\mu(x) \partial_r^\mu \\ &\approx V_\mu(x) \partial_x^\mu + (r \cdot \partial_x V_\mu(x)) \partial_r^\mu \end{aligned} \quad (66)$$

where  $r \cdot \partial_x$  denotes a four-vector product. Similar one obtains

$$\begin{aligned} m_K^{*2}(x_1) - m_K^{*2}(x_2) &\approx 2m_K^*(x) (r \cdot \partial_x m_K^*(x)) \\ V_\mu(x_1) V^\mu(x_1) - V_\mu(x_2) V^\mu(x_2) &\approx 2V_\mu(x) (r \cdot \partial_R V^\mu(x)) \quad . \end{aligned} \quad (67)$$

Inserting Eqs. (66), (67) into (64) gives

$$\begin{aligned} & \left[ \partial_\mu^x \partial_r^\mu + i \left( V_\mu(x) \partial_x^\mu + (r \cdot \partial_x V_\mu(x)) \partial_r^\mu \right) + m_K^*(x) (r \cdot \partial_x m_K^*(x)) \right. \\ & \left. - V_\mu(x) (r \cdot \partial_x V^\mu(x)) \right] \phi\left(x + \frac{r}{2}\right) \phi^*\left(x - \frac{r}{2}\right) = 0 \quad . \end{aligned} \quad (68)$$

Integration of Eq. (68) over  $\int d^4r e^{ik \cdot r}$  yields the Vlasov equation

$$[k^* \partial_\mu^x + (k_\nu \partial_x^\mu V^\nu - V_\nu \partial_x^\mu V^\nu + m_K^* \partial_x^\mu m_K^*) \partial_\mu^k] (af)(x, k) = 0 \quad (69)$$

for the scalar phase-space distribution  $f(x, k)$ . The phase-space distribution is defined as the Wigner transform of the density matrix  $\phi \phi^*$

$$f(x, k) = \int d^4r e^{ik \cdot r} \phi\left(x + \frac{r}{2}\right) \phi^*\left(x - \frac{r}{2}\right) \quad . \quad (70)$$

Introducing the field strength tensor  $F^{\mu\nu} = \partial^\mu V^\nu - \partial^\nu V^\mu$  and kinetic momenta  $k_\mu^* = k_\mu \mp V_\mu$ , Eq. (69) can now be written as

$$[k^{*\mu} \partial_\mu^x + (k_\nu^* F^{\mu\nu} + m_K^* \partial_x^\mu m_K^*) \partial_\mu^{k^*}] f(x, k^*) = 0 \quad . \quad (71)$$

The corresponding equation for  $K^-$  mesons is obtained by replacing in Eq. (71) the field strength tensor  $F^{\mu\nu}$  with  $F^{\nu\mu} = -F^{\mu\nu}$ .

Equation (71) has exactly the same structure as the relativistic Vlasov equation for nucleons which is obtained from the projection onto the scalar component of the Wigner density matrix for spin- $\frac{1}{2}$  fermions in the spinor representation. Thus, in the semi-classical limit the information of the fermionic/bosonic character of the particles is lost at the mean field level. In the collision integral differences are retained, e.g. fermionic Pauli-blocking factors are replaced by Bose-enhancement factors.

#### 4.1.2 Equations of motion

From the Vlasov eq. (71) classical equations of motion are obtained in the quasi-particle limit which implies to put the phase space distribution on mass shell

$$f(x, k^*) \equiv f(\mathbf{q}, t; \mathbf{k}^*) \delta(k_0^* - E^*(\mathbf{q}, \mathbf{k})) \quad , \quad (72)$$

with

$$E^* = \sqrt{\mathbf{k}^{*2} + m_K^{*2}} \quad . \quad (73)$$

Inserting (72) into (71) yields the covariant equations of motion

$$\frac{dq^\mu}{d\tau} = \frac{k^{*\mu}}{m_K^*} = u^\mu \quad (74)$$

$$\frac{dk^{*\mu}}{d\tau} = \frac{k_\nu^*}{m_K^*} F^{\mu\nu} + \partial^\mu m_K^* \quad . \quad (75)$$

Again the classical equations of motion are identical to those for nucleons, obtained e.g., in relativistic mean field theory [20]. Only the different structure of the effective mass reflects the bosonic character of the kaons.

Alternatively the equations of motion can also be obtained from the dispersion relation  $E = k_0 = E^* \pm V_0$  through the Hamilton equations

$$\frac{d\mathbf{q}}{dt} = \frac{\partial E}{\partial \mathbf{k}} \quad , \quad \frac{d\mathbf{k}}{dt} = -\frac{\partial E}{\partial \mathbf{q}} \quad . \quad (76)$$

Thus one obtains

$$\frac{d\mathbf{q}}{dt} = \frac{\mathbf{k}^*}{E^*} \quad (77)$$

$$\frac{d\mathbf{k}}{dt} = -\frac{m_K^*}{E^*} \frac{\partial m_K^*}{\partial \mathbf{q}} \mp \frac{\partial V^0}{\partial \mathbf{q}} \pm \frac{\mathbf{k}_i^*}{E^*} \frac{\partial \mathbf{V}_i}{\partial \mathbf{q}} \quad . \quad (78)$$

Eq. (78) provide the non-covariant version of (75). The term proportional to the space-like component of the vector potential gives rise to a momentum dependence in Eq. (78) which can be attributed to a Lorentz force term. This structure becomes more evident when Eq. (78) is rewritten in terms of kinetic momenta

$$\frac{d\mathbf{k}^*}{dt} = -\frac{E^*}{m_K^*} \frac{\partial m_K^*}{\partial \mathbf{q}} \mp \frac{\partial V^0}{\partial \mathbf{q}} \pm \frac{\mathbf{k}^*}{E^*} \times \left( \frac{\partial}{\partial \mathbf{q}} \times \mathbf{V} \right) = -\frac{\partial U_K}{\partial \mathbf{q}} \pm \mathbf{v}_i \frac{\partial \mathbf{V}_i}{\partial \mathbf{q}} \quad . \quad (79)$$

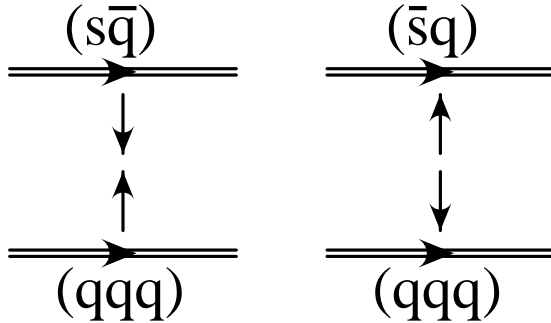


Figure 18: Action of the Lorentz force between nucleons ( $qqq$ ) and kaons. The force acts opposite for  $K^-(s\bar{q})$  and  $K^+(\bar{s}q)$ .

with  $\mathbf{v} = \mathbf{k}^*/E^*$  the kaon velocity. The appearance of the velocity dependent ( $\mathbf{v} = \mathbf{k}^*/E^*$ ) Lorentz force in Eqs. (75)-(79) is a genuine feature of the relativistic kaon dynamics as soon as a vector field is involved. In addition to the trivial  $|\mathbf{k}|$  momentum dependence of the optical potential the  $\mathbf{k}$  dependent part of the interaction appears in reference frames where the spatial components  $\mathbf{V}$  and  $\mathbf{k}$  do not vanish. Hence, in nuclear matter at rest or  $p+A$  reactions no Lorentz force is present. The importance of this interaction for the nucleon dynamics in heavy ion collisions is well known since a long time, see e.g. [168]. For the kaon dynamics it was first discussed by Fuchs et al. [46]. The physical picture behind is completely analogous to electrodynamics: assuming that the interaction between kaons and nucleons is determined by the non-strange quark content of the hadrons, two parallel currents are attracted, two anti-parallel currents are repelled. Hence the Lorentz force acts opposite for  $K^-(s\bar{q})$  and  $K^+(\bar{s}q)$  as illustrated in Fig.18. In heavy ion reactions kaons are primordially produced in the early non-equilibrium

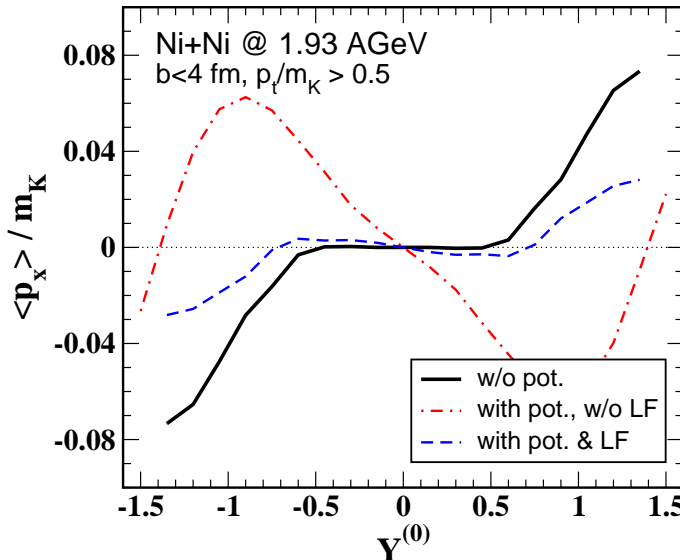


Figure 19: Transverse  $K^+$  flow in 1.93 AGeV  $^{58}\text{Ni} + ^{58}\text{Ni}$  reactions at impact parameter  $b \leq 4$  fm. The calculations are performed without and including the kaon mean field dynamics. In the latter case results without and including the contribution from the Lorentz-force (LF) are shown.

phase. In contrast to  $p+A$  reactions, there the baryon vector current is in general locally non-zero even in the c.m. frame of the colliding nuclei. Thus a Lorentz force will be acting on the kaon. As discussed in [46] the Lorentz force counterbalances to large extent the influence of the time-like  $V_0$  component of the vector field acting on the  $K^+$  mesons. This cancellation can easily be understood from Eq. (78). The vector field is proportional to the baryon current  $j_\mu = (\rho_B, \mathbf{u}\rho_B)$  where  $\mathbf{u}$  denotes the streaming

velocity of the surrounding nucleons. If  $\mathbf{u}$  is locally constant, then the total contribution of the vector field in Eq. (78) can be written as  $\mp \frac{3}{8f_\pi^2} (1 - |\mathbf{v}||\mathbf{u}| \cos \Theta) \partial \rho_B / \partial \mathbf{q}$ . Now the angle  $\Theta$  between the kaon and the baryon streaming velocities determines the influence of the Lorentz force. For  $\Theta = 0$  one obtains an attraction (repulsion) for  $K^+$  ( $K^-$ ) and the opposite in the case of  $\Theta = 180^\circ$ .

Such dynamics have e.g. consequences for the kaon transverse flow. This is illustrated in Fig. 19 where the  $K^+$  transverse flow in Ni+Ni reactions at 1.93 AGeV is shown for various cases. It is seen that the strongly repulsive static  $K^+$  potential  $U_K$  in (79) tends to push the kaons away from the spectator matter, leading to a strong anti-flow around mid-rapidity. The Lorentz force pulls the kaons back to the spectator matter, resulting finally in a flow pattern which is close to that obtained without any in-medium potential. However, the magnitude of the cancellation effect and the final flow pattern depends also on the strength of the vector potential and the interplay between repulsive vector and the attractive scalar potential. In the early works on kaon flow [39, 159] the Lorentz force has been disregarded which led to an overestimation of the vector repulsion. One has, however, to keep in mind that correlations beyond mean field lead to an explicit momentum dependence of the scalar and vector potentials. Such an explicit momentum dependence reduces e.g. in the case of the nucleons the size of the scalar and vector potentials and, correspondingly the Lorentz force which softens the nucleon optical potential. A detailed discussion of the kaon flow and a comparison to data will be performed in chapter 5.

## 4.2 Off-shell transport

Essential for the validity of the classical equations of motion is the quasi-particle approximation (QPA) which assumes that the spectral strength of a hadron is concentrated around its quasi-particle pole. Since kaons have practically zero width this condition is readily fulfilled in the vacuum. Particle widths can, however, dramatically change in a dense hadronic environment. To first order in density the in-medium width of a hadron in nuclear matter can be estimated by the collision width  $\Gamma^{\text{tot}} = \Gamma^{\text{vac}} + \Gamma^{\text{coll}}$ ,

$$\Gamma^{\text{coll}} = \gamma v \sigma \rho_B , \quad (80)$$

with  $v$  the hadron velocity relative to the surrounding matter and  $\sigma$  the total hadron-nucleon cross section. Due to their long mean free path the collisional broadening of kaons is small. The kaon-nucleon cross section is dominated by its elastic part which is about 10 mb and the majority of kaons is produced with relatively small velocity. Thus for  $K^+$ 's in-medium widths can be expected to be small and the quasi-particle-approximation appears to be justified. For antikaons the situation is completely different. The strong coupling of the  $K^-N$  system to the  $\Lambda(1405)$  and  $\Sigma(1385)$  hyperons leads not only to a shift of the quasi-particle pole but also to a strong distortion of the  $K^-$  spectral function [61, 37] (see Fig. 5). The application of mean field dynamics is therefore questionable.

First attempts to account for in-medium spectral properties in a more consistent way within the framework of semi-classical transport models were already made some time ago. A fully consistent treatment of the off-shell dynamics, i.e. a solution of the full Kadanoff-Baym equations has up to now only been performed for toy models and simplified geometries. Danielewicz [19] was the first to solve the quantum evolution equations for the correlation functions  $G^{<>}$  (59,60) for an infinite cylindrically symmetric system using a simplified two-body potential of Gaussian form. The work of Köhler [169] who solved the Kadanoff-Baym equations under the same conditions on a Cartesian momentum space grid can be viewed as the first step towards a realization of quantum transport on a lattice. To develop a lattice quantum transport for non-uniform systems and realistic interactions will be one of the future challenges in theoretical heavy ion physics.

On the other hand, substantial progress has been made in the recent years to map part of the off-shell dynamics on a modified test-particle formalism [28, 166, 172, 174]. This allows to apply off-shell dynamics, although in a simplified form, to the complex space time evolution of a heavy ion reaction.

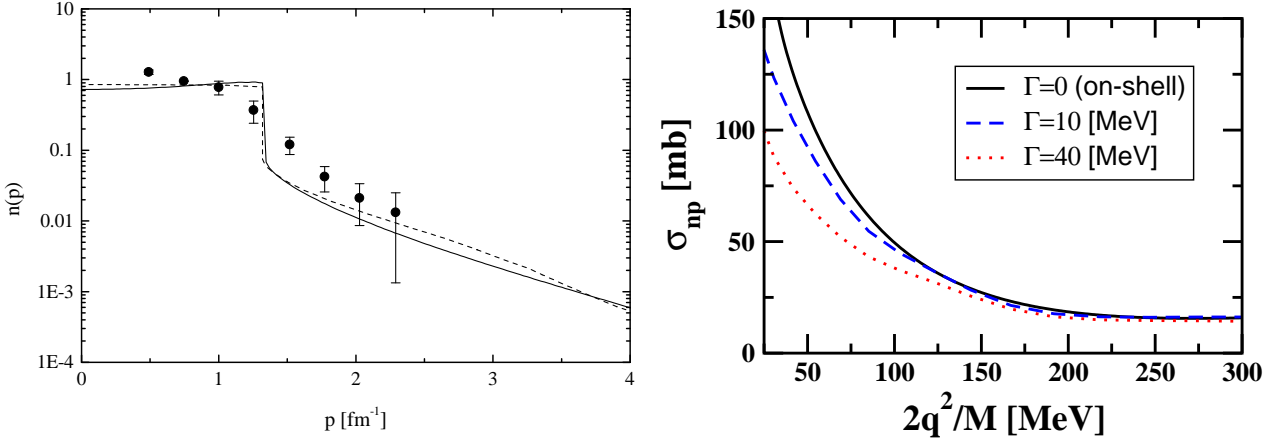


Figure 20: Left: momentum distribution in nuclear matter at  $\rho_0$  from a self-consistent off-shell transport (solid) is compared to a many-body calculation [170] (dotted) and to data from electron scattering [171]. The figure is taken from [172]. Right: Off-shell dependence of the elastic in-medium  $np$  cross section at  $\rho_0$ . Off-shell DBHF matrix elements are folded over nucleon spectral functions of different width. Results are from [173].

That such type of approach is able to describe essential features of nuclear correlations beyond mean field has e.g. been demonstrated in Ref. [172]: in the left part of Fig. 20 the nucleon phase space distribution  $f(\mathbf{k})$  in nuclear matter resulting from a self-consistent off-shell calculation is compared to a microscopic many-body calculation [170] and to electron scattering data [171]. Although these results were obtained with adjusted on-shell scattering matrix elements the agreement with the realistic distribution function is remarkably good.

The present knowledge of off-shell matrix elements is rather limited. Except of particular cases of interest, e.g.  $\pi Y \leftrightarrow K^- N$  matrix elements [62, 63], theoretical investigations are scarce. In Ref. [173] in-medium half-off-shell matrix elements for elastic nucleon-nucleon scattering have been determined from relativistic DBHF many-body calculations based on realistic meson exchange potentials. The results indicate that a smooth transition from on-shell to off-shell matrix elements is possible and the usage of on-shell cross sections is justified for  $NN$  scattering. The right part of Fig. 20 displays the elastic off-shell in-medium neutron-proton cross section at  $\rho_0$ , folded over nucleon spectral functions of different width, as a function of the c.m. momentum. The mean  $NN$  cross section is in general only little affected which justifies the standard on-shell transport approach for the overall reaction dynamics.

The question to what degree a depletion of the Fermi surface due to particle-hole excitations and the high momentum tails of the nuclear spectral functions will affect subthreshold particle production is, however, not so obvious to answer. The high momentum tails correspond to deeply bound states which are off-shell and to treat such states in a standard transport approach like on-shell quasi-particles would violate energy-momentum conservation. The contribution of the nuclear short-range correlations to subthreshold  $K^+$  production in  $p+A$  reactions have been estimated in [144], based on the spectral distributions of Benhar et al. [170] shown in Fig. 20. The removal energy for a high momentum state compensates the naively expected energy gain and the short-range correlations do therefore not significantly contribute to subthreshold particle production [144]. The situation changes, however, when the medium is heated up and high momentum particles become on-shell or when the spectral distributions of the produced hadrons themselves are broadened.

Possible implications of off-shell dynamics connected to a spectral broadening of the kaons have first

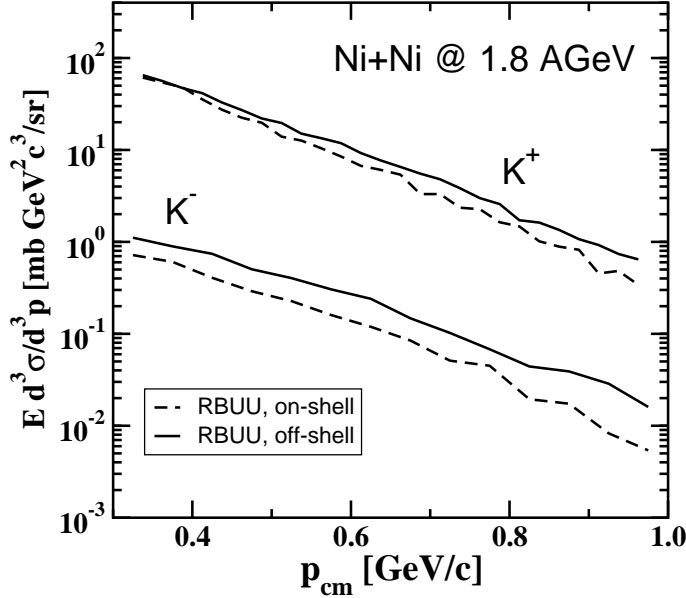


Figure 21: Influence of hadron off-shell propagation on  $K^\pm$  spectra in Ni+Ni reactions at 1.8 AGeV. On-shell cross sections have been used for the strangeness production and exchange reactions in the RBUU calculation of [174].

been studied by Cassing and Juchem [174, 121]. These calculations were based on *on-shell* cross sections and hadronic spectral functions ( $N, \pi, \Delta, K^+, K^-$ ) which are exclusively determined by the collisional broadening (80) of these particles. Nucleons and pions were found to be practically unaffected by the off-shell propagation while the high momentum tails of the  $K^+$  spectra are enhanced. But even at subthreshold energies the effect on the  $K^+$  yield was found to be moderate which justifies the standard quasi-particle approach and is in line with the observations of Ref. [144]. As expected, the off-shell effects were found to be much stronger for antikaons.  $K^-$ 's acquire a large spectral width in the medium and it is energetically favorable to produce them off-shell in the low momentum tails of their spectral functions. During the propagation through the medium these particles become on-shell as they reach the detector. Obviously this transition must take place in a controlled way which is guaranteed within consistent off-shell dynamics [174, 121]. As can be seen from Fig. 21 where the corresponding  $K^\pm$  spectra in Ni+Ni reactions at 1.8 AGeV are shown, the collisional broadening leads to an enhancement of the  $K^-$  yield by about a factor of 2-3 compared to the on-shell treatment. However, in particular for  $K^-$  the off-shell behavior of the in-medium strangeness exchange cross sections  $\pi Y \longleftrightarrow NK^-$  plays an important role [121]. Results based on off-shell cross sections will be discussed in the following chapter.

### 4.3 Collisions

Transport models treat particle production at subthreshold energies usually in a perturbative way. In each individual hadron-hadron collision the incident energy  $\sqrt{s}$  must be above the production threshold. However, such processes are rare and the corresponding cross sections lie in the vicinity of thresholds usually several orders of magnitude below the total cross sections. Since Monte-Carlo methods which are applied to solve the collision integral of the kinetic equation [175] select the actual reaction channel

$i$  with probability

$$P_i = \frac{\sigma_i(\sqrt{s})}{\sigma_{\text{tot}}(\sqrt{s})} , \quad \sum_{\text{all channels}} P_i = 1 , \quad (81)$$

meson production is at subthreshold energies an extremely rare process. To obtain nevertheless reasonable statistics, for such reactions a perturbative treatment is applied [176, 177, 178]. In short, this means that the meson is produced if kinematically allowed. Phase space and Pauli-blocking factors for the final states are determined and the produced meson  $k$  gets the probability

$$P_k = \sum_X \frac{\sigma^{Y \rightarrow K^+ X}(\sqrt{s})}{\sigma_{\text{tot}}} \quad (82)$$

assigned.  $Y$  denotes the initial state and the sum runs over all possible final states. From the set of possible final states the actual reaction channel  $k$ , i.e.  $Y \rightarrow K^+ X_k$ , is selected by Monte-Carlo. Thus, e.g. the total  $K^+$  multiplicity is given

$$N_{K^+} = \sum_{\text{all } K^+} P_k . \quad (83)$$

Finally the initial particles are reset to their initial values and the cascade continues as if no such reaction would have taken place. The perturbatively produced mesons are propagated as 'virtual' particles parallel to the ongoing reaction dynamics in such a way that they are influenced by the bulk of particles, however, without any feed back to the global reaction dynamics. The perturbative treatment is justified as long as the considered particles are rare enough not to influence the average reaction dynamics.

#### 4.3.1 Elementary cross sections

As discussed in the previous chapter, the elementary production mechanism for  $K^+$  mesons can be divided into baryon induced reactions  $BB \rightarrow BYK^+$  ( $B$  stands either for a nucleon or a  $\Delta$ -resonance and  $Y$  for a  $\Lambda$  or a  $\Sigma$  hyperon, respectively) and processes  $\pi B \rightarrow YK^+$  induced by pion absorption. Here and in the previous works of the Tübingen group [46, 109, 123, 159, 179, 180, 181, 182] for pion induced reactions the elementary cross sections of Tsushima et al. [110] have been used. The cross sections are derived within the resonance model in Born approximation, including all baryonic resonances with masses below 2 GeV as intermediate states. In the meantime they are standardly and applied in most transport calculations [116, 183, 25, 39, 154, 98, 184, 96].

For baryon induced channels there are presently several different parameterizations on the market: Those from Li and Ko [154] used by the Texas and Stony Brook groups; those given by Sibirtsev [97] which are used by the Giessen group [116, 25] and have been applied in some of our previous works [109, 159, 123, 46]; and more recent calculations within the resonance model by Tsushima et al. [100, 101, 102]. In principle it would be desirable to base the cross sections for both, pion and baryon induced reactions on the same model [110, 102]. However, the resonance model [102] under-predicts the COSY-11 data [87] for  $pp \rightarrow p\Lambda K^+$  at threshold. Thus, here and in [181, 182] the cross sections from [97] were used for  $NN \rightarrow N\Lambda(\Sigma)K^+$  and those of ref. [102] for reactions involving nucleon resonances ( $NN \rightarrow \Delta YK^+$ ,  $N\Delta \rightarrow BYK^+$  and  $\Delta\Delta \rightarrow BYK^+$ ). Figure 22 compares the model predictions for  $pp$  and  $\pi p$  channels to available data. In the vicinity of the threshold the nucleon-hyperon final state interaction is attractive and strong which tends to increase the cross section [188]. Since both, the OBE as well as the resonance model calculations do not account for FSI effects, the COSY data are under-predicted near threshold [87]. As pointed out in [189] the modification of the energy dependence of the cross section due to FSI is determined by the on-shell T-matrix. Since in the semi-classical

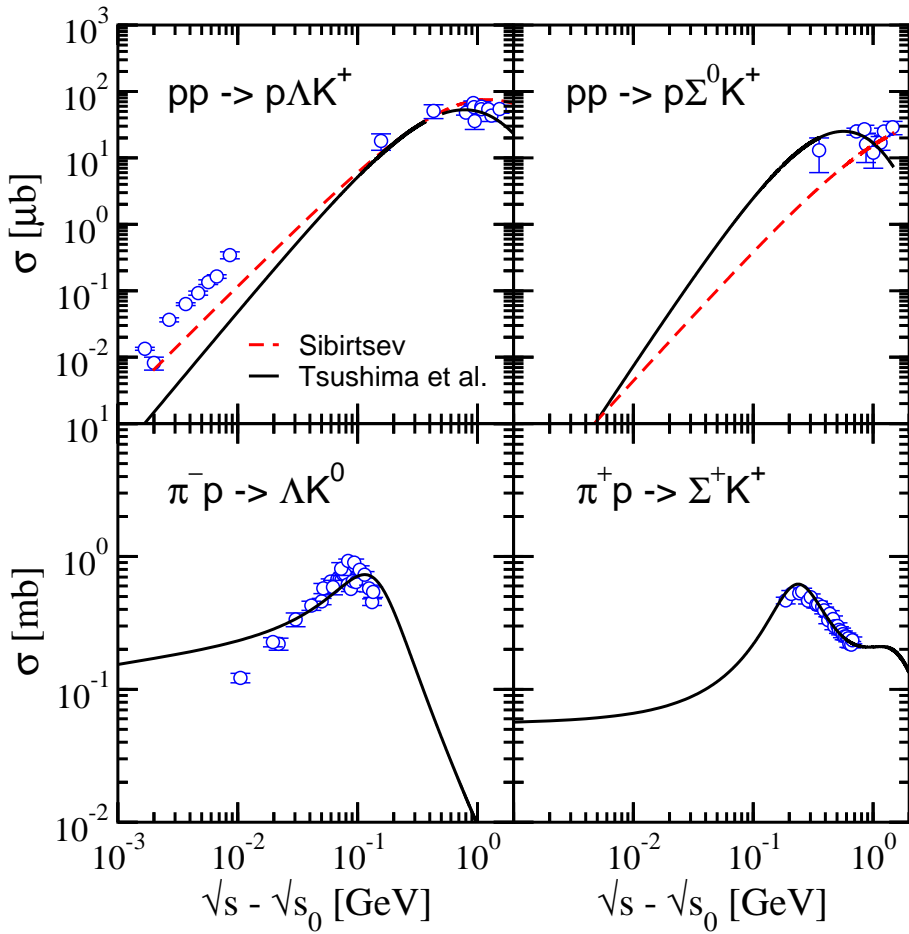


Figure 22: Elementary cross section for kaon production. Resonance model calculations from Tsushima et al. [110, 102] and OBE calculations from Sibirtsev [97] are compared to data [87, 185, 186, 187].

transport models on-shell potentials enter into the evaluation of the scattering amplitude, e.g. by shifts of thresholds, some FSI contribution is effectively included which justifies the usage of the cross sections from [97].

In contrast to the  $NN$  channel, cross sections with an incoming  $\Delta$  resonance  $N\Delta \rightarrow BYK^+$  are not constrained by data. Here the largest differences between various parameterizations occur. Fig. 23 compares the resonance model results [102] with parameterizations based on isotopic relations for  $pp$  [25, 94]. The latter cross sections turn out to be about one order of magnitude smaller. This difference is crucial since the  $N\Delta \rightarrow K^+X$  is one of the primary production channels for kaons. It explains why there existed a significant inconsistency between transport calculations from different groups concerning the total kaon multiplicity in heavy ion reactions. Kaon yields obtained from the Giessen group [25, 94, 116] turned out to be systematically smaller than those of the Texas and Stony Brook [95, 154], the Nantes [96] and the Tübingen [181, 182] groups. The source of this discrepancy, which is crucial with respect of an interpretation of corresponding data in terms of kaon in-medium potentials, could finally be traced back to the usage of the different cross sections for kaon production in  $N\Delta$  collisions [96].

Reactions with multi-particle final states, such as  $NN \rightarrow N\pi YK$ ,  $NN \rightarrow N\pi\pi YK$ , are subdominant at subthreshold energies. If taken into account they can either be treated by direct parameterizations of experimental data [154] or by two-step processes via resonance production  $NN \rightarrow RYK$  and subsequent decay  $R \rightarrow N(n \cdot \pi)$ . Fig. 23 compares resonance model calculations [102] to data. The experimental values in Fig. 23 are normalized to the iso-spin factors of the corresponding  $\Delta \rightarrow N\pi$  decays. The present calculations include reactions with a  $\Delta$  resonance in the final state with cross

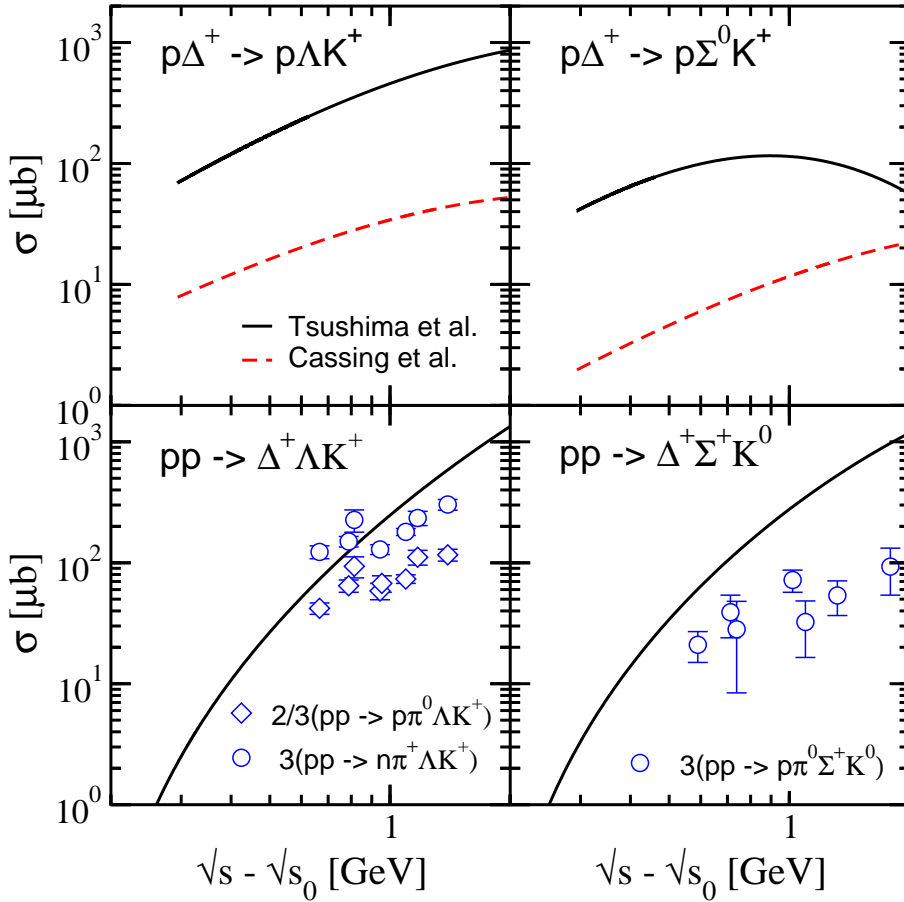


Figure 23: Cross sections involving  $\Delta$  resonances. Upper part: for the experimentally unknown  $p\Delta \rightarrow pYK^+$  cross sections resonance model calculations [102] are compared to the parameterizations of [25]. Lower part: Resonance model calculations [102] for  $pp \rightarrow \Delta YK$  are compared to  $pp \rightarrow N\pi YK$  data [185].

sections taken from [102].

#### 4.3.2 Shift of thresholds

The cross sections are obtained for free scattering. The incorporation of medium effects in the scattering process is a peculiar question, in particular since at SIS energies most kaons are created near threshold. A shift of the thresholds by in-medium potentials affects the production mechanism significantly. However, the treatment of the threshold conditions and the determination of the phase space of final states is in the medium a subtle problem. Since there exists up to now no unified description of relativistic and non-relativistic approaches we will discuss this point in more detail. In this context problems arise generally due to on-shell scattering of quasi-particles. In the presence of the medium mass-shell conditions are modified and phase space relations valid in free space have to be modified as well.

Let us for example consider baryon-baryon induced  $K^+$  production  $BB \rightarrow BYK^+$ . In free space the momenta of the outgoing particles are distributed according to the 3-body phase space

$$d\Phi_3(\sqrt{s}, m_B, m_Y, m_K) = d\Phi_2(\sqrt{s}, m_B, M) dM^2 \Phi_2(M, m_Y, m_K) \quad (84)$$

with  $\sqrt{s}$  the center-of-mass energy of the initial baryons. The two-body phase space in Eq. (84) has the well known form

$$\Phi_2(\sqrt{s}, m_1, m_2) = \frac{\pi p^*(\sqrt{s}, m_1, m_2)}{\sqrt{s}} \quad (85)$$

where

$$p^*(\sqrt{s}, m_1, m_2) = \frac{\sqrt{(s - (m_1 + m_2)^2)(s - (m_1 - m_2)^2)}}{2\sqrt{s}} \quad (86)$$

is the momentum of the particles 1 and 2 in their center-of-mass frame.

Concerning the in-medium description differences arise also between non-relativistic and relativistic approaches. In the relativistic case the mean field is generally composed by scalar and vector parts, a feature which is absent in purely non-relativistic approaches. However, also the kaon mean field is of a scalar-vector type structure which makes a non-relativistic treatment somewhat ambiguous. The reason lies in the fact that in most non-relativistic approaches canonical momenta  $k_\mu$  are propagated whereas in relativistic approaches usually kinetic momenta  $k_\mu^*$  are used. To illustrate this effect we consider first nucleon-nucleon scattering.

In relativistic dynamics, e.g. given by the  $\sigma\omega$  model of Quantum Hadron Dynamics [47] the nucleon mean field is also composed by a scalar  $\Sigma_S$  and a vector  $\Sigma_\mu$  part. Like for kaons the vector field enters into the kinetic momenta  $k_\mu^* = k_\mu - \Sigma_\mu$  and the scalar field into the effective mass  $m^* = m + \Sigma_S$  of the particles. The dressed quasi-particles fulfill the mass shell condition

$$k_\mu^{*2} - m^{*2} = 0 \quad , \quad E^* = \sqrt{\mathbf{k}^{*2} + m^{*2}} \quad (87)$$

and thus transport models are usually formulated in terms of these kinetic quasi-particle quantities. If two nucleons are scattered, energy-momentum conservation requires

$$k_{1\mu} + k_{2\mu} = k'_{1\mu} + k'_{2\mu} \quad (88)$$

which is equivalent to the conservation of the kinetic quantities

$$k_{1\mu}^* + k_{2\mu}^* = k'^*_{1\mu} + k'^*_{2\mu} \quad (89)$$

as long as the fields are density dependent but do not explicitly depend on momenta, i.e.  $\Sigma_{\mu,S} = \Sigma_{\mu,S}(\rho)$ . Then both conditions (88) and (89) can be fulfilled simultaneously. This means that the phase space relations (84–86) can be used by replacing the bare quantities  $s, m_B, m_Y, m_K$  by the effective quantities  $s^*, m_B^*, m_Y^*, m_K^*$ .

However,  $K^+$  mesons are created by associated strangeness production which leads automatically to a shift of the corresponding production thresholds in the medium, even when no modifications of the kaon properties are taken into account. The reason is the creation of the associated hyperon. Due to its reduced non-strange quark content the mean field of the hyperon should scale – at least in a simple  $SU(3)$  flavor picture – with about a factor of 2/3 compared to the nucleon field. Such a scaling is in rough agreement with mean field calculations for hyper nuclei [190, 191, 192]. Now the baryon fields are no more conserved and therefore it is no more possible to conserve both, kinetic and canonical momenta simultaneously. From the derivation of kinetic equations [19, 20] it is clear that in this case single particle energies

$$E = k_0 = E^* + \Sigma_0 \quad (90)$$

and canonical momenta  $k_\mu = (E, \mathbf{k})$  are the quantities which have to be conserved. Consequently, the usage of on-shell phase space relations (84–86) with the quantities  $s^*, m_B^*, m_Y^*, m_K^*$  will lead to a violation of energy conservation.

To overcome this problem and to make nonetheless use of on-shell relations it is useful to formulate the mass-shell conditions in terms of canonical momenta. This can be achieved with the help of the optical potential defined in (29) which allows to rewrite the in-medium dispersion relation as  $0 = k_\mu^{*2} - m_K^{*2} = k_\mu^2 - m_K^2 - 2m_K U_{\text{opt}}$ . Since  $U_{\text{opt}}$  is a Lorentz scalar it can be absorbed into an newly defined effective mass  $\tilde{m}_K$

$$\tilde{m}_K(\rho, \mathbf{k}) = \sqrt{m_K^2 + 2m_K U_{\text{opt}}(\rho, \mathbf{k})} \quad (91)$$

which sets the canonical momenta on mass-shell

$$0 = k_\mu^{*2} - m_K^{*2} = k_\mu^2 - \tilde{m}_K^2 \quad . \quad (92)$$

The single particle energy follows from the dispersion relation (27) written now as

$$E = \sqrt{\mathbf{k}^2 + \tilde{m}_K^2} \quad . \quad (93)$$

The threshold condition for  $K^+$  production in baryon induced reactions reads now

$$\sqrt{s} \geq \tilde{m}_B + \tilde{m}_Y + \tilde{m}_K \quad (94)$$

with  $\sqrt{s}$  the center-of-mass energy of the colliding baryons. The momenta of the outgoing particles are distributed according to the 3-body phase space

$$d\Phi_3(\sqrt{s}, \tilde{m}_B, \tilde{m}_Y, \tilde{m}_K) = d\Phi_2(\sqrt{s}, \tilde{m}_B, M) dM^2 \Phi_2(M, \tilde{m}_Y, \tilde{m}_K) \quad . \quad (95)$$

The integration over the mass distribution of the  $\tilde{m}_B, \tilde{m}_Y, \tilde{m}_K$  system in Eqs. (86) and (95) has to be performed numerically. The introduction of  $\tilde{m}_K$  is thereby of practical use. However, in contrast to the quasi-particle mass  $m_K^*$  which is in mean field approximation only density dependent,  $\tilde{m}_K$  depends on density and momentum. This means that 3-body-phase-space of the final states and the corresponding final state  $\tilde{m}$  masses for the final state hadrons have to be determined self-consistently by iteration. Thus the production threshold depend also on the final momentum distribution. The usage of a simply shifted in-medium mass  $\tilde{m}_K = m_K \pm \alpha \rho$  in eq. (93) neglects such a momentum dependence.

The potential of the final state hyperons is usually determined under the assumption of SU(3) symmetry. The scaling with the non-strange quarks leads than to the reduction by 2/3 compared to the nucleon potential. Such a scaling has been found to be in reasonable agreement with the  $\Lambda$  dynamics in heavy ion reactions, in particular the  $\Lambda$  flow [179, 98] and is also close to the value extracted from hyper nuclei [190, 191, 192]. Thus one obtains an additional shift of the thresholds by  $U_Y - U_B = -\frac{1}{3}U_B$ . In the QMD calculations discussed in the work the shifts of the thresholds due to the different initial and final state in-medium potentials have been treated within a relativistic framework, i.e.  $U_Y - U_B = -\frac{1}{3}(\Sigma_s - \Sigma_0)$ . This allows well defined Lorentz transformations of the kaon and baryon mean fields concerning their scalar-vector structure. In correspondence with the soft/hard Skyrme forces a soft/hard version of the non-linear  $\sigma\omega$ -model [133] with  $K=200$  MeV and  $K=380$  MeV are used to determine the reaction threshold.

Besides the scaling of the hyperon optical potential also the momentum dependence of baryon optical potentials influences the production thresholds. The nucleon optical potential is repulsive at high momenta which are necessary for the incoming states to overcome the production threshold. The momenta of the final states are significantly smaller. Due to the less repulsive optical potential experienced by the final states additional energy is gained to overcome the production threshold. At subthreshold energies all these effects are essential and have to be taken into account in the transport calculations.

### 4.3.3 Angular distributions

For most reactions elementary cross sections are assumed to be isotropic. In some cases there exists experimental evidence for anisotropic angular distributions. However, from heavy ion spectra it is difficult to disentangle the possible sources for anisotropic kaon emission. One source are final state interactions such as  $KN$  rescattering and the mean field propagation [122, 123, 94]. For a reproduction of the strongly forward-backward peaked  $K^+$  pattern reported in [193] these sources turned out to be not sufficient and an additional forward-backward anisotropy was introduced into the pion induced

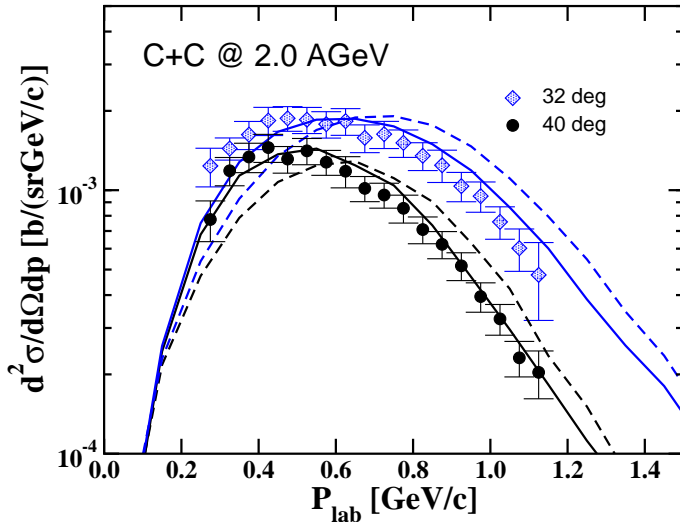


Figure 24: Inclusive  $K^+$  spectra at  $\theta_{\text{lab}} = 32^\circ, 40^\circ$  in C+C reactions at 2.0 AGeV. The calculations are performed with different  $BB \rightarrow BYK^+$  final state 3-body phase space distributions and compared to KaoS data [194]. The dotted curves refer to an isotropic 3-body phase space while the solid curves are obtained using the parameterization of Eq. (19) with an additional empirical c.m. angular anisotropy (see text). The figure is taken from [182].

$\pi N \rightarrow YK^+$  channel in [123]. Instead of an ideal 3-body final state phase space in the baryon induced reactions  $NN \rightarrow NYK^+$  Li et al. [14] proposed an empirical parameterization of the form

$$d\Phi_3(\sqrt{s}, \tilde{m}_B, \tilde{m}_Y, \tilde{m}_K) = dW_K(\sqrt{s}, \tilde{m}_B, \tilde{m}_Y, M_K) dM_K^2 \Phi_2(\sqrt{s} - M_K, \tilde{m}_Y, \tilde{m}_B) \quad (96)$$

where the kaon momentum  $p$  is distributed according to

$$dW_K \simeq \left( \frac{k}{k_{\max}} \right)^3 \left( 1 - \frac{k}{k_{\max}} \right)^2, \quad (97)$$

with  $k_{\max} = p^*(\sqrt{s}, \tilde{m}_B + \tilde{m}_Y, \tilde{m}_K)$  the maximal kaon momentum in the  $BB$  c.m. frame.  $M_K = \sqrt{k^2 + \tilde{m}_K^2}$  in Eq. (96). The parameterization of Eq. (96) has been motivated by analyzing corresponding  $pp \rightarrow p\Lambda K^+$  data [195]. Compared to the ideal 3-body phase space it shifts the kaon spectrum towards lower momenta. The influence of different treatments is illustrated in Fig. 24 where  $K^+$  spectra in C+C collisions at 2.0 AGeV are shown. KaoS measured inclusive  $K^+$  spectra at various c.m. angles with high precision [194]. From the comparison to data one sees that an isotropic 3-body phase space in the  $BB \rightarrow BYK^+$  channel shifts the spectra to too high momenta. The empirical parameterization of Eq. (97) improves the situation but is still not fully sufficient to account for the angular asymmetry of the data [194]. A relatively good agreement can be achieved introducing an empirical angular dependence

$$d\sigma \propto (1 + a \cos^2 \theta_{\text{c.m.}}) d\cos \theta_{\text{c.m.}} \quad (98)$$

in the elementary cross sections. An asymmetry parameter of  $a = 1.2$  leads to slightly forward/backward peaked elementary  $BB \rightarrow BYK^+$  cross sections and the corresponding spectra shown in Fig. 24 are then well reproduced.

#### 4.4 Comparison of different transport models

This subsection addresses the question how consistent the results of present transport models are. Differences may occur due to the use of different physical input such as e.g. elementary cross sections.

The type of the model, i.e. BUU or QMD should not be of relevance. However, the corresponding simulation codes are complex and sometimes based on different numerical and methodical solution techniques. Although physical observables should be independent on such technical questions one has to exclude them as possible sources of uncertainties as far as possible. This was the major goal of two workshops held in Trento 2001 and 2003 where all major groups doing transport model calculations in the SIS energy range participated. In a first round of homeworks the default versions of the codes were compared, in a second round further specifications were made for the comparison. The results of the second round have been published in [196].

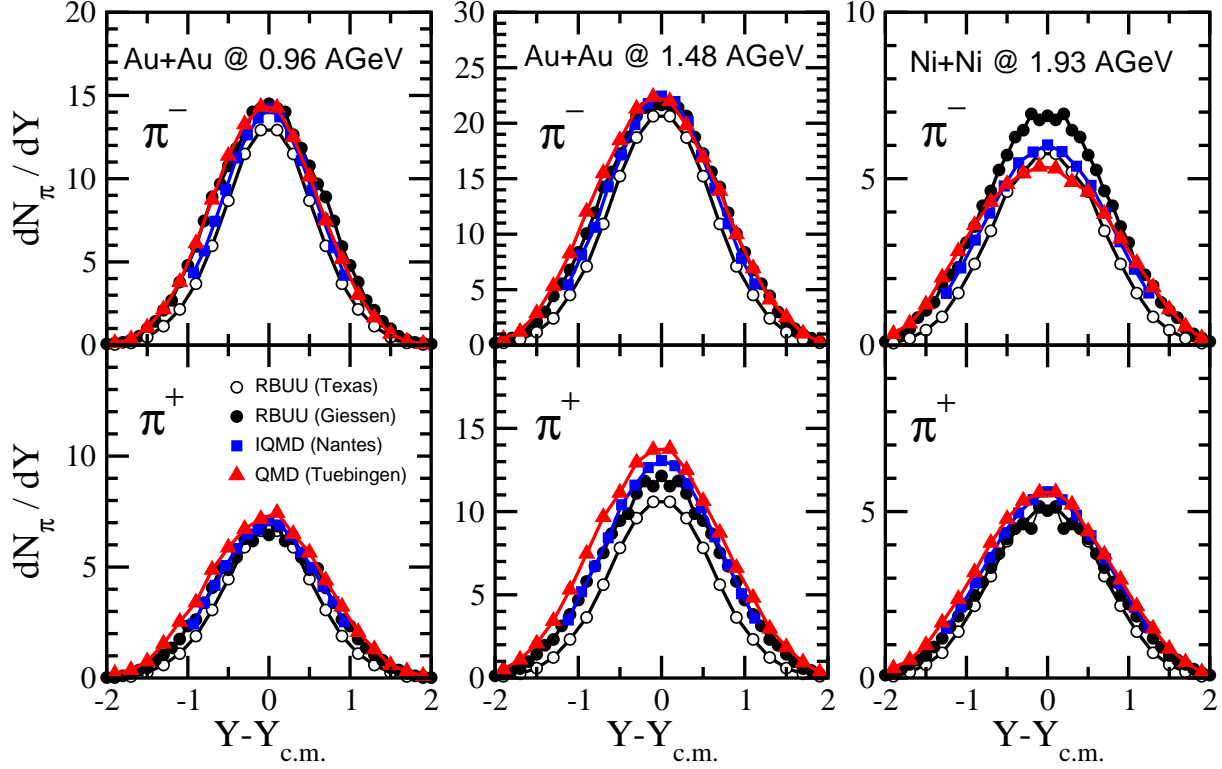


Figure 25:  $\pi^\pm$  rapidity distributions in central ( $b=1$  fm) Au+Au reactions at 0.96 and 1.48 AGeV and Ni+Ni reactions at 1.93 AGeV from various transport models: RBUU (Texas, open circles), RBUU (Giessen, full circles), IQMD (Nantes, full squares) and QMD (Tübingen, full triangles).

In the following I compare results for pion and kaon production from four state of the art transport models which participated in that benchmark test. This selection represents only a subset of the models compared in [196] and is motivated by the fact that most of the publications on subthreshold  $K^+$  production over the last five to ten years are based on one of these codes. Of course each of the models experienced a steady development during this period but the selection represents well established transport models used to describe  $K^+$  production at subthreshold energies: the RBUU model of the Texas A&M group [95, 197], the RBUU model of the Giessen group [25], the IQMD model of the Nantes group [96] and the QMD model of the Tübingen group [181, 182]. Additional reasons why the present discussion is restricted to the four mentioned approaches instead of all models presented in [196] are the following ones: the BUU model of Danielewicz [198] does not contain explicit kaonic degrees of freedom, UrQMD (Reiter) [24] treats kaon production non-perturbatively through resonance excitations and is not well suited for an application at subthreshold energies, the Munich/Catania RBUU model (Gaitanos) [199] uses the Tübingen kaon package and gives therefore similar results. The status of the Rossendorf/Budapest BUU model (Barz/Wolf) is hard to estimate since there exist no publications on  $K^+$  production based on this model from recent years. Finally the Giessen BUU model (Larionov) included for the benchmark test all baryonic resonances with masses below 2 GeV under the assumption

that the excited  $\Delta^*$  and  $N^*$  resonances contribute to the  $K^+$  production with the same cross sections as the  $\Delta$  and the nucleon, respectively. Hence a comparision to the four models which include only the  $\Delta(1232)$  and  $N^*(1440)$  for kaon production can be missleading, in particular since the contributions from higher excited nucleon resonances to the kaon production will be suppressed by a quenching of the elementary resonance production cross sections at finite density. The resonance quenching is taken into account in [200] where the Giessen BUU model shows a much better agreement with the four selected models than the benchmark test from [196] would suggest. For the benchmark results of this model we refer the reader to [196]. However, the model is included in Fig. 27 where the default versions of the various codes are compared.

The bechmark tests were performed for three different systems, Au+Au at 0.96 and 1.48 AGeV and Ni+Ni at 1.93 AGeV, all at impact parameter  $b=1$  fm. For this comparison a soft nuclear EOS with momentum dependent forces was applied. Except of the Giessen RBUU model<sup>||</sup> the results were obtained with a constant  $\Delta$  width  $\Gamma_\Delta = 120$  MeV, respectively a constant lifetime  $\tau = 1/\Gamma_\Delta$ . A constant resonance life time is unphysical and not used in the default versions of the codes but it simplifies such a comparison to some extent, in particular when predictions for pion production are considered. In QMD<sup>\*\*</sup> and IQMD only the  $\Delta(1232)$  and  $N^*(1440)$  resonances have been included, while the Giessen RBUU includes additionally the  $N^*(1535)$ . Fig. 25 shows the resulting  $\pi^-$  and  $\pi^+$  rapidity distributions: For Au+Au at 0.96 and 1.48 AGeV the agreement between the different codes is quite satisfactory, i.e. within a 5-10% level. Only at the highest considered energy of 1.93 stronger deviations are visuable since the Giessen calculations includes one higher lying resonance. In this context it should be mentioned that the  $\pi^\pm$  yields from Texas RBBU shown in Fig. 25 differ from those of [196]. There isospin averaged rapidity distributions are shown while here the isospin dependence is taken into account by the isobar model. The default versions of the codes use different descriptions of the energy dependence of the resonance life times. As discussed in [196] the two RBUU models under consideration use  $\tau \propto 1/\Gamma_\Delta(|\mathbf{k}|)$  with an energy dependent width. The QMD [26] and IQMD [201] models apply the time delay description [202] where the lifetime is obtained from the phase shift  $\tau = 2d\delta(E)/dE$  which results in a Breit-Wigner form  $\tau(\mu) = 4\pi\mu dW_\Delta(\mu)/d\mu^2$  with

$$dW_\Delta(\mu) = \frac{1}{\pi} \frac{\mu\Gamma_\Delta(\mu)d\mu^2}{(\mu^2 - m_\Delta^2)^2 + (\mu\Gamma_\Delta(\mu))^2} \quad (99)$$

In Eq. (99)  $m_\Delta$  is the resonance pole mass and  $\mu$  the running mass. The pion yields obtained by such a description are lower than those shown in Fig. 25 (15-20% for QMD and about 30% for IQMD) while they do not much change when the constant width is replaced by an energy dependent width in the RBUU calculations.

Though pion yields agree well the situation is not yet as clear concerning the kaon production. Fig. 26 shows the  $K^+$  rapidity distributions obtained without in-medium effects and including an in-medium kaon potential. First we will discuss the results without medium effects:

The results are based on comparable, however, not completely identical input. The Giessen RBUU, IQMD and QMD calculations are based on exactly the same set of elementary cross sections, i.e. the parameterizations of [97] for  $NN \rightarrow NYK^+$  and those of [102] for  $N\Delta \rightarrow NYK^+$  (in contrast to previous publications of the Giessen group). Pion induced reactions are based on the cross sections of [110]. Hence the RBUU results from Giessen agree relatively well with those of the Tübingen QMD, i.e. on a 10-15% level. Compared to these two models the Nantes IQMD leads to an about 30% higher kaon yield, in particular at higher energies. This discrepancy can probably not be traced back to the level of elementary input and further clarification is needed. The Texas RBUU yields lie significantly below

---

<sup>||</sup>Private communication with E.L. Bratkovskaya.

<sup>\*\*</sup>An extended version of the QMD model which includes all nucleon resonances with masses below 2 GeV was used for the description of dilepton production at SIS energies [26].

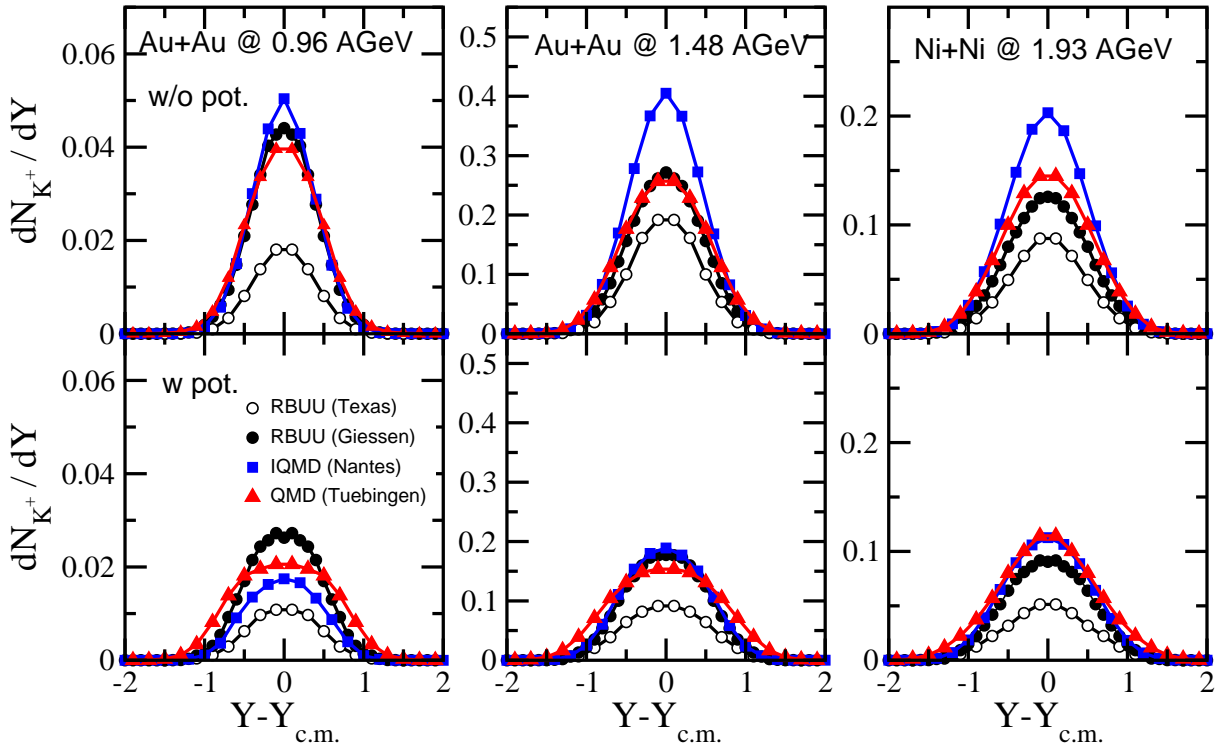


Figure 26:  $K^+$  rapidity distributions in central ( $b=1$  fm) Au+Au reactions at 0.96 and 1.48 AGeV and Ni+Ni reactions at 1.93 AGeV from various transport models [203]: RBUU (Texas, open circles), RBUU (Giessen, full circles), IQMD (Nantes, full squares) and QMD (Tübingen, full triangles). The upper curves show results without kaon in-medium potentials while the lower curves include potentials.

the other ones. This discrepancy is, however, understandable since the Tsushima cross sections [102] have been used for the  $NN \rightarrow NYK^+$  channel which are at threshold about one order of magnitude smaller than those of [97], see Fig. 22. Consequently, the suppression of the RBUU Texas yields is most pronounced at the lowest energy of 0.96 AGeV. Here the impact of the elementary input is clearly reflected.

All models show the same qualitative in-medium effect, namely a sizable reduction of the  $K^+$  yield. One has, however, to be aware that the different models use repulsive in-medium potentials of different strength and treat their momentum in different ways. When the kaon potential is parameterized in the form of an effective mass

$$m_K^* = m_K(1 + \alpha \rho / \rho_0) \quad (100)$$

the coefficients for the results shown in Fig. 26 are  $\alpha = 0.07$  (QMD; MFT ChPT+corr. potential), 0.075 (IQMD), 0.04 (RBUU Giessen) and 0.04 (RBUU Texas) [196]. This leads automatically to different predictions for the kaon yields. According to the weakest potential the relative suppression of the kaon yields is least pronounced in the RBUU calculations. There exist, however, not only differences in the size of the potentials but also in the way how the kaon mean field is treated. The present QMD [46, 181] calculations (and those of [200]) are the only ones which account for the full covariant structure including the Lorentz force from the spatial components of the vector field (79). RBUU Texas and IQMD neglect these contributions and in the RBUU Giessen model the total kaon potential according to expression (100).

From the above comparison it seems surprising that all four models are able to fit the experimental  $K^+$  data for Ni+Ni at 1.93 AGeV [182, 96, 204, 197] (see also Fig. 30). Therefore in Fig. 27 the predictions of the default versions of the codes are shown, again for Ni+Ni at 1.93 AGeV at impact parameter  $b=1$  fm. This figure contains in addition the predictions of the BUU model of Larionov

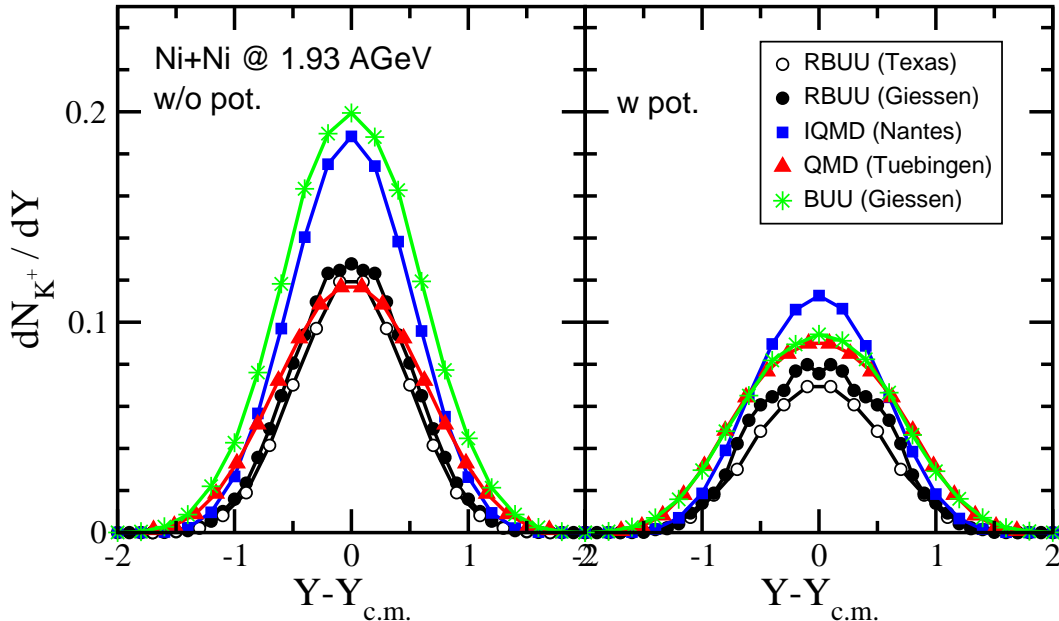


Figure 27:  $K^+$  rapidity distributions in central ( $b=1$  fm) Ni+Ni reactions at 1.93 AGeV from various transport models in their default versions: RBUU (Texas, open circles), RBUU (Giessen, full circles), IQMD (Nantes, full squares), QMD (Tübingen, full triangles) and BUU (Giessen). The left figure shows results without kaon in-medium potentials while the right one includes potentials.

and Mosel (BUU Giessen) which is also able to reproduce experimental kaon multiplicities when a quenching of higher nucleon resonances is taken into account [200]. This model uses exactly the same in-medium  $K^+$  potential as is used in the present QMD calculations. From Fig. 27 it becomes clear that the unphysical constraint of a constant  $\Delta$  width (which violates detailed balance in the codes if pion absorption is not modified accordingly) has a strong influence on the kaon yields. Similar to the pion yields the kaon yields are smaller in the QMD/IQMD default versions, in particular when in-medium potentials are used. For the Texas RBUU the behavior is opposite, i.e. the kaon yields are now enhanced. Considering the case without potential one sees that the models group into two fractions: (IQMD, BUU (Giessen)) and (QMD, RBUU (Texas), RBUU (Giessen)). The latter ones yield an about 30-40% smaller kaon yield. The reason for this discrepancy is still an open question which has to be settled in future.

When in-medium potentials are taken into account, the QMD and BUU rapidity distribution are slightly broader than the other ones. This is due to the momentum dependence originating from the relativistic Lorentz force which is only accounted for in these two models. The relative potential effect is now larger for the Giessen RBUU compared to Fig. 30 since the stronger chiral RHA potential of [204] is applied, corresponding to  $\alpha \simeq 0.055$  in the above parameterization. When in-medium potentials are applied, the uncertainty of the present model calculations, is of similar magnitude than experimental error bars. However, as mentioned above, the agreement of the codes in their bare versions is still not completely satisfactory and requires further efforts to improve on this.

For a compilation of the predictions for  $K^-$  production, which turned out to be still burdened with much higher uncertainties, we refer the reader to Ref. [196].

## 5 Probing in-medium kaon potentials

In-medium kaon potentials shift the single particle energies (26) and the thresholds for kaon production (91-94). The measurement of kaon multiplicities should therefore provide a direct access to such in-medium potentials and, consequently probe an expected partial restoration of chiral symmetry at supra-normal nuclear densities [122]. For  $K^+$  mesons the repulsive mean field reduces the yields while the situation is opposite for  $K^-$  where the yields should be significantly enhanced by the attractive potential. The hope is to extract information about the existence and size of such potentials from heavy ion reactions by transport calculations. However, the situation turned out to be more complex than originally expected:

Despite the fact that the kaon mean field has indeed a strong influence on the multiplicities their absolute values depend as well on the elementary cross sections. Uncertainties due to an incomplete knowledge of the cross sections turned out to be of the same order as the potential effects. However, in the meantime a more or less consistent picture has emerged concerning the  $K^+$  mesons. For antikaons the situation is less satisfying since cross sections are known with less precision and the  $K^-$  yield itself is strongly coupled to the  $K^+$  production rate via strangeness exchange reactions.

As a way out of this dilemma there were also strong attempts to extract the potential from dynamical observables which are altered by the in-medium optical potential while uncertainties in the total production rates drop out. Promising probes are, e.g., collective flow pattern.

### 5.1 Total Yields

For  $K^+$  mesons the various transport models now provide a relatively consistent picture what concerns the net potential effect on the kaon multiplicities. The repulsive mean field leads to a reduction of the yields by about 30-50%, depending on the actual strength of the potential, the system size and the energy of the reaction. The magnitude of the reduction within different transport model realizations can be read off from Fig. 26. Figures. 28 to 30 demonstrate the energy and system size dependence and the conclusion which can be drawn from the comparison to data. Fig. 28 shows the potential effect in

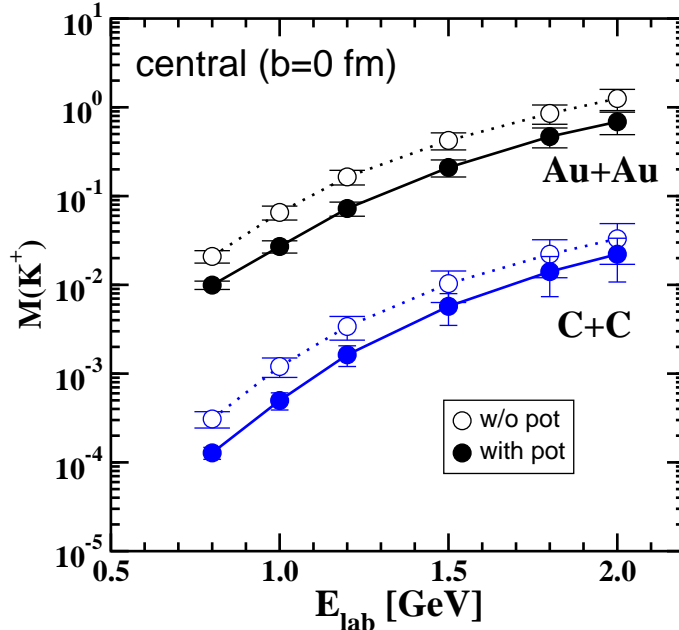


Figure 28: Influence of  $K^+$  in-medium potential on the kaon yields. Multiplicities obtained with and w/o in-medium potential are shown for central ( $b=0$ ) Au+Au and C+C reactions.

central Au+Au and C+C reactions as a function of beam energy. Throughout this work the calculations which include an in-medium potential are based on the  $K^+$  mean field proposed by Brown and Rho [31], denoted in Figure 1 as MFT ChPT+corr., which has been derived from ChPT and includes effectively higher order corrections beyond mean field. The reduction of the  $K^+$  yield due to the repulsive potential is, as expected, slightly larger in heavy systems than in light systems and most pronounced at energies far below threshold. The excitation functions of the  $K^+$  cross sections in inclusive Au+Au and C+C

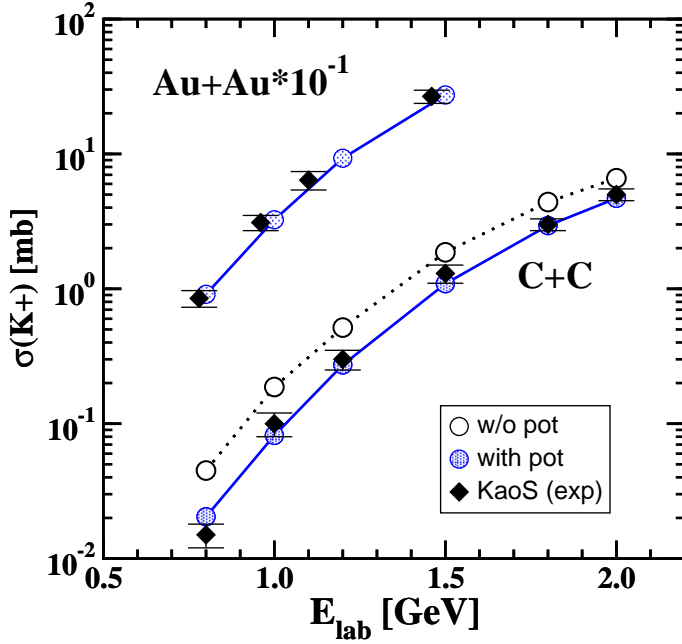


Figure 29: The  $K^+$  excitation functions in Au+Au (scaled by  $10^{-1}$ ) and C+C reactions are compared to data from KaoS [205, 142]. Calculations include an in-medium kaon potential. For C+C also results w/o in-medium potential are shown.

are shown in Fig 29. Calculations were performed with  $b_{\max} = 11$  fm for Au+Au and  $b_{\max} = 5$  fm for C+C and are normalized to the experimental reaction cross sections. The comparison to data from KaoS [142, 205] clearly supports the existence of such a repulsive  $K^+$  potential.

The same conclusion has been obtained by other groups, e.g. the Texas and Stony Brook groups [95, 154, 14, 206] and the Nantes group [96]. For some time these findings were in contradiction to calculations from the Giessen group [94, 116, 25, 121] where the in-medium suppression of the  $K^+$  yield was found to be of similar size but corresponding data were then underpredicted. The reason for this discrepancy could be traced back to the usage of different elementary cross sections, in particular for the  $N\Delta \leftrightarrow NYK^+$  channels (see also Fig. 23). The cross sections used by the Giessen group have been derived from  $pp \leftrightarrow p\Lambda K^+$  by isotopic relations while the calculations of the present work (Tübingen group) are based on the cross sections of Tsushima et al. [207] for the  $N\Delta$  channel. The latter ones have a better theoretical foundation and are now standardly used in transport calculations. However, in earlier calculations the uncertainty due to this channel (not constrained by data) was of the same order as the net potential effect. When model calculations are based on comparable sets of elementary cross sections the results of the various transport models are rather consistent, as can be seen from Figs. 26 and 30.

Fig. 30 compares the  $K^+$  rapidity distributions in Ni+Ni reactions at 1.93 AGeV to data from FOPI [135] and KaoS [157] \*. Again the description of the data requires the repulsive mean field. The same conclusions are obtained from IQMD [96] and the RBUU calculations of Mishra et al. [204], now with

\* $Y^{(0)}$  denotes the center-of-mass rapidity normalized to the projectile rapidity  $Y^{(0)} = (Y/Y_{\text{proj}})_{\text{c.m.}} = 2Y_{\text{lab}}/Y_{\text{beam}} - 1$ .

the  $N\Delta \rightarrow XK^+$  cross sections of Tsushima et al. [207]. The RBUU calculations shown here are based on a chiral mean field evaluated in relativistic Hartree approximation with  $\Sigma_{KN} = 450$  MeV [204]. The range term is included and thus the mean field is close to that one used in the present QMD calculations. The IQMD calculations are based on the RMF kaon optical potential of Schaffner et al. [56] which is also of similar strength than the chiral mean field. The suppression of the kaon production by the repulsive

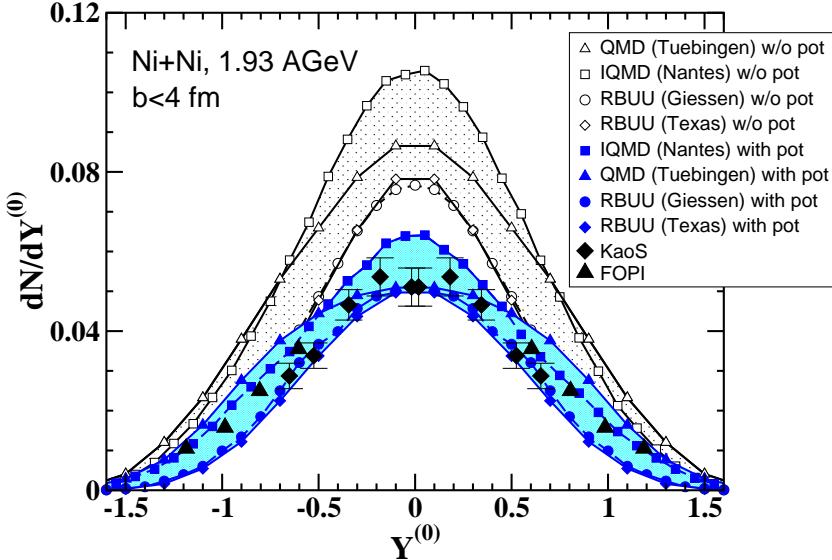


Figure 30:  $K^+$  rapidity distributions in Ni+Ni reactions at 1.93 AGeV obtained including and w/o an in-medium kaon potential. QMD, IQMD [96] and RBUU (Giessen from [204], Texas from [197]) and calculations are compared to data from FOPI [135] and KaoS [157].

in-medium potential is most pronounced at mid-rapidity which is understandable from kinematical reasons. Since subthreshold particle production takes dominantly place around mid-rapidity the kaons are produced close to threshold where in-medium shifts have maximal impact. As already reflected in Fig. 26 the in-medium effect is slightly stronger in the IQMD calculations [96] compared to QMD and RBUU. Both RBUU calculations use a slightly weaker in-medium potential (RBUU Giessen is based on the chiral RHA potential of [204] and RBUU Texas on the empirical potential of [197]). In the QMD calculation the in-medium potential leads not only to a suppression but also to a slight broadening of the rapidity distribution which is due to the covariant dynamics including the Lorentz force. This contribution is absent in the IQMD and RBUU calculations. Although the theoretical descriptions show still same variance they allow nevertheless to distinguish clearly between the two scenarios with and without in-medium effects. Data support the first one.

Another parameter which has influence on the kaon multiplicities is the stiffness of the nuclear equation of state. The EOS dependence will in detail be discussed in the next chapter. The usage of a stiffer nuclear EOS reduces the  $K^+$  yields to some extent, in particular in heavy systems and thus one might be worried that the combination of a hard EOS w/o kaon potential might also be able to match with existing data. But here one can take advantage from the fact that light systems like C+C show almost no nuclear EOS dependence while the influence of the kaon potential is still present. Hence the two effects can be disentangled and the scenario without in-medium kaon potential can be ruled out from the light reaction systems.

Concerning the  $K^-$ 's mesons the situation is more complex and less clear. This is to large part due to the interplay of two different production mechanisms, i.e. strangeness production and strangeness

exchange reactions. Here transport model calculations do not yet deliver a consistent picture. On a qualitative level the in-medium energy shifts can easily be understood within the mean field picture. In  $K^+K^-$  pair production reactions the vector potentials  $\pm V_0$  cancel due to alternating signs for  $K^+$  and  $K^-$  and only the attractive scalar parts  $\Sigma_S$  (30) lead to a shift  $\Delta Q$  of the production thresholds

$$BB \rightarrow BBK^+K^- , \quad \Delta Q = -2\Sigma_S . \quad (101)$$

The same holds for the combination of strangeness production and strangeness exchange which involves the excitation of an intermediate hyperon

$$\left. \begin{array}{l} BB \rightarrow BYK^+ , \quad \Delta Q = V_0 - \Sigma_S \\ \pi Y \rightarrow BK^- , \quad \Delta Q = -V_0 - \Sigma_S \end{array} \right\} \Delta Q = -2\Sigma_S . \quad (102)$$

The latter can be viewed as a three-body process  $\pi BB \rightarrow BBK^+K^-$  which is energetically favored compared to the two-body process  $BB \rightarrow BBK^+K^-$ . Exactly the same arguments can be applied to the pion induced pair production  $\pi B \rightarrow BK^+K^-$  and effective three-body process  $\pi\pi B \rightarrow BK^+K^-$  which runs over strangeness exchange via an intermediate hyperon. If there are enough pions in the system these processes are the dominant sources for  $K^-$  production [116, 120]. From these considerations one would conclude that the  $K^-$  production threshold is generally lowered by  $\Delta Q = -2\Sigma_S$  and the corresponding  $K^-$  should be significantly enhanced by the presence of the in-medium potentials.

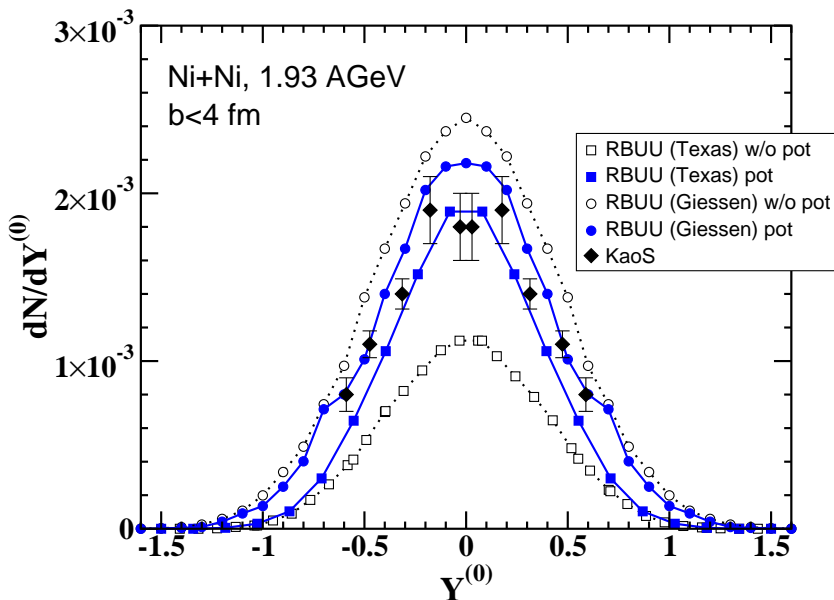


Figure 31:  $K^-$  rapidity distributions in Ni+Ni reactions at 1.93 AGeV obtained including and without in-medium kaon and antikaon potentials. RBUU calculations (Giessen from [204], Texas from [197]) are compared to data from KaoS [157].

However, these arguments are only valid if strangeness production and strangeness exchange reactions take place at equal nuclear densities where the corresponding potentials are of equal size. This is generally not the case (see also Chap. 3). While strangeness production takes predominantly place in the early high density phase, strangeness exchange reactions are the driving processes for  $K^-$  production and absorption at later stages and lower nuclear densities [111, 120]. Now the balance between attractive and repulsive potential shifts is violated. The same holds when less attractive  $K^-$  potentials, e.g. from coupled channel calculations are used instead of mean fields potentials. Hence the net effect of

the in-medium potentials on the  $K^-$  yield may be small [120, 121, 204]. Also the data situation is much less satisfying than for  $K^+$ . Some older transport calculations explain the available  $K^-$  yields better using in-medium potentials [154, 25]. The comparison to old Ni+Ni in 1997 data clearly needed strong  $K^-$  potentials. In more recent measurements the  $K^-$  yield was found to be about a factor of two lower [157]. Fig. 31 compares recent RBUU results from Giessen [204] and Texas [197] to  $K^-$  multiplicities measured by KaoS in semi-central Ni+Ni reactions at 1.93 AGeV. Both models support the  $K^-$  in-medium scenario, but on the basis of a qualitatively different behavior. While the results of Chen et al. [197] follow the argumentation above, leading to an enhanced  $K^-$  yield when potentials are switched on, the results from Mishra et al. [204] show the opposite behavior. The  $K^-$  yields depend not only on the strength of the attractive  $K^-$  potential but, due to strangeness exchange, also on the strength of the repulsive  $K^+$  potential. Around threshold the number of  $K^+$  mesons and, correspondingly, that of  $\Lambda$ 's in the system is about one order of magnitude larger than that of primary  $K^-$  mesons. Small relative changes in the  $\Lambda$  abundances can have large impact on the final  $K^-$  yields. This complicated interplay can even lead to a reversed potential dependence of the  $K^-$  yield as has first been pointed out by Hartnack et al. [120]. The results from Ref. [204] shown in Fig. 31 are based on the chiral RHA potential, i.e. the same model as applied in Fig. 30 for  $K^+$ , which is able to reproduce both sets of data. Slightly different mean fields which reproduce the  $K^+$  data as well were found to fail for  $K^-$  [204]. Hence, the measured  $K^-$  yields allow at present no definite conclusions on the strength of the attractive  $K^-$  potential. The situation is further complicated by a possible strong medium dependence of the strangeness exchange reactions  $\pi Y \longleftrightarrow NK^-$  which is, however, theoretically not yet completely settled. The predictions obtained within coupled channel calculations range from a moderate enhancement close to threshold [68, 37] to a strong suppression [121]. A consistent treatment of these effects requires in any case to account for the off-shell dynamics within the transport approach. The off-shell calculations of [121] support the scenario of in-medium potential shifts for  $K^-$ .

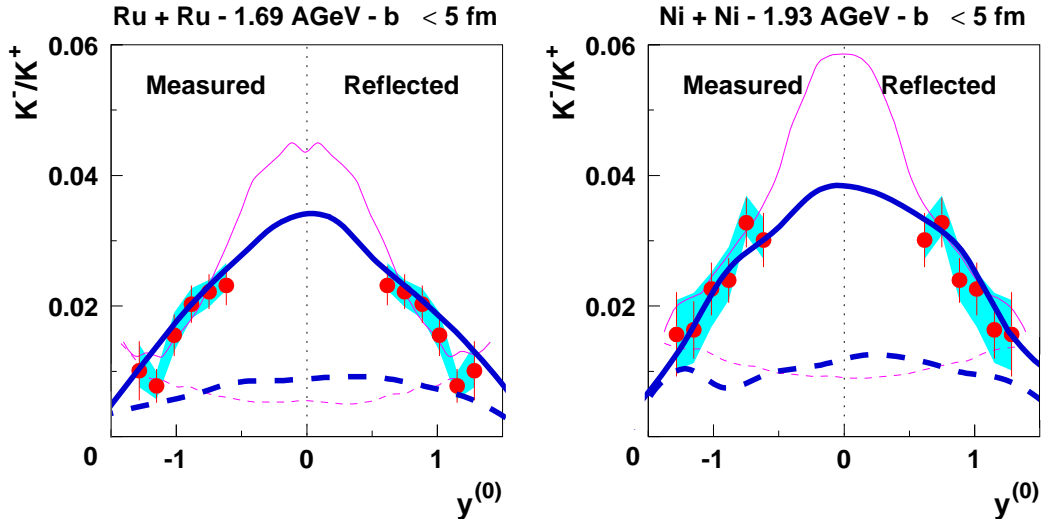


Figure 32:  $K^-/K^+$  ratio as a function of rapidity in Ru+Ru reactions at 1.69 AGeV and Ni+Ni reactions at 1.93 AGeV. RBUU calculations (thick lines: Ref. [25], thin lines: Ref. [206]) are compared to FOPI data [155]. In both cases solid lines include in-medium potentials, dashed lines refer to calculations without in-medium potentials. The figure is taken from [155].

The situation should become clear if one considers the  $K^-/K^+$  ratio, in particular its phase space dependence. This is done in Fig. 32 where FOPI data [155] for the  $K^-/K^+$  ratio as a function of rapidity are compared to transport results from [206] and [25]. Without further in-medium effects the distributions are predicted to be flat as also expected within a statistical approach. The presence of the potentials pushes the kaons outwards to higher rapidities while the attractive antikaon potential binds

$K^-$ 's at mid-rapidity. Both effects lead to an increase of the  $K^-/K^+$  ratio around mid-rapidity as also seen in the data. Supplementary data from KaoS [157] show that  $K^-/K^+$  ratio reaches in Ni+Ni at 1.93 AGeV a value of about 0.04 at mid-rapidity which is in good agreement with the predictions from [25] (with pot.) but in contrast to those of [206] where the in-medium effects are over estimated. However, more recent calculations which include in-medium modifications of the pion induced  $K^-$  production cross sections  $\pi Y \rightarrow NK^-$  and the corresponding absorption cross sections do no longer deliver such a clear picture [68, 62]. The  $K^-$  chemistry and the freeze-out time depends crucially on the magnitude of the strangeness exchange cross sections and this seems also to be reflected in the corresponding rapidity distributions. As already mentioned, the medium modifications of the cross sections are still a matter of current debate.

## 5.2 Dynamical Observables

Dynamical observables such as collective flow patterns are to large extent free from uncertainties in the total production rates. They depend on the phase space pattern of the primordial sources and the final state interaction. For  $K^+$  mesons the final state interaction is well under control since only elastic (and charge exchange) reactions occur, the total elastic cross section is of the order of  $10 \div 15$  mb.

### 5.2.1 In-plane flow

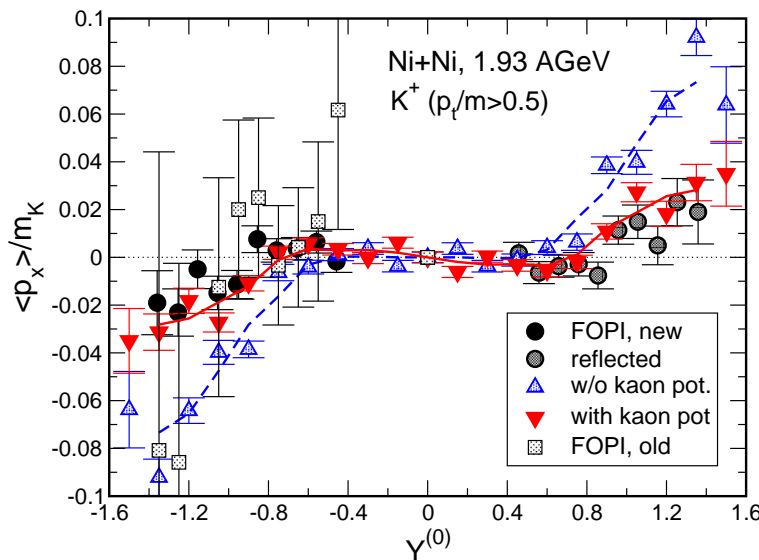


Figure 33: Transverse  $K^+$  flow in 1.93 AGeV  $^{58}\text{Ni} + ^{58}\text{Ni}$  reactions at impact parameter  $b \leq 4$  fm. Calculations with and w/o kaon in-medium potential are compared to FOPI data [3] (old) and [208] (new). The MFT ChPT+corr. potential is used brown96b and the Lorentz force is included.

The transverse or in-plane flow of  $K^+$  mesons is a particularly attractive observable. It was first proposed by Ko and Li [39] that the kaon flow pattern should provide a sensitive probe for the in-medium kaon potential. The repulsive potential should push the kaons away from the nuclear matter and produce slight anti-flow at spectator rapidities and a zero flow signal around mid-rapidity. This was found to be consistent with the first available flow data from FOPI [3]. Other theoretical studies predicted similar features for the kaon flow [94, 183, 159, 160]. However, as pointed out by Fuchs et al. [46] the scalar-vector type structure of the kaonic mean field implies the occurrence of a Lorentz-force (LF) in moving frames which has been disregarded in the previous investigations. The Lorentz-force from the vector field counterbalances the influence of the time-like vector potential on the  $K^+$  in-plane

flow to large extent (see discussion in Chap. 4) which makes it more difficult to draw definite conclusions from transverse flow pattern.

In Refs. [182, 200] the  $K^+$  flow in Ni+Ni reactions was re-investigated since in the meantime FOPI data with improved statistics became available [208]. As can be seen from Fig. 33 it is difficult to distinguish between the scenarios w/o in-medium potentials and full covariant in-medium dynamics around mid-rapidity. However, at spectator rapidities clear differences appear and the data favor again the in-medium scenario. The QMD calculations are based on the MFT ChPT+corr. potential brown96b including the LF. Very similar results have been obtained in [200] where the same potential (including LF) has been used. In both, QMD [182] and BUU [200], the data are best described by the relatively strong MFT ChPT+corr. mean field while the weaker MFT ChPT potential or no potential at all lead to too strong flow at spectator rapidities. The dependence of the kaon flow on the nuclear EOS and the Coulomb force is quite weak [159, 182]. The present calculations are based on a soft nuclear EOS and the Coulomb force is included.

Since the magnitude of the Lorentz-force depends on the size of the vector potential an explicit momentum dependence of these potentials beyond mean field can reduce the Lorentz force. Such a momentum dependence reduces the nucleon flow in relativistic approaches compared to a mean field description, e.g. within QHD. An explicit momentum dependence is necessary in order to comply with the empirical optical nucleon-nucleus potential and nucleon flow data above 1 AGeV [209, 210, 211]. Similarly, spectra ( $p_{\text{lab}}$ ,  $p_T$  and  $m_T$ ) imply that the  $KN$  interaction is less repulsive at high  $p_T$  which might be an indication for an explicit momentum dependence counterbalancing the Lorentz force to some extent. Slopes obtained – in particular in central – Au+Au reactions are too hard while C+C spectra spectra are well described [200] (see also Fig. 24). The FOPI Collaboration measured also the  $p_T$  dependence of  $v_1$  in Ni+Ni and Ru+Ru reactions at spectator rapidities where a transition from anti-flow to flow with rising  $p_T$  was observed [212]. Also these data require a repulsive in-medium potential as found in RBUU [212]. Recent BUU calculations [200] indicate that the Lorentz force is thereby essential not to overestimate the data. Hence, for a precise determination of the density *and* momentum dependence of the  $K^+$  potential more theoretical efforts are needed.

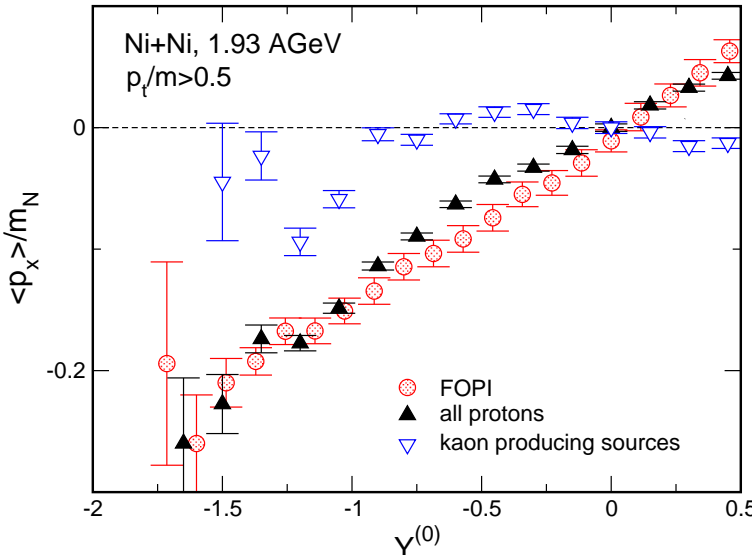


Figure 34: Transverse flow of the kaon production sources in 1.93AGeV  $^{58}\text{Ni} + ^{58}\text{Ni}$  reactions. The total proton flow is compared to FOPI data [3].

In this context one might worry about conclusions based on the small kaonic flow signal (about  $10^{-3}$  of the initial kinetic energy) if it is not completely clear how well the flow of the primordial sources is under control. The proton flow, shown in Fig. 34, is reasonably well described by present transport

models but there exist still deviations from data which are generally on the 10% level. The situation is, however, less severe since the final proton and kaon flow pattern are only very loosely connected [184]. The production sources carry a large in-plane flow while the kaons themselves carry a much smaller flow fraction since, at given rapidity, they are produced from two baryons originating from very different rapidity regions. Therefore baryon sources with positive and negative  $p_x$  add up to an almost vanishing net flow (see the results given by open down triangles in Fig. 34.  $\Lambda$ 's which are produced in association with  $K^+$ 's have very similar flow pattern as protons, i.e. they show almost the same  $p_x/m$  scaling [208]. In [180] the  $\Lambda$  flow was investigated within the present model and the data were best reproduced including the hyperon mean field according to SU(3) scaling  $U_{\text{opt}}^Y = \frac{2}{3}U_{\text{opt}}^B$ . As also observed in [160] the primordial  $\Lambda$  flow is moderate but strongly enhanced by the  $\Lambda N$  final state interactions, i.e. rescattering and the  $\Lambda$  mean field.

### 5.2.2 Out-of-plane flow

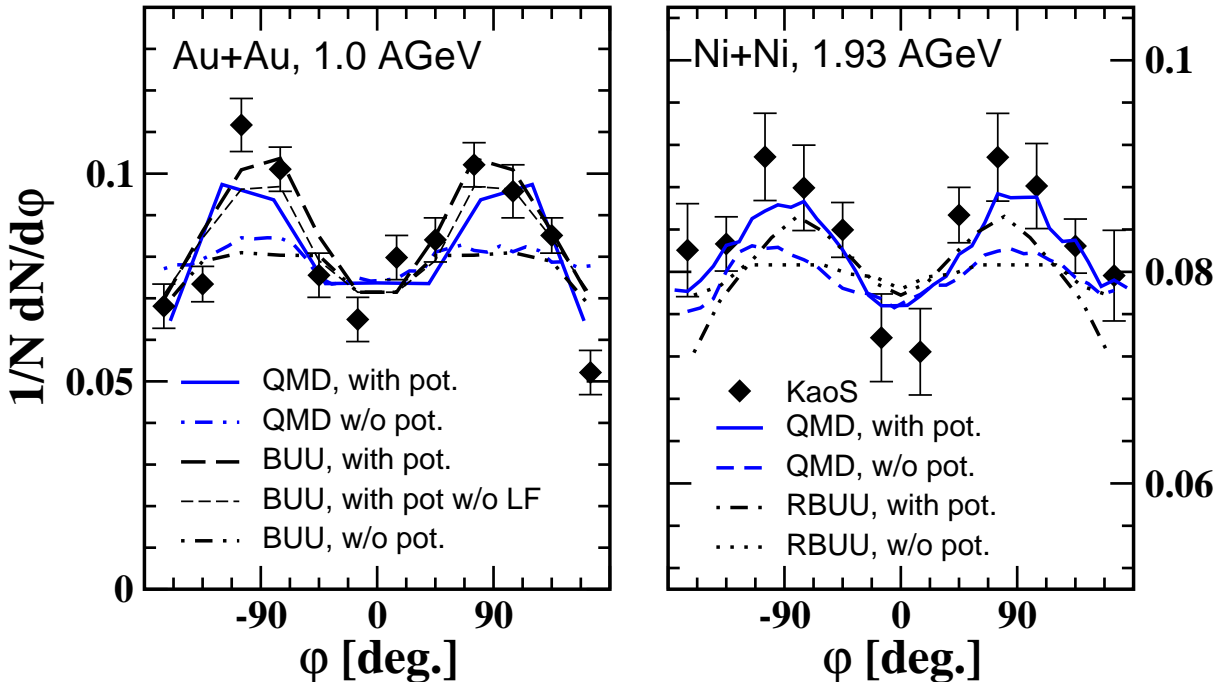


Figure 35:  $K^+$  azimuthal angular distributions in semi-central  $\text{Au+Au}$  reactions at  $1.0 \text{ AGeV}$  and  $\text{Ni+Ni}$  reactions at  $1.93 \text{ AGeV}$ . QMD, BUU [200] and RBUU [213] calculations without and with in-medium potential are compared to data from KaoS [161, 214].

The phenomenon of collective flow can generally be characterized in terms of anisotropies of the azimuthal emission pattern, expressed in terms of a Fourier series

$$\frac{dN}{d\phi}(\phi) \propto 1 + 2v_1 \cos(\phi) + 2v_2 \cos(2\phi) + \dots \quad (103)$$

which allows a transparent interpretation of the coefficients  $v_1$  and  $v_2$ . The dipole term  $v_1$  arises from a collective sideward deflection of the particles in the reaction plane and characterizes the transverse flow in the reaction plane. The second harmonics describes the emission pattern perpendicular to the reaction plane. For negative  $v_2$  one has a preferential out-of-plane emission, called *squeeze-out*. Pions exhibit a clear out-of-plane preference [215, 216] which is due to shadowing by spectator nucleons. The short mean free path of the pions hinders pions produced in the central reaction zone to traverse the spectator matter located in the reaction plane. Therefore it is easier for them to escape perpendicular

to the reaction plane [136]. Since the  $K^-$  mean free path is comparable to that of the pions one might expect the same phenomenon for  $K^-$  while the mean free path of  $K^+$  mesons is large and no squeeze-out signal should be observed. These arguments hold when the final state interaction is exclusively determined by scattering and absorption processes. However, the presence of a mean field changes the dynamics. Azimuthal anisotropies are therefore considered as a suitable tool to study medium effects.

The azimuthal asymmetry of the  $K^+$  production in heavy ion reactions has been first studied by Li et al. [217]. First data from KaoS [161] for semi-central Au+Au at 1 AGeV showed a clear squeeze-out signal for midrapidity kaons. In corresponding transport calculations from the Texas/Stony Brook group [217, 161] and the Tübingen group [179] the data could only be reproduced by the presence of the repulsive  $K^+$  mean field. Elastic rescattering of  $K^+$  mesons was found to be too weak to create the observed squeeze-out signal. However, if the repulsive potential is taken into account, the kaons are driven by potential gradients preferentially out-of-plane since gradients are larger perpendicular than parallel to the reaction plane. With other words, in the reaction plane the kaons are repelled by the spectator matter. Thus, the potential leads to an additional dynamical focusing out of the reaction plane.

Fig. 35 shows the azimuthal distributions for semi-central Au+Au reactions at 1 AGeV and Ni+Ni at 1.93 AGeV [214]. In both cases a transverse momentum cut of  $0.2 < p_t < 0.8$  GeV/c and a mid-rapidity cut of  $|Y^{(0)}| < 0.2$  (Au+Au) and  $|Y^{(0)}| < 0.4$  (Ni+Ni) has been applied. The corresponding impact parameters ranges are  $5 < b < 10$  fm (Au+Au) and  $3.8 < b < 6.5$  fm (Ni+Ni). In the Au+Au case we compare QMD calculations and recent BUU calculations from Larionov et al. [200] to the KaoS data [161]. The results confirm the findings that the in-medium potential is needed in order to explain the experimental squeeze-out signal. Another interesting observation is the fact that the Lorentz force, present in covariant dynamics, has only a small influence on the out-of-plane flow, contrary to the in-plane flow discussed above [200] <sup>†</sup>. The BUU calculations are based on the same kaon mean field as QMD, i.e. on Ref. [31]. For the Ni+Ni system shown in the right panel of Fig. 35 also full experimental filter cuts are applied ( $0.267 < p_{\text{lab}} < 1.182$  GeV/c and a  $28 < \Theta_{\text{lab}} < 54$ ). The calculations with in-medium potential include the full covariant dynamics. For completeness the right panel of Fig. 35 shows also recent RBUU/HSD calculations [213] based on the chiral RHA potential [204] which agree well with QMD. In summary, there exists a convergence of the various transport models on the conclusion that the azimuthal  $K^+$  emission pattern require a repulsive mean field.

Turning to  $K^-$  the situation is less clear. The first predictions for  $K^-$  out-of-plane emission pattern were made by Wang et al. [179] and are shown in Fig. 36. The energy of 1.8 AGeV has been chosen threshold equivalent to  $K^+$  at 1 GeV. The results shown in Fig. 36 were obtained at mid-rapidity ( $|Y^{(0)}| < 0.2$ ) for a semi-central ( $b=8$  fm) reaction. Standard strangeness exchange reactions  $\pi Y \leftrightarrow K^- N$  ( $Y = \Lambda, \Sigma$ ) have been taken into account and the MFT ChPT mean field (see Fig. 1) has been used. These calculations concentrated on the dynamical mean field effect in the particle propagation and thus shifts of the  $K^+$  and  $K^-$  production threshold by the in-medium potentials have been disregarded.

Under these assumptions a very transparent picture was predicted: due to the short mean free path  $K^-$  behave similar like pions, i.e. they show a clear squeeze-out signal caused by absorption and rescattering. By the presence of a strongly attractive potential this signal is destroyed. In summary: without in-medium potential no squeeze-out signal for  $K^+$  and a strong squeeze-out signal for  $K^-$ , with in-medium potentials a sizable squeeze-out signal for  $K^+$  and an isotropic emission pattern for  $K^-$ . However, already in [179] a freeze-out time or  $p_T$  correlation has been observed, reflected in the  $p_T$  dependence of the  $R_{\text{out/in}}$  ratio.  $R_{\text{out/in}}$  quantifies the strength of the azimuthal asymmetry and is defined by the ratio of the particle multiplicity emitted perpendicular to that emitted parallel to the

---

<sup>†</sup>In contrast to the earlier statement made in [179] we agree with [200] on this point.

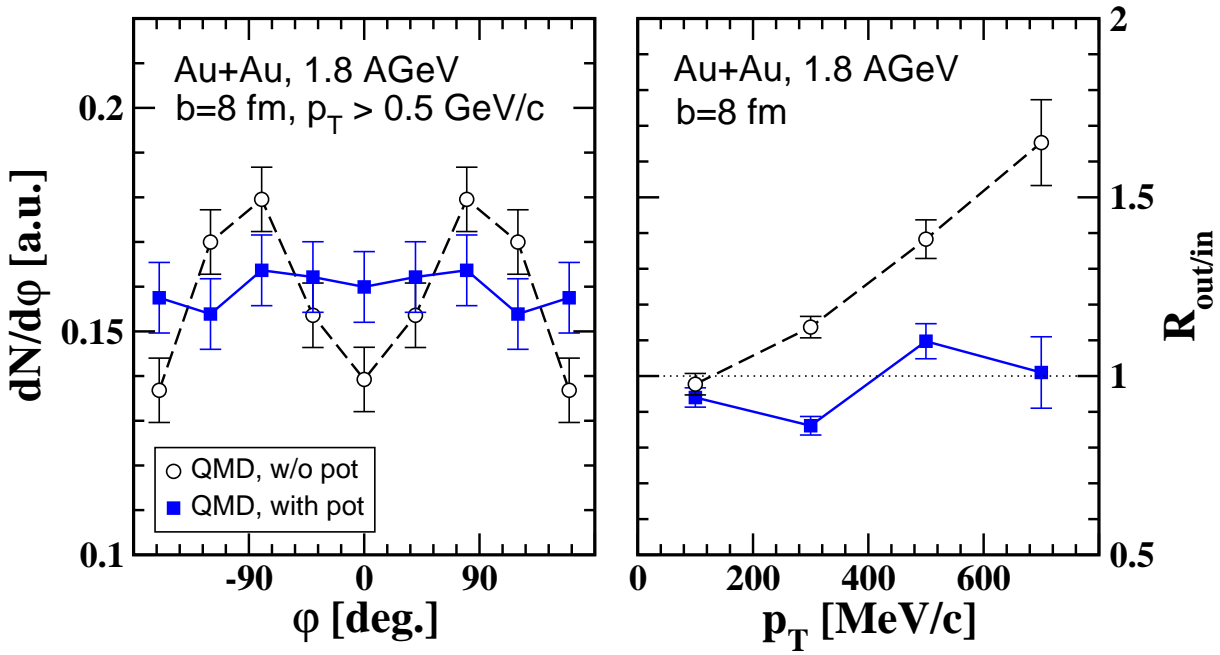


Figure 36:  $K^-$  azimuthal angular distribution and the  $R_{\text{out/in}}$  ratio as a function of  $p_T$  as predicted in Ref. [179] for semi-central Au+Au reactions at 1.8. The calculations have been performed with in-medium  $K^-$  potential. A mid-rapidity cut of  $|Y^{(0)}| < 0.2$  has been applied.

reaction plane

$$R_{\text{out/in}} = \frac{N(\phi = 90^\circ) + N(\phi = 270^\circ)}{N(\phi = 0^\circ) + N(\phi = 180^\circ)} = \frac{1 - 2v_2}{1 + 2v_2} \quad (104)$$

$R_{\text{out/in}} > 1$  corresponds to a preferential out-of-plane emission. The calculation without  $K^-$  potential shows a steady rise of  $R_{\text{out/in}}$  with  $p_T$ , reflected in the emission pattern (Fig. 36 left part) where a  $p_T > 0.5\text{GeV}/c$  cut has been applied. When the potential is switched on  $R_{\text{out/in}}$  is close to unity but high  $p_T$  particles which are assumed to freeze out early carry still some squeeze. The low  $p_T$   $K^-$  mesons are, on the other hand, equilibrated and have flat emission pattern or even a slight in-plane flow. Such a transition from in-plane to out-of-plane flow has recently been observed by KaoS in Au+Au at 1.5 AGeV [218] but the experimental signal is much larger than that obtained in [179].

First data on  $K^-$  azimuthal emission pattern have only recently been delivered by KaoS for the Ni+Ni system at 1.93 AGeV [214]. The data agree with none of the two predicted scenarios but a preferred in-plane emission of the  $K^-$  mesons at mid-rapidity has been observed. Although IQMD transport calculations from the Nantes group match the data when the in-medium potential is used it is not really obvious how such in-plane flow can develop. In [214] it is argued that it might be due to late emission times caused by strangeness exchange reactions  $K^-N \rightarrow Y\pi \rightarrow K^-N$ . However, the same holds for pions which undergo several absorption cycles  $\pi N \rightarrow \Delta \rightarrow \pi N$ , have late emission times but show a clear squeeze-out signal. The main difference between the 1997 QMD calculations from Wang et al. [179] and recent IQMD and RBUU results shown in Fig. 37 lies in the fact that in [179] *free* cross sections without in-medium shifts, both for  $K^+$  and  $K^-$  production and absorption, have been used. Shifts of the thresholds change the  $K^+$  and  $K^-$  multiplicities which, at a first glance, one would not expect to affect flow pattern significantly. However, reduced  $K^+$  multiplicities go in line with a reduced number of hyperons in the system which reduces the  $K^-$  absorption rate and the rate of strangeness exchange reactions  $Y\pi \rightarrow K^-N$ .

Thus the  $K^-$  flow pattern are determined by the interplay between mean field and in-medium cross

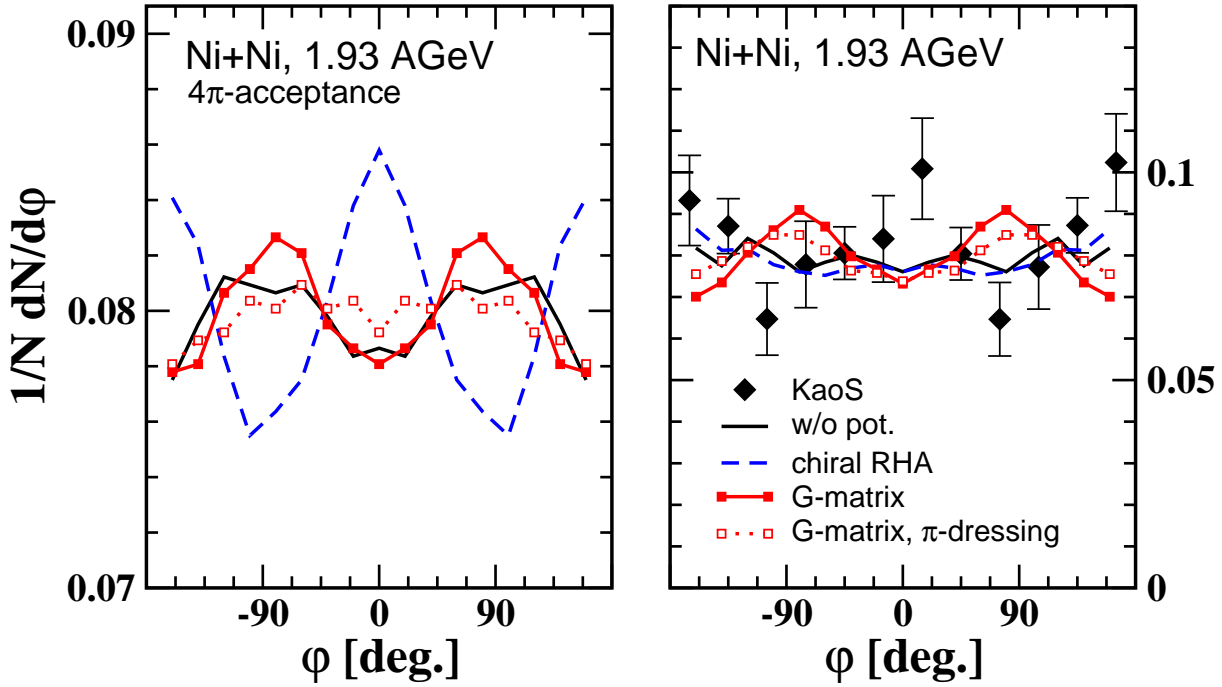


Figure 37:  $K^-$  azimuthal angular distribution in Ni+Ni at 1.93 AGeV. RBUU calculations [213] without and using  $K^\pm$  in-medium potentials of different type are shown for  $4\pi$ -acceptance (left) and compared to the KaoS data [214] with the corresponding acceptance cuts (right).

sections. The medium dependence of the cross sections is significant, in particular when off-shell effects are included. The  $4\pi$  pattern from recent RBUU calculations [213] demonstrate the following: Without any medium effects a clear squeeze-out signal is observed, as predicted in [179]. Using off-shell dynamics based coupled channel G-matrix potentials and in-medium cross sections of Tolos et al. [158, 121] this signal is even enhanced. This potential see Fig. 3, is significantly weaker than the chiral RHA mean field but the  $K^-$  absorption cross sections are strongly enhanced at threshold. This means that the shadowing wins against the attractive potential in this scenario which leads to an even stronger squeeze-out than without in-medium effects. When, on the other hand, pion dressing is taken into account (G-matrix with  $\pi$ -dressing) the situation changes and the azimuthal pattern are almost flat. The corresponding potential is slightly less attractive than in the previous case but the absorption cross sections are now strongly reduced. The last case, namely the strongly attractive chiral RHA potential with free cross sections leads to an anti-squeeze-out which is also seen in the data. However, the KaoS acceptance cuts lead to a strong distortion of the flow pattern and none of the discussed scenarios is able to explain the observed distribution shown in the right panel of Fig. 37. Thus the observed  $K^-$  emission pattern are at present not really understood and further experimental and theoretical efforts are needed to clarify the picture.

## 5.3 Consistency of the results

### 5.3.1 Consistency between transport predictions

Now the question arises up to which degree a consistent picture has emerged after more than ten years of intensive experimental and theoretical efforts to understand kaon production in heavy ion reactions at intermediate energies. Since one of the major goals was to extract information on the existence and size of in-medium potentials we summarize in Table 3 the answers which are provided by present transport calculations. This summary is organized in the following way: for the most important

model	QMD <sup>1</sup>	IQMD <sup>2</sup>	RBUU <sup>3</sup>	RBUU <sup>4</sup>	BUU <sup>5</sup>
$K^+$ multiplicity	●○ [181, 182]†	●○ [96]	●○ [204]	●○ [154, 14, 197]	●○ [200]
$K^+$ flow	●★ [159, 182]†	○★ [184]	●○ [25, 204]	●○ [39, 160]	●○ [200]
$K^+$ squeeze	●○ [179]†	●● [214]	●○ [204]	●○ [161]	●○ [200]
$K^-/K^+$ ratio	—	—	●○ [25]	●○ [154, 206]	○● [68]
$K^-$ multiplicity	—	—	★★ [116, 121, 204]	●○ [154, 197]	—
$K^-$ squeeze	○○ [179]	●○ [214]	○○ [204], ●○ [121]	—	—

Table 3: Comparison of various transport model calculations with existing data: the calculations are from <sup>1</sup>Tübingen († besides the given references also results from the present work are included), <sup>2</sup>Nantes, <sup>3</sup>Giessen (RBUU/HSD), <sup>4</sup>Texas/Stony Brook, <sup>5</sup>Giessen(Berkeley). Symbols denote: ●≡ good description of available data within error bars; ○≡ clear failure to describe available data within error bars; ★≡ situation unclear. The first symbol corresponds to calculations based on kaon in-medium potentials while the second one corresponds to the case w/o in-medium potential.

measured observables the agreement or disagreement of transport calculations of different groups, using independent simulation codes and models, is classified by three classes:

A filled bullet (●) denotes a good agreement within error bars with the bulk of existing data for this observable, an open bullet (○), on the other hand, denotes a clear disagreement. When the situation is unclear, i.e. when calculations match part of the data and fail for other parts, this is indicated by a star (★). In each case two symbols are shown. The first one corresponds to the in-medium scenario, i.e. the calculations using in-medium potentials, while the second one corresponds to calculations without kaon potentials. Hence a combination (●○) means that the corresponding observable allows to clearly distinguish between the two scenarios and data support the existence of in-medium potentials, (○●) would mean the opposite.

It is clear that such a classification is rough since the data situation strongly differs from observable to observable, the transport models differ at least partially in their input and the level of sophistication and do not in each case compare to the complete set of available data in one observable class. Nevertheless, there exists the necessity to bring some systematics into the theoretical predictions.

As already discussed in Chapters 3 and 4 the various transport approaches differ partially in the elementary input and in the technical realizations. Table 4 summarizes the most relevant differences. These lie in usage of different parameterizations for the strangeness production cross sections  $NN \leftrightarrow NYK^+$ <sup>‡</sup>,  $N\Delta \leftrightarrow NYK^+$  and the medium dependence of the strangeness exchange cross sections  $N\pi \leftrightarrow YK^-$ . The  $K^+$  production cross sections are either based on one-boson-exchange (OBE) or resonance model (R) calculations where parameters are fixed by the measured  $pp \leftrightarrow p\Lambda K^+$  reaction. For the pion induced  $K^+$  production all approaches apply the cross section of [110]. (P) denotes parameterizations of experimental cross sections which are in particular used for the well constrained strangeness exchange reactions. However, here the intrinsic medium dependence of these cross sections is crucial and has been explored in chiral coupled channel (CC) [68] and coupled channel G-matrix (CCG) [63] calculations. The medium dependence due to shifts of the threshold by the attractive/repulsive  $K^\pm$  mean field are usually taken into account (mass shifts). Concerning the dynamics one has to distinguish between a non-relativistic treatment of the mean field (nonrel.) and full covariant dynamics (covariant) which includes the vector Lorentz force according to (79) and the off-shell dynamics of [28, 121].

By far the best measured quantity are  $K^+$  multiplicities. High precision data exist for a broad range of energies and different mass systems. For the dynamical observables  $K^+$  flow and squeeze, data are in the meantime also precise enough to constrain the models. For  $K^+$  mesons one can summarize the

<sup>‡</sup>In QMD different parameterizations are applied for the  $\Lambda$  and  $\Sigma$  channel which is indicated in Tab. 4.

Model	$NN \mapsto XK^+$	$N\Delta \mapsto XK^+$	$\pi B \mapsto YK^-$	cross section	dynamics
QMD: [179] [181, 182] present	[97] $\Lambda$ (OBE) [100] $\Sigma$ (R) [97] $\Lambda$ (OBE) [100] $\Sigma$ (R)	[100] (R) [100] (R)	[25] (P) –	free mass shift	nonrel. covariant
IQMD: [184, 96] [214]	[184] (P) [97] $\Lambda$ (OBE) [100] $\Sigma$ (R)	[184] (P) [100] (R)	– (P)	mass shift mass shift	nonrel. nonrel.
RBUU: [116, 25] [121] [204]	[25] (OBE) [25] (OBE) [25] (OBE)	[25] (OBE) [25] (OBE) [100] (R)	[25] (P) [63] (CCG) [63] (CCG)	mass shift mass shift ( $K^+$ ) off-shell ( $K^-$ ) mass shift	nonrel. nonrel. ( $K^+$ ) off-shell ( $K^-$ ) nonrel.
RBUU: [14, 154, 161] [160, 206, 197]	[154] (OBE)	[154] (OBE)	[154] (P)	mass shift	nonrel.
BUU: [68] [200]	[68] (OBE) [100] (R)	– [100] (R)	[68] (CC) –	mass shift ( $K^+$ ) in-med. ( $K^-$ ) mass shift	nonrel. covariant

Table 4: Elementary input, realization of the medium dependence of the cross sections and mean field dynamics in the transport models summarized in Table 3.

situation as follows: there exist no data which contradict the in-medium scenario. In contrast, most observables can *only* be described within the in-medium scenario. For  $K^-$  the data situation as well as the theoretical situation is much less satisfying. No consistent picture has yet emerged which allows to discriminate between the two scenarios.

### 5.3.2 $p + A$ reactions

The picture was recently complemented by measurements of the  $K^+$  production in proton-nucleus reactions [219, 88]. Although such reactions test only subnormal nuclear densities they are much easier to handle than the complicated dynamical evolution of heavy ion reactions. A particularly sensitive

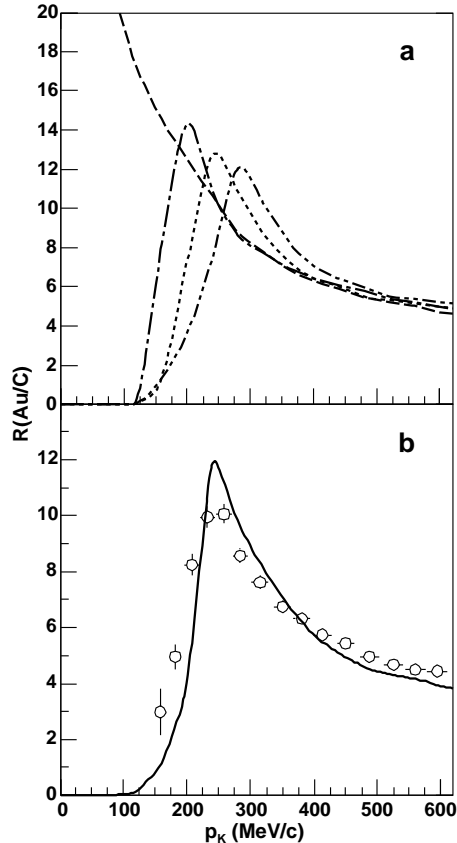


Figure 38: Ratios of  $K^+$  production cross sections for  $p+\text{Au}/p+\text{C}$  at  $T_p = 2.3 \text{ GeV}$  as a function of the kaon momentum. a) Transport calculations including only the Coulomb potential (dash-dotted) and in addition a kaon potential of different strength, i.e. 20 MeV (dotted) and 40 MeV (dashed-double-dotted) at  $\rho_0$ . The broken line corresponds to simulations without Coulomb and nuclear kaon potentials. In all cases considered here,  $K^+$  rescattering in the nucleus has been taken into account. b) The open circles are the experimental data. The solid line shows the result of RBUU transport calculations starting from the dotted line in the top figure with a baryon potential added. The figure is taken from [219].

observable was based on the measurement of the kaon momenta in  $p+\text{Au}$  and  $p+\text{C}$  reactions. A repulsive potential leads to a momentum shift which, in the absence of further final state interactions, results in minimal possible momenta

$$p_{\min} = \sqrt{2m_K(V_C(r) + V_0(r))} . \quad (105)$$

This feature is, e.g. well known from the suppression of  $\beta^+$  emission in heavy nuclei at low positron momenta due to the Coulomb shift. Naturally, such a low momentum shift is more pronounced in a heavy nucleus. Building now the ratio between the heavy and the light system one is sensitive to density effects and thus to the size of the potential.

This is demonstrated in Fig. 38 where the ratio of the  $K^+$  cross section in  $p+Au/p+C$  reactions is shown as a function of the kaon momentum. Taking the Coulomb potential  $V_C$  into account one can determine the strength of  $V_0$  from the peak in the data. This has been done in [219, 85] using transport calculations and a repulsive kaon potential of  $V_0 \sim 20 \pm 5$  MeV at  $\rho_0$  has been extracted. Hence the result is consistent with heavy ion reactions and the magnitude of  $V_0$  as predicted by effective chiral Lagrangians. Such a potential was also found to be consistent with the measured  $K^+$  spectra in  $p+A$  reactions at subthreshold energies [85].

## 6 Probing the nuclear equation of state

Heavy ion reactions provide the only possibility to reach nuclear matter densities beyond saturation density  $\rho_0 \simeq 0.16 \text{ fm}^{-3}$ . Transport calculations indicate that in the intermediate energy range  $E_{\text{lab}} \simeq 1 \text{ AGeV}$  nuclear densities between  $2 \div 3\rho_0$  are accessible while the highest baryon densities ( $\sim 8\rho_0$ ) will probably be reached in the energy range of the future GSI facility FAIR [220] between  $20 \div 30 \text{ AGeV}$ . At even higher incident energies transparency sets in and the matter becomes less baryon rich due to the dominance of meson production. Since the knowledge of the nuclear equation-of-state (EOS) at supranormal densities is essential for our understanding of the nuclear forces as well as for astrophysical purposes, the determination of the EOS was already one of the primary goals when first relativistic heavy ion beams started to operate in the beginning of the 80ties [221]. In the following we will briefly report the knowledge on the nuclear EOS from a theoretical point of view, then turn to the compression phase in heavy ion reactions, give a short review on possible observables and finally discuss the recent progress achieved by the kaon measurements.

### 6.1 Modeling the nuclear EOS

#### 6.1.1 Predictions for the nuclear EOS

Models which make predictions on the nuclear EOS can roughly be divided into three classes:

1. **Phenomenological density functionals:** These are models based on effective density dependent interactions such as Gogny or Skyrme forces [222] or relativistic mean field (RMF) models [57]. The number of parameters which are fine tuned to the nuclear chart is usually larger than six and less than 15. This type of models allows the most precise description of finite nuclear properties.
2. **Effective field theory approaches:** Models where the effective interaction is determined within the spirit of effective field theory (EFT) become recently more and more popular. Such approaches lead to a more systematic expansion of the EOS in powers of density, respectively the Fermi momentum  $k_F$ . They can be based on density functional theory [223, 224] or e.g. on chiral perturbation theory [225, 226]. The advantage of EFT is the small number of free parameters and a correspondingly higher predictive power. However, when high precision fits to finite nuclei are intended this is presently only possible by the price of fine tuning through additional parameters. Then functionals based on EFT have approximately the same number of parameters as phenomenological density functionals.
3. **Ab initio approaches:** Based on high precision free space nucleon-nucleon interactions, the nuclear many-body problem is treated microscopically. Predictions for the nuclear EOS are parameter free. Examples are variational calculations [227, 228], relativistic [167, 229, 230, 231] or non-relativistic Brueckner calculations and Greens functions Monte-Carlo approaches [232].

Phenomenological models as well as EFT contain parameters which have to be fixed by nuclear properties around or below saturation density which makes the extrapolation to supra-normal densities somewhat questionable. However, in the EFT case such an extrapolation is safer due to a systematic density expansion. One has, nevertheless, to keep in mind that EFT approaches are in general based on low density expansions. Many-body calculations, on the other hand, have to rely on the summation of relevant diagram classes and are still too involved for systematic applications to finite nuclei. In the following we will restrict the discussion mainly to the prediction from many-body calculations.

In the relativistic Brueckner approach the nucleon inside the nuclear medium is viewed as a dressed particle in consequence of its two-body interaction with the surrounding nucleons. The in-medium interaction of the nucleons is treated in the ladder approximation of the relativistic Bethe-Salpeter (BS) equation

$$T = V + i \int V Q G G T \quad , \quad (106)$$

where  $T$  denotes the T-matrix, while  $V$  is the bare nucleon-nucleon interaction. The intermediate off-shell nucleons in the scattering equation are described by a two-particle propagator  $iGG$ . The Pauli operator  $Q$  accounts for the influence of the medium by the Pauli-principle and projects the intermediate scattering states out of the Fermi sea. The Green's function  $G$  fulfills the Dyson equation

$$G = G_0 + G_0 \Sigma G \quad . \quad (107)$$

$G_0$  denotes the free nucleon propagator while the influence of the surrounding nucleons is expressed by the nucleon self-energy  $\Sigma$ . In Brueckner theory this self-energy is determined by summing up the interaction with all the nucleons inside the Fermi sea in Hartree-Fock approximation

$$\Sigma = -i \int_F (Tr[GT] - GT) \quad . \quad (108)$$

The coupled set of equations (106)-(108) represents a self-consistency problem.

Fig. 39 compares the saturation points of nuclear matter obtained by relativistic Dirac-Brueckner-Hartree-Fock (DBHF) calculations using the Bonn potentials [233] as bare  $NN$  interactions to non-relativistic Brueckner-Hartree-Fock calculations for various  $NN$  interactions. The DBHF results are taken from Ref. [167] (BM) and more recent calculations based on improved techniques are from [229] (Tübingen). In these calculations the Bonn A interactions matches with the empirical region of saturation, however, still at a slightly too high density. For various  $NN$  potentials the non-relativistic results lie on the so called *Coester line* which misses the empirical region of saturation. Only by the inclusion of 3-body-forces (shown by the dashed square in Fig. 39) the situation can be improved [234, 235]. The contributions from 3-body-forces (3-BFs) are in total repulsive which makes the EOS harder and non-relativistic calculations come close to their relativistic counterparts when 3-BFs are included. The same effect is observed in variational calculations [228]. The variational approach shown contains relativistic boost corrections to the potential which lead to additional repulsion [228]. Both, the BHF calculations from [234] and the variational calculations from [228] are based on the latest AV<sub>18</sub> version of the Argonne potential. In both cases phenomenological 3-body-forces are used, the Tucson-Melbourne 3-BF in [234] and the Urbana IX 3-BF (using boost corrections the repulsive contributions of the UIX interaction are reduced by about 40% compared to the original ones) in [228]. Except of ChPT [236] there exists no systematic generation of 3-BF contributions \*. On the other hand, contributions from 3-body-forces are to large extent canceled by box diagrams containing resonance excitations and/or are partially effectively included in the relativistic approach (see e.g. the discussion in [230, 237]). This fact should make an application of DBHF at supra-normal densities more reliable. Fig. 40 compares

---

\*Next to leading order all 3-BFs cancel while non-vanishing contributions appear at NNLO [236].

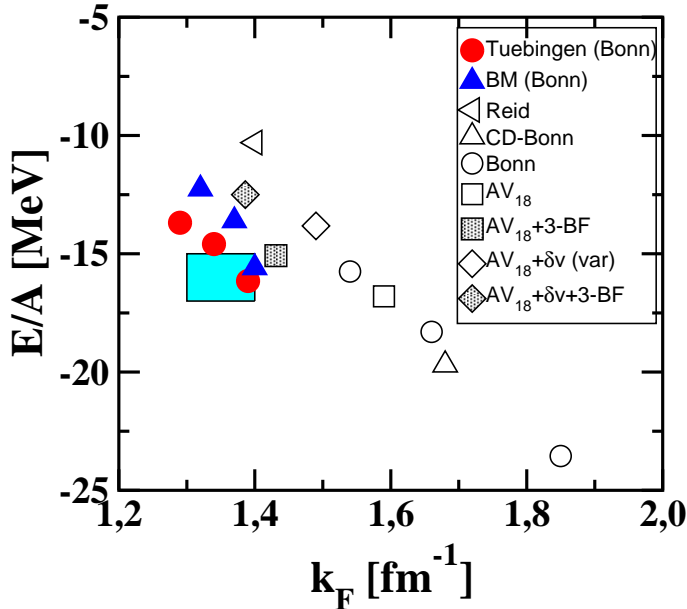


Figure 39: Nuclear matter saturation points from relativistic (full symbols) and non-relativistic (open symbols) Brueckner-Hartree-Fock calculations based on different nucleon-nucleon forces. The diamonds show results from variational calculations. Shaded symbols denote calculations which include 3-body forces. The shaded area is the empirical region of saturation.

the equations of state from the different approaches, i.e. relativistic DBHF from Ref. [229] based on the Bonn A interaction<sup>†</sup> [233], non-relativistic BHF [234] and variational calculations [228]. The latter ones are based on the Argonne AV<sub>18</sub> potential and include 3-body forces. All the approaches use modern high precision  $NN$  interactions and represent state of the art calculations. The corresponding EOSs can also be compared to phenomenological parameterizations.

In Fig. 40 two Skyrme EOSs are shown which correspond to the limiting cases of a soft ( $K=200$  MeV) and a hard ( $K=380$  MeV) EOS. One can conclude from Fig. 40 that *ab initio* calculations predict throughout a soft EOS in the density range relevant for heavy ion reactions at SIS energies, i.e. up to about three times  $\rho_0$ . There seems to be no way to obtain an EOS as stiff as the hard Skyrme force shown in Fig. 40. This observation stands somehow in contrast to the observations made from fits to finite nuclei. When density functionals are fine tuned to the nuclear chart, e.g. in RMF theory, the corresponding EOS turns out to be relatively stiff [57]. The same observation can be made within EFT. E.g. the EOS obtained from chiral pion-nucleon dynamics by Finelli et al. [226] is rather soft but when phenomenological correction terms are added in order to improve the description of the finite nuclei this results in much stiffer EOS. However, one has to keep in mind that finite nuclei constrain the interaction at saturation density and below. The predictive power of such density functionals at supra-normal densities is therefore restricted.

### 6.1.2 Skyrme forces in QMD

Like for QMD calculations shown in the foregoing chapter the following investigations are based on the soft and hard Skyrme parameterizations. These forces are easy to handle, cover the range of uncertainty concerning the EOS for isospin symmetric nuclear matter and are therefore widely used in transport calculations for heavy ion collisions.

<sup>†</sup>The high density behavior of the EOS obtained with different interaction, e.g. Bonn B or C is very similar. [229]

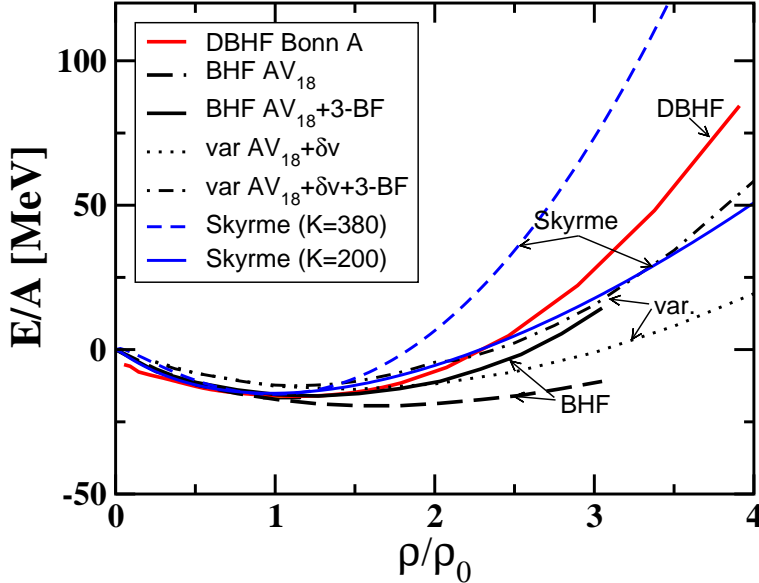


Figure 40: The nuclear matter EOS from soft and hard Skyrme forces are compared to the predictions from microscopic ab initio calculations, i.e. relativistic DBHF [229], non-relativistic BHF [234] and variational [228] calculations.

The QMD N-particle Hamiltonian is given by [23, 24, 238]

$$H = \sum_i \sqrt{\mathbf{k}_i^2 + m_i^2} + \frac{1}{2} \sum_{\substack{i,j \\ (j \neq i)}} (V_{ij}^{\text{Sk}} + V_{ij}^{\text{Yuk}} + V_{ij}^{\text{Coul}}) \quad . \quad (109)$$

The Hamiltonian (109) contains 2-body interactions which are determined as classical expectation values from local Skyrme forces  $V_{ij}^{\text{Sk}}$  supplemented by a phenomenological momentum dependence, an effective Coulomb interaction  $V_{ij}^{\text{Coul}}$  and a Yukawa-type potential  $V_{ij}^{\text{Yuk}}$ . The Yukawa potential mainly serves to improve the surface properties and the stability of the initialized nuclei when used in heavy ion collisions. The individual nucleons are described by Gaussian wave packets with fixed width  $2\sqrt{L}$ . This leads to a one-particle Wigner density

$$f_i(\mathbf{q}, \mathbf{k}, t) = \frac{1}{\pi^3} e^{-(\mathbf{q}-\mathbf{q}_i(t))^2 2/L} e^{-(\mathbf{k}-\mathbf{k}_i(t))^2 L/2} \quad . \quad (110)$$

The Skyrme interaction contains an attractive local two-body part, an effective density dependent repulsive two-body part and an nonlocal momentum dependent two-body part. The elementary two-body potentials entering into (109) read then

$$V^{\text{Sk}} = t_1 \delta^3(\mathbf{q} - \mathbf{q}') + t_2 \delta^3(\mathbf{q} - \mathbf{q}') \rho^{\gamma-1}(\mathbf{q}) + t_3 \ln^2(\epsilon |\mathbf{k} - \mathbf{k}'|^2 + 1) \delta^3(\mathbf{q} - \mathbf{q}') \quad (111)$$

$$V^{\text{Yuk}} = t_4 \frac{e^{-|\mathbf{q}-\mathbf{q}'|/\mu}}{|\mathbf{q}-\mathbf{q}'|/\mu} \quad , \quad V^{\text{coul}} = \left(\frac{Z}{A}\right)^2 \frac{e^2}{|\mathbf{q}-\mathbf{q}'|} \quad . \quad (112)$$

In the case  $\gamma = 2$  the density dependent interaction can be derived from a local three-body interaction. The parameterizations of [23, 24, 238] treat  $\gamma$  as a phenomenological parameter. The folding over the Wigner distributions (110) yields the expectation values

$$\begin{aligned} V_{ij}^{\text{Sk}} &= \int d^3q \, d^3q' \, d^3k \, d^3k' \, f_i(\mathbf{q}, \mathbf{k}, t) \, V^{\text{Sk}}(\mathbf{q}, \mathbf{k}; \mathbf{q}', \mathbf{k}') \, f_j(\mathbf{q}', \mathbf{k}', t) \\ &= \alpha \left(\frac{\rho_{ij}}{\rho_0}\right) + \beta \left(\frac{\rho_{ij}}{\rho_0}\right)^\gamma + \delta \ln^2(\epsilon |\mathbf{k}_i - \mathbf{k}_j|^2 + 1) \frac{\rho_{ij}}{\rho_0}, \end{aligned} \quad (113)$$

where  $\rho_{ij}$  is an interaction density

$$\rho_{ij} = \frac{1}{(4\pi L)^{\frac{3}{2}}} e^{-(\mathbf{q}_i - \mathbf{q}_j)^2/4L}, \quad (114)$$

which arises due to the folding of the two Gaussian wave packets with fixed width  $2\sqrt{L}$  in coordinate space. In analogous way the expectation values of the Yukawa and Coulomb potentials are obtained. The parameters  $\alpha, \beta, \gamma, \delta, \epsilon$  in Eq. (113) are fitted to the saturation point ( $\rho_0 = 0.16 \text{ fm}^{-3}$ ,  $E_B = -16 \text{ MeV}$ ) and the momentum dependence of the real part of the nucleon-nucleus optical potential. The linear density dependence of  $V^{\text{Sk}}$  is obtained from the point-like 2-body interaction in Eq. (111) while the nonlinear density dependence is motivated by point-like 3-body interactions<sup>‡</sup> With this Hamiltonian (109) the EOS of isospin saturated nuclear matter, i.e. the binding energy per particle, is of the simple form[23]<sup>§</sup>

$$E_{\text{bind}} = \frac{E}{A} = \frac{3k_F^2}{10M} + \frac{\alpha}{2} \left( \frac{\rho}{\rho_0} \right) + \frac{\beta}{1+\gamma} \left( \frac{\rho}{\rho_0} \right)^\gamma + \frac{\delta}{2} \ln^2 \left( \epsilon \left( \frac{\rho}{\rho_0} \right)^2 + 1 \right) \frac{\rho}{\rho_0}. \quad (115)$$

In contrast to the Skyrme functional (115) where the high density behavior is fixed by the compression modulus, in microscopic approaches the compression modulus is only loosely connected to the curvature at saturation density. Below  $3\rho_0$ , e.g. the DBHF EOS with  $K=230 \text{ MeV}$  is close to the soft Skyrme EOS but becomes significantly stiffer at higher densities.

## 6.2 Particle production and the compression phase in HICs

### 6.2.1 Pions

With the start of the first relativistic heavy ion programs the hope was that particle production would provide a direct experimental access to nuclear EOS [239]. Without additional compression two times saturation density should be reached in the participant zone of the reactions where the difference between the soft and hard Skyrme EOS is about 13 MeV in binding energy. If the matter could be compressed up to  $3\rho_0$  the difference is already  $\sim 55 \text{ MeV}$ . It was expected that the compressional energy should be released into the creation of new particles, primarily pions, when the matter expands [239]. However, pions have large absorption cross sections and they turned out not to be suitable messengers of the compression phase. They undergo several absorption cycles through nucleon resonances [136, 137, 27] and freeze out at final stages of the reaction and at low densities. Hence pions loose most of their knowledge on the compression phase and are not very sensitive probes for stiffness of the EOS. This fact is illustrated in Fig. 41 which shows the  $\pi^+$  excitation function in minimal bias Au+Au and C+C reactions and compares to data from KaoS [205, 142]<sup>¶</sup>. For C+C there exists practically no dependence of the pion yield on EOS, in Au+Au the dependence is moderate, i.e. of the order of  $\sim 15 - 20\%$ .

A second and important observation, in particular with respect to the  $K^+$  production discussed below, is the fact that the enhancement of the pion multiplicities in Au+Au when using a soft compared to a hard EOS is almost completely independent of the beam energy. This feature becomes even more transparent from the lower part of Fig. 41 which shows the ratio of the total pion multiplicities in  $Au + Au$  over  $C + C$  reactions scaled by the corresponding mass numbers. For this observable the data from KaoS [205, 142] are qualitatively well reproduced. The usage of different nuclear forces leads to a small shift of the theoretical curves but does not change their slope. The fraction is generally below

<sup>‡</sup>A parameter  $\gamma \neq 2$  is purely phenomenological.

<sup>§</sup>The small Coulomb and Yukawa terms as well as relativistic corrections to the kinetic energy corrections have been suppressed.

<sup>¶</sup>Details on the treatment of pions in the present QMD calculations can be found in [27, 26]

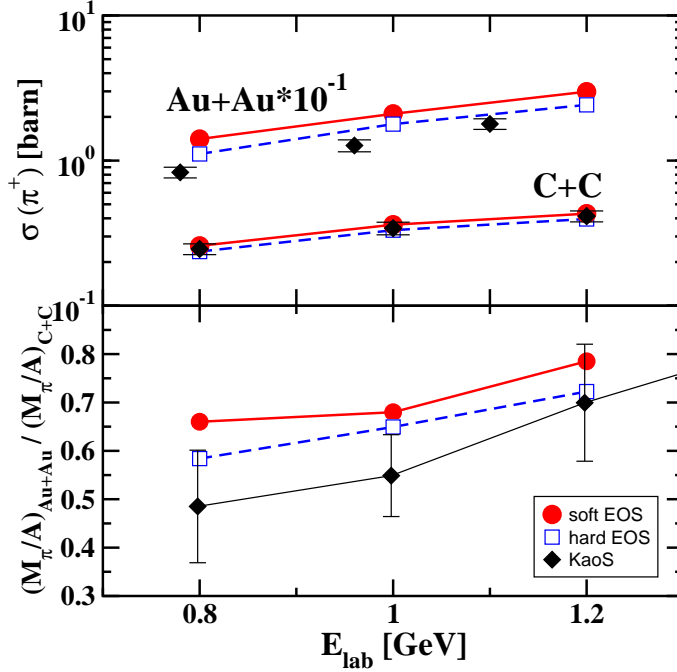


Figure 41: Excitation function of the  $\pi^+$  production cross section in Au+Au (scaled by  $10^{-1}$ ) and C+C reactions (top), and ratio of the total pion multiplicities in Au+Au over C+C. The calculations are performed using a hard/soft nuclear EOS and are compared to data from KaoS [205, 142].

unity indicating the larger absorption rate in  $Au + Au$  compared to  $C + C$ . With rising energy the pion suppression in the heavy compared to the light system becomes smaller as also seen in the data. The dependence of this observable on the nuclear EOS is rather moderate and would not allow to draw some definite conclusions from the model calculations.

The other observation from Fig. 41, namely that experimental pion multiplicities are in the SIS energy range systematically overestimated in large systems like Au+Au is a common (and well known) feature of transport models, independent if they are of BUU or QMD type [136, 137, 241, 27, 242]. It demonstrates that the pion production and/or absorption mechanisms are theoretically not yet fully understood. The pion as a Goldstone boson is the lightest meson with a large Compton wave length and quantum aspects beyond the semi-classical treatment in transport models could be of particular relevance. However, several attempts to go beyond the standard treatments and to account for particular quantum effects such as the coupling to  $\Delta N^{-1}$  excitations [243, 244, 241] or non-localities, i.e. memory effects and time delays in resonance decays [245, 246] did not really improve on this discrepancy and solve the problem. Since pions are a source for kaon production through pion induced reactions one could consider this fact as a severe uncertainty. Fortunately, the situation is less worse since the overestimation of the experimental pion multiplicities is restricted to low momentum pions which dominate the yields. These pions are, however, not energetic enough to contribute to subthreshold kaon production and the relevant high momentum tails of the pion spectra are generally well described by the transport models [136, 137, 27].

However, for a fair comparison of experiment and theory it should be mentioned that also the experimental situation, in particular the  $A_{\text{part}}$  dependence of the multiplicities, is not yet completely settled for the SIS/BEVALAC energy range. Fig.42 shows a compilation of published pion multiplicities ( $\pi^- + \pi^0 + \pi^+$ ) for different mass systems as a function of  $A_{\text{part}}$  [134] at 1 AGeV incident energy. The data set consists of measurements with the streamer chamber at LBL [247] and with the TAPS [248, 249, 250], KaoS [251, 205] and FOPI [252] spectrometers at the GSI. In none of the experiments

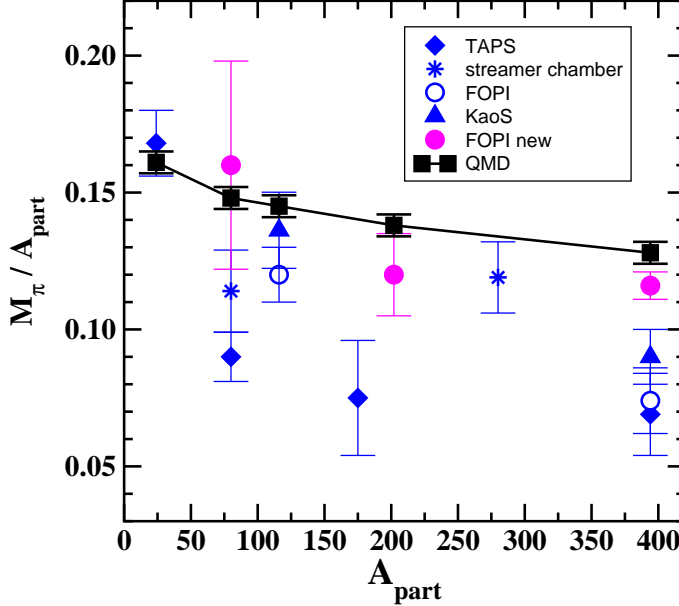


Figure 42: Pion multiplicities as a function of  $A_{\text{part}}$  for various mass systems at 1 AGeV incident energy. QMD calculations for central reactions ( $b=0$  fm) are compared to a compilation of experimental data taken from [134]. Recent preliminary results from FOPI [240] are denoted as FOPI new.

all pion charges have been measured simultaneously and thus each data set contains extrapolations in isospin space which are based on the isotopic relations for the  $\Delta$  production and decay [252]. The largest experimental uncertainty lies probably in the determination of  $A_{\text{part}}$ . On the one side this quantity is biased by the impact parameter resolution but it depends on model assumptions as well. <sup>||</sup> The corresponding QMD calculations are performed for central reactions ( $b=0$  fm) with  $A_{\text{part}} = A + A$ . The experimental yields are well described in light and intermediate mass systems but are significantly overestimated in heavy systems with  $A_{\text{part}} \geq 120$ . The La+La data point [247], which falls off the general systematics, is compatible with the transport result within error bars. Interesting is, however, that the FOPI Collaboration re-measured  $\pi^\pm$  yields and a new analysis, denoted in Fig.42 as FOPI new, is compatible with the streamer chamber systematics and also with the transport model predictions.

### 6.2.2 Kaons - historical overview

After pions turned out to fail as suitable messengers,  $K^+$  mesons were suggested as promising tools to probe the nuclear EOS. This idea was first put forward by Aichelin and Ko almost 20 years ago [132]. At subthreshold energies  $K^+$  mesons are produced in the high density phase and due to the absence of absorption reactions they have a long mean free path and leave the matter undistorted by strong final state interactions. Moreover, at subthreshold energies nucleons have to accumulate energy by multiple scattering processes in order to overcome the threshold for kaon production and therefore these processes should be particularly sensitive to collective effects.

Already in the first theoretical investigations by transport models it was noticed that the  $K^+$  yield reacts rather sensitive on the EOS [176, 90, 92, 133]. Both, in non-relativistic QMD calculations based on soft/hard Skyrme forces [90, 92] and in RBUU [176, 133, 93] with soft/hard versions of the (non-linear)  $\sigma\omega$ -model for the nuclear mean field it turned out that the  $K^+$  yield is about a factor 2–3

<sup>||</sup>For the determination of the overlapping volume of the two interpenetrating nuclei as function of the impact parameter.

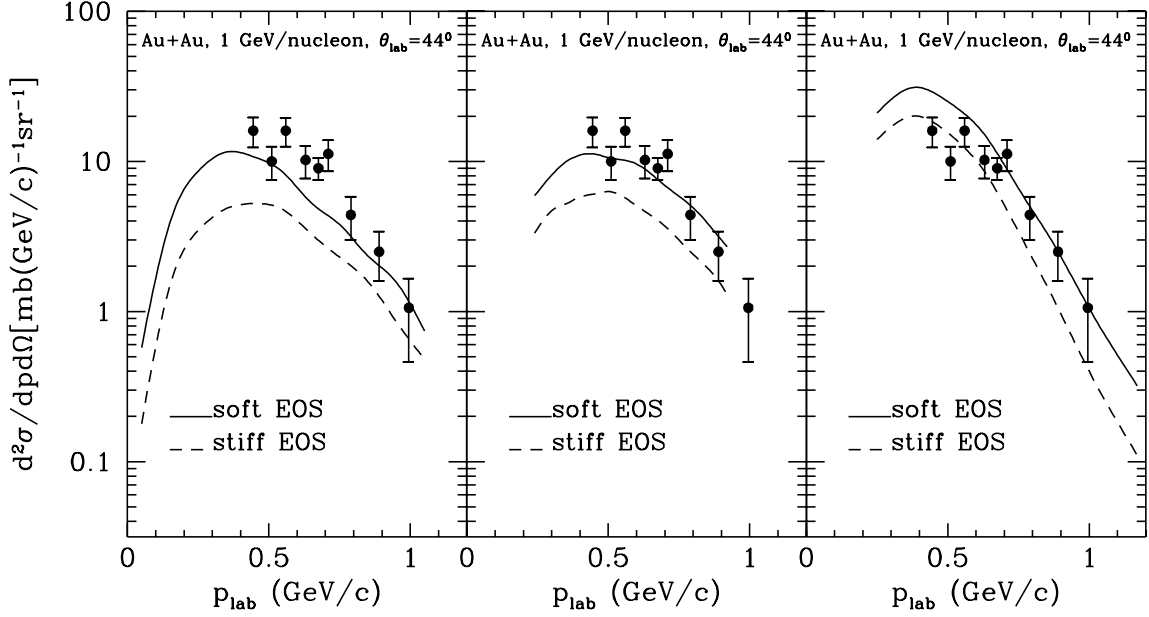


Figure 43: QMD and RBUU transport model calculations from Nantes, Texas and Giessen are compared to the first KaoS data [2] for  $Au + Au$ . The figure is taken from [95].

larger when a soft EOS is applied compared to a hard EOS. At that time the available data favored a soft equation of state. This fact is illustrated in Fig. 43 which compares QMD calculations from the Nantes [92] and RBUU calculations from the Texas/Stony Brook [133] and Giessen [93] groups to the first KaoS data for  $Au + Au$  [2]. However, at that stage the theoretical calculations were still burdened with large uncertainties. First of all, it was noticed [90, 92] that the influence of the repulsive momentum dependent part of the nuclear interaction, Eq. (111), leads to a strong suppression of the kaon abundances which made a quantitative description of the available data more difficult. Moreover, at that time the pion induced reaction channels  $\pi B \rightarrow Y K^+$  have not yet been taken into account explicitly. In [176] the frozen  $\Delta$  approximation has been used which includes pionic degrees of freedom implicitly. The importance of this channel was first pointed out by Fuchs *et al.* [109]. These additional channels which contribute up to  $30 \div 50\%$  to the total yield allowed to explain the measured yields with realistic momentum dependent interactions [109, 94]. However, the dependence of the total  $K^+$  yield on the nuclear EOS turned now out to be much smaller than originally expected, i.e. in the order of 15–20%.

A further breakthrough was achieved when the COSY-11 Collaboration measured the  $pp \rightarrow pK^+\Lambda$  reactions at threshold [87]. The strangeness production cross sections  $NN \rightarrow NK^+Y$  [97, 102] which are nowadays in use are based on these data and are in particular close to threshold three orders of magnitude smaller than the parameterizations of Randrup and Ko [86] which were used in the early QMD and RBUU/Texas calculations shown in Fig. 43.

### 6.3 The ratio Au+Au/C+C

Within the last decade the KaoS Collaboration has performed systematic measurements of the  $K^+$  production far below threshold [2, 141, 205, 140, 142]. Based on the new data situation, in Ref. [181] the question if valuable information on the nuclear EOS can be extracted has been revisited and it has been shown that subthreshold  $K^+$  production provides indeed a suitable and reliable tool for this purpose. These results have been confirmed by the Nantes group later on [96]. In subsequent

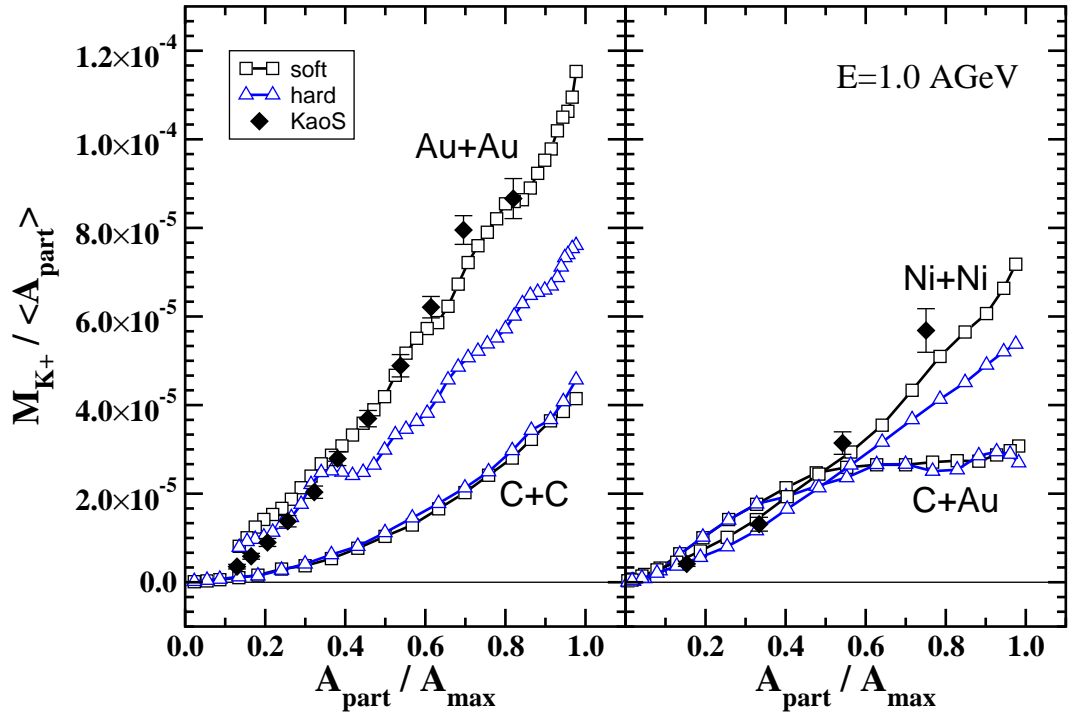


Figure 44: EOS dependence of the  $K^+$  multiplicities as a function of  $A_{\text{part}}$  in Au+Au, Ni+Ni, C+Au and C+C reactions at 1 AGeV. For Au+Au and Ni+Ni data from KaoS [134, 141] are shown as well.

publications these findings were worked out in more detail [253, 254]. Here we summarize and complete these investigations. If not denoted differently, throughout this section all model calculations contain a repulsive in-medium  $K^+$  potential as discussed in Chap. 5.

In Chap. 3 we discussed already the  $A_{\text{part}}$  dependence of the  $K^+$  yield on a qualitative bases. The calculations shown in Fig. 13 were based on a soft EOS. Fig. 44 demonstrates the interplay between  $A_{\text{part}}$ , system size and the nuclear EOS. It shows the  $K^+$  multiplicities as a function  $A_{\text{part}}$  in Au+Au, Ni+Ni, C+Au and C+C reactions at 1 AGeV. The multiplicities are normalized to the mean  $A_{\text{part}}$ :  $\langle A_{\text{part}} \rangle = A_{\text{max}}/2$  with  $A_{\text{max}} = A + A$  for symmetric systems and  $A_{\text{max}} = 56$  for C+Au. A significant dependence of the kaon multiplicities on the nuclear EOS requires a large amount of collectivity which is easiest reached in central reactions of heavy mass systems. Consequently, the EOS dependence is most pronounced in central Au+Au reactions. Also in Ni+Ni effects are still sizable while the small C+C system is completely insensitive on the nuclear EOS even in most central reactions. The available data for Au+Au and Ni+Ni [134, 141] support the soft EOS. Interesting is in this context the asymmetric C+Au system: Though in central C+Au reactions the number of participants is comparable to Ni+Ni the  $K^+$  yield does not depend on the EOS. This indicates again that a sensitivity on the EOS is not only a question of  $A_{\text{part}}$  but of the compression which can be reached by the colliding system. Remarkable is the saturation of the kaon yield as a function of  $A_{\text{part}}$  predicted by the transport calculations. It stands in clear contradiction to the  $A_{\text{part}}$  dependence predicted by the thermal model [150, 151] and a measurement of the quantity would allow to distinguish between these two approaches. In Fig. 45 the QMD calculations for inclusive reactions are compared to KaoS data from [255]. The data are generally described within error bars by the soft EOS. Compared to Fig. 44 in inclusive reactions the EOS dependence survives for large mass systems although the large difference between the soft and hard – seen in most central Au+Au reactions – is washed out to some extent. In minimal bias reactions the bulk of kaons originates from semi-central reactions  $b \sim 5$  fm, corresponding to  $A_{\text{part}}/A_{\text{max}} \sim 0.7$ . The fact that the  $K^+$  multiplicities in C+Au are significantly smaller than in Ni+Ni reactions although both

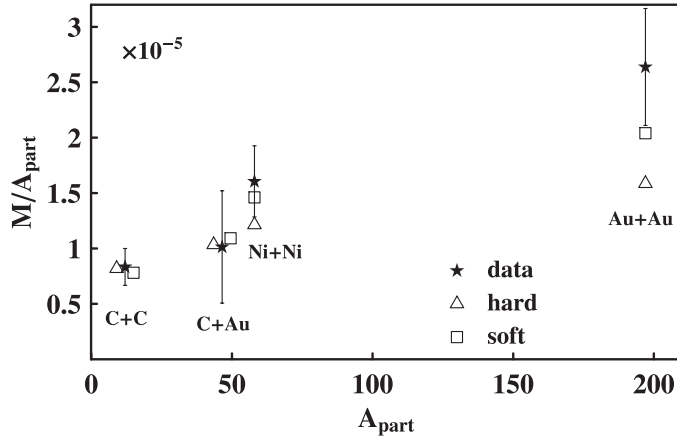


Figure 45:  $K^+$  multiplicities in inclusive C+C, Ni+Ni, Au+Au and C+Au reactions at 1 AGeV. QMD calculations using a hard/soft nuclear EOS are compared to KaoS data [255]. The figure is taken from [255].

systems correspond to comparable mean  $A_{\text{part}}$  is a strong experimental evidence for a strong sensitivity of the kaon production on the compression. As also discussed in [255] even in central reactions the carbon projectile is simply too small in order to achieve a high compression of the gold target. The situation is different in central Ni+Ni reactions. Hence the mass dependence of the kaon multiplicities seems not primordially to be an  $A_{\text{part}}$  effect but a compression effect. This is also clearly reflected by the transport calculations. The next and natural step is to consider the energy dependence of the EOS effect. It is expected to be most pronounced most far below threshold because there the highest degree of collectivity, reflected in multi-step collisions, is necessary to overcome the production thresholds (see also discussion in chapter 3.2). The calculations for the excitation function shown in Fig. 29 were obtained for a soft EOS and are performed under minimal bias conditions with  $b_{\text{max}} = 11$  fm for  $Au+Au$  and  $b_{\text{max}} = 5$  fm for  $C+C$  and normalized to the experimental reaction cross sections [142, 205]. For both systems the agreement with the KaoS data is quite good.

The effects become even more evident when the ratio  $R$  of the kaon multiplicities obtained in Au+Au over C+C reactions (normalized to the corresponding mass numbers) is built [181, 142]. Such a ratio has moreover the advantage that possible uncertainties which might still exist in the theoretical calculations should cancel out to large extent.

This ratio is shown in Fig. 46. Both, soft and hard EOS, show an increase of  $R$  with decreasing energy down to 1.0 AGeV. However, this increase is much less pronounced when the stiff EOS is employed. In the latter case  $R$  even decreases at 0.8 AGeV whereas the soft EOS leads to an unrelieved increase of  $R$ . At 1.5 AGeV which is already very close to threshold the differences between the two models become small. The strong increase of  $R$  can be directly related to higher compressible nuclear matter. The comparison to the experimental data from KaoS [142], where the increase of  $R$  is even more pronounced, strongly favors a soft equation of state.

### 6.3.1 Phase space dependence

To obtain a quantitative picture of the explored density effects in Fig. 47 the baryon densities are shown at which the kaons are created. The energy is chosen most below threshold, i.e. at 0.8 AGeV and only central collisions are considered where the effects are maximal.  $dM_{K^+}/d\rho$  is defined as in Eq. (50). For the comparison of the two systems the curves are normalized to the corresponding mass numbers.

Fig. 47 illustrates several features: Only in the case of a soft EOS the mean densities at which kaons

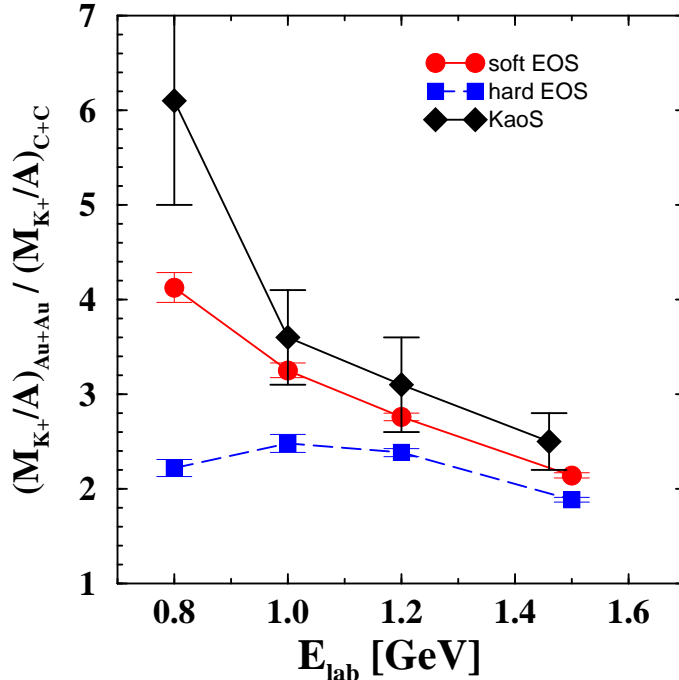


Figure 46: Excitation function of the ratio  $R$  of  $K^+$  multiplicities obtained in inclusive Au+Au over C+C reactions. The calculations are performed with a hard/soft nuclear EOS and compared to the data from the KaoS Collaboration [142].

are created differ significantly for the two different reaction systems, i.e.  $\langle \rho / \rho_0 \rangle = 1.46 / 1.40$  for C+C and  $1.47 / 1.57$  for Au+Au using the hard/soft EOS. Generally, in C+C reactions densities above  $2\rho_0$  are rarely reached whereas in Au+Au the kaons are created at densities up to three times saturation density. Furthermore, for C+C the density distributions are weakly dependent on the nuclear EOS. The situation changes completely in Au+Au. Here the density profile shows a pronounced EOS dependence [133]. Moreover, the excess of kaons obtained with the soft EOS originates almost exclusively from high density matter. A second quantitative measure for the collectivity is the average number of collisions for those hadrons which were involved in the  $K^+$  production displayed in Fig. 47. Again only central collisions are considered where the effects are maximal.  $\langle N_C \rangle$  is defined as in Fig. (11). In average the particles undergo about twice as much relevant collisions in the heavy compared to the light system. Furthermore, the collectivity, i.e. the accumulation of energy by multiple scattering, increases with decreasing energy. Thus one can conclude that the increase of  $R$  is not due to a trivial phase space effect, namely the fact that far below threshold the C+C system is simply too small to provide enough collectivity for the kaon production. If such a scenario - which in principle also explain the rise of  $R$  seen in the KaoS data - would be true,  $\langle N_C \rangle$  would have to saturate for C+C at low energies. This demonstrates that  $K^+$  production far below threshold always requires a certain amount of collectivity which can be provided also in a very small colliding system, though such processes are rare. There is, however, no sharp limit where such collision histories become impossible. Thus trivial phase space effects can be excluded for an explanation of the increase of  $R$ . In [142] a similar argument was based on the measurement of high energy pions which can test the phase space available for particle production.

### 6.3.2 Stability of the EOS dependence

Now the question arises, how firm the conclusions on the nuclear EOS are. The influence of the repulsive in-medium potential has been discussed in [181] and can be seen from Fig. 48 which shows the ratio  $R$

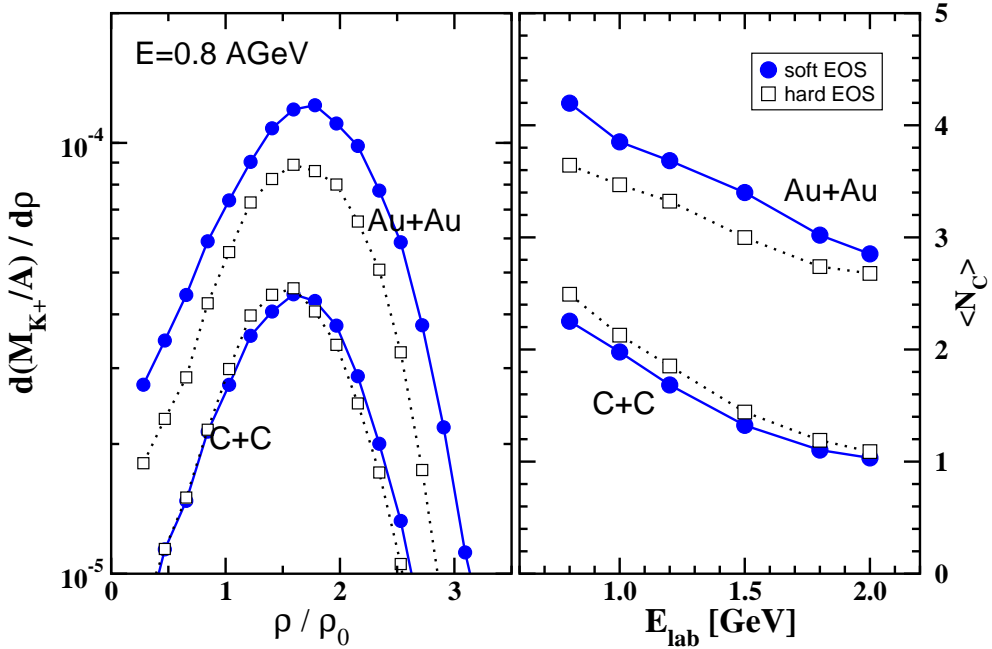


Figure 47: Phase space dependence of the  $K^+$  production. Left: nuclear density at the production of  $K^+$  mesons. Right: number of collisions which the particles encountered prior to  $K^+$  production. In both cases the EOS dependence in central Au+Au and C+C reactions is studied.

in central reactions from simulations with and without kaon potential. It is remarkable and at a first glance surprising that  $R$  shows for both cases qualitatively the same behavior. The in-medium kaon potential acts opposite to the EOS effect: a higher compression increases the kaon yield but also the value of the in-medium kaon mass which, on the other hand, tends to lower the yield again. However, the increase of the in-medium mass goes linear with density whereas the collision rate per volume increases approximately with  $\rho^2$ . E.g. in central Au+Au reactions at 0.8 AGeV the average density  $\langle \rho \rangle$  at kaon production is enhanced from  $1.47$  to  $1.57 \rho_0$  switching from the hard to the soft EOS. This leads to an average shift of the in-medium mass (91) compared to the vacuum value of  $55/61$  MeV using the hard/soft EOS, i.e. a relative shift of 6 MeV between soft and hard. However, collective effects like the accumulation of energy by multiple scattering show a higher sensitivity on the compression resulting in an enhancement of the available energy  $\langle \sqrt{s} \rangle = 90$  MeV applying the soft EOS.

The next question concerns the knowledge of the elementary reaction cross sections. As discussed in Chapter 4 the  $NN$  and  $\pi N$  cross sections are well under control since these channels are constrained by data. The reactions which involve nucleon resonances in the initial states ( $i = N\Delta, \pi\Delta, \Delta\Delta$ ) are less secure due to the lack of data and one has to rely on model assumptions. The cross sections which have been used in the present transport calculations are based on the effective Lagrangian model of Refs. [102, 110, 207]. The isospin dependence of the cross sections was determined by isotopic relations assuming isospin independent matrix elements.

In summary, some uncertainty in the transport calculations is still existing due to the fact that elementary production channels involving  $\Delta$  resonances are not constrained by data \*\*. The ratio built from different mass systems should, however, be robust against such uncertainties:

- Changes of the production cross sections shift absolute yields but considering the ratio possible

\*\*Elementary reactions with a  $N^*(1440)$  resonance in the initial states are included in the present calculations. For these reactions the same cross sections as for nucleons are used. Higher lying nucleon resonances can be neglected at subthreshold energies.

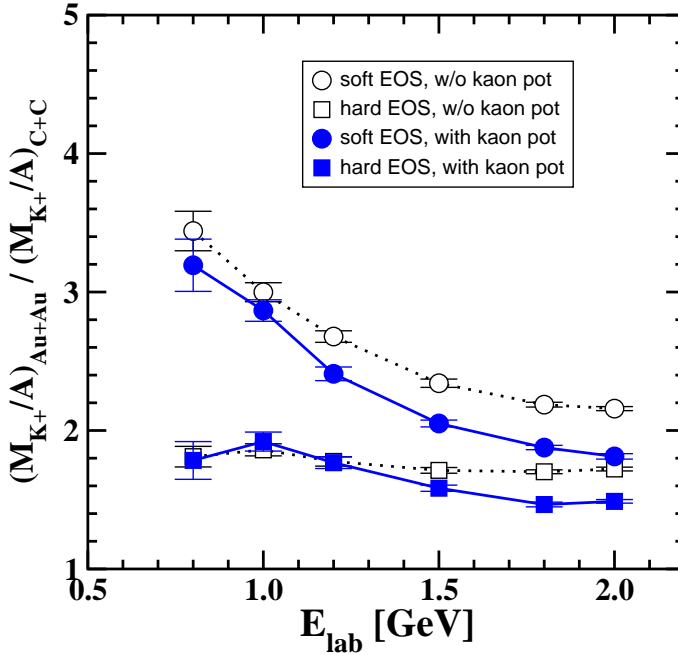


Figure 48: Excitation function of the ratio of  $K^+$  multiplicities obtained in central ( $b=0$  fm) Au+Au over C+C reactions. The calculations are performed with/without in-medium kaon potential and using a hard/soft nuclear EOS. The figure is taken from [181].

errors drop out in leading order.

- Conclusions are based on the slope of this ratio as a function of energy. It is extremely unlikely that an incomplete knowledge of cross sections, i.e. an unknown isospin dependence, can create the observed energy dependence. The systematics of spurious contributions should rather be flat as a function of energy.

To illustrate these arguments the influence of the different elementary channels is shown in Fig. 49. There the ratios  $R_i$  are built separately for the production channels with initial states  $i = NN, \pi N, N\Delta, \pi\Delta, \Delta\Delta$ . The shape of  $R$  is not strongly influenced by the  $N\Delta, \pi\Delta$  channels which are the most insecure ones. The excitation function for the  $N\Delta$  contribution varies only little as a function of energy and is similar using the different EOSs. The contribution of the  $\pi\Delta$  channel is decreasing for both, a hard and a soft EOS. The shape of  $R$  is to most extent determined by the  $NN$  and  $\pi N$  contributions which are well under control.

These findings are generally confirmed by independent transport calculations of the Nantes group using the IQMD transport model [96] shown in Fig. 50 together with the present QMD results. The IQMD calculations include an in-medium kaon potential derived in relativistic mean field theory (RMF) [56] which is somewhat less repulsive than that one used in the present calculations. For the soft EOS the IQMD calculations coincide almost with the present results [181]. The two sets of transport calculations show a good overall agreement and both rule out the hard EOS from the comparison with data. The shaded area in Fig. 50 can be taken as the existing range of uncertainty in the theoretical model description of the considered observable.

Moreover, the IQMD calculations were also repeated with an alternative set of  $N\Delta; \Delta\Delta \leftrightarrow NYK^+$  cross sections taken from [25] which are almost one order of magnitude smaller than those from Tsushima et al. [102] (see Fig. 23). The ratio  $R$  is almost completely independent on this change in elementary cross sections and also total yields. An even more systematic study of possible uncertainties concerning this observable has been performed by Hartnack in [256]. A possible medium dependence of the

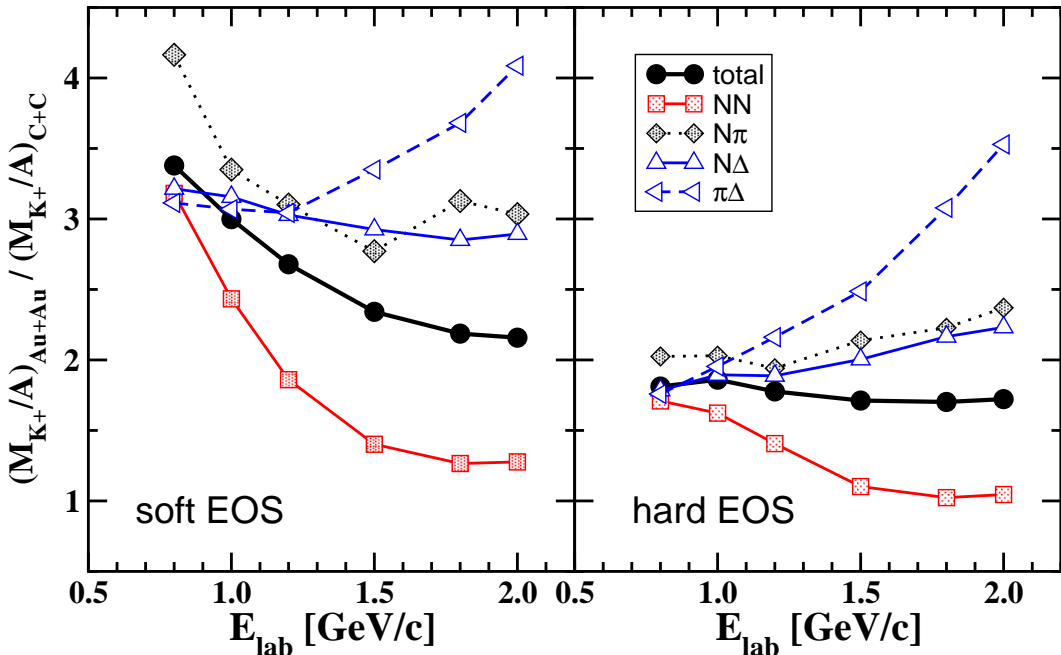


Figure 49: Dependence of the excitation function of  $R$  on the various  $K^+$  production channels. Central ( $b=0$  fm) Au+Au and C+C reactions are considered. The results are taken from [253].

elementary cross sections, i.e. a density dependent reduction, as well as a general scaling has been investigated. Also in these extreme cases the EOS dependence of the ratio  $R$  survived and conclusions stayed stable. This demonstrates once more the robustness of this observable.

## 6.4 Constraints from other sources

### 6.4.1 Nucleon flow

Concerning the nuclear equation of state one has to confront the information from subthreshold  $K^+$  production with the knowledge obtained from other sources: At intermediate energies heavy ion reactions test the density range between one and two, maximally three times nuclear density. The information from kaon production implies that in this density range the EOS shows a soft behavior. One has of course to be aware that the adopted Skyrme forces are simplified interactions which are easy to handle but must not be very realistic.

Another observable which helps to constrain the nuclear mean field and the underlying EOS at supra-normal densities is the collective nucleon flow [258]. The transverse flow  $v_1$  has been found to be sensitive to the EOS and, in particular in peripheral reactions, to the momentum dependence of the mean field [198, 209, 259]. The elliptic flow  $v_2$ , in addition, is very sensitive to the maximal compression reached in the early phase of a heavy ion reaction. The cross over from preferential in-plane flow  $v_2 < 0$  to preferential out-of-plane flow  $v_2 > 0$  around 4-6 AGeV has also led to speculations about a phase transition in this energy region which goes along with a softening of the EOS [260]. However, the corresponding AGS data can also be explained conventionally [261].

The present situation can be summarized as follows: Flow data at SIS energies are consistent with a soft EOS [210, 198]. The full flow excitation function, ranging from low SIS ( $E_{\text{lab}} \simeq 0.2 \div 2$  AGeV) up to top AGS energies ( $E_{\text{lab}} \simeq 2 \div 11$  AGeV), has been studied in [257, 261]. The conclusion from Ref. [257] was that, both, super-soft equations of state ( $K=167$  MeV) as well as hard EOSs ( $K>300$  MeV) are ruled out by data. Fig. 51 displays the pressure-density area which, according to the analysis

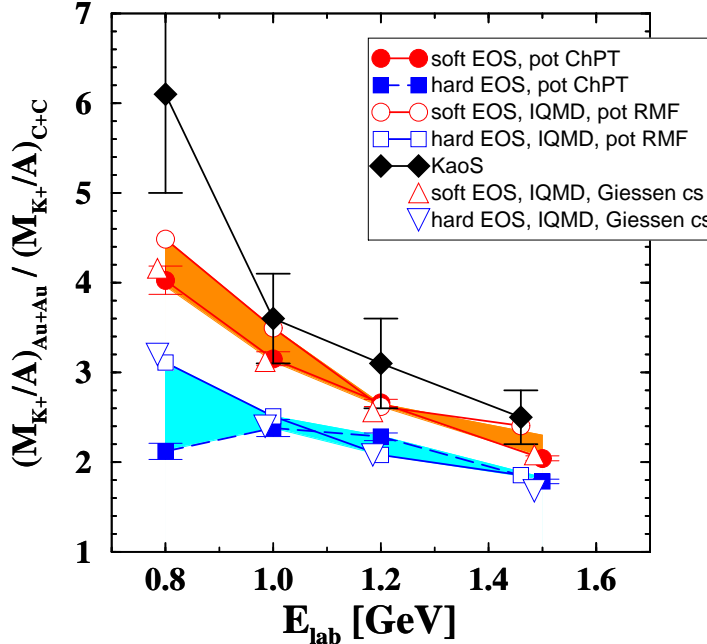


Figure 50: Excitation function of the ratio  $R$  of  $K^+$  multiplicities obtained in inclusive Au+Au over C+C reactions. Our results are compared to IQMD calculations [96]. The shaded area indicates thereby the range of uncertainty in the theoretical models. In addition IQMD results based on an alternative set of elementary  $K^+$  production cross sections are shown.

of [257], is consistent with heavy ion flow data. The soft Skyrme EOS is in agreement with flow data. The boundaries of Fig. 51 are the result of a compilation from the analysis of sideward and elliptic anisotropies. In the models used by Danielewicz et al. [198, 257] sideward flow favors indeed a rather soft EOS with  $K=210$  MeV while the development of the elliptic flow requires slightly higher pressures. The BHF and variational calculations including 3-body-forces<sup>††</sup> fit well into the constrained area up to  $4\rho_0$ . At higher densities the microscopic EOSs, also DBHF, tend to be too repulsive.

However, conclusions from flow data are generally complicated by the interplay of the compressional part of the nuclear EOS and the momentum dependence of the nuclear forces. A detailed comparison to  $v_1$  and  $v_2$  data below 1 AGeV from FOPI [262] and KaoS [263] favors again a relatively soft EOS with a momentum dependence close to that obtained from microscopic DBHF calculations [198, 209, 264]. In Fig. 51 the microscopic DBHF EOS ( $K=230$  MeV) lies at the upper edge of the boundary, but is still consistent in the density range tested at SIS energies, i.e. up to maximally  $3\rho_0$ . This fact is further consistent with the findings of Gaitanos et al. [209, 264] where a good description of  $v_1$  and  $v_2$  data at energies between 0.2 and 0.8 AGeV has been found in RBUU calculations based on DBHF mean fields. However, as pointed out in Refs. [209, 18, 264, 211] is thereby essential to account for non-equilibrium effects and the momentum dependence of the forces which softens the EOS compared to the equilibrium case shown in Fig. 51.

In summary,  $K^+$  production and nucleon flow provide a consistent picture so far that stiff equations-of-state are ruled out. Details concerning the interplay between density and momentum dependence have still to be settled and require future efforts.

<sup>††</sup>For the BHF + 3-BF calculation the pressure shown in Fig. 51 has been determined from the parameterization given in [235] which is based on the Urbana IX 3-BF different to that used in [234].

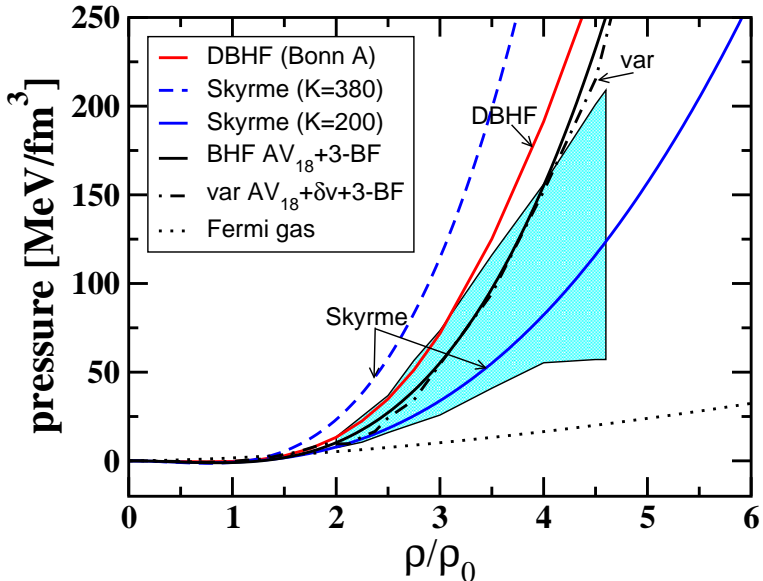


Figure 51: Constraints on the nuclear EOS from heavy ion flow data. The shaded area shows the pressure-density which is compatible with heavy ion flow data according the analysis on [257]. The equations-of-state from the models shown in Fig. 40 are displayed.

#### 6.4.2 Neutron stars and symmetry energy

Models for neutron stars are constrained by the lower limit of the maximal neutron star mass. This means that any equation-of-state must be stiff enough to produce a neutron star of mass greater than 1.44 solar masses, the largest neutron star in the PSR 1913+16 system. The upper limit for a nuclear EOS is thereby obtained by the conventional neutron star consisting of neutrons and protons. The occurrence of additional degrees of freedom such as pion,  $K^-$  or H-dibaryon condensation or the excitation of hyperons in hybrid stars softens the EOS and reduces the maximal neutron star mass. The same is true when quark cores or cores of strange matter are considered. Conventional neutron stars put only weak constraints on the nuclear EOS. Super-soft EOSs with a compressibility less than  $K \lesssim 120$  MeV can be ruled out [13]. The microscopic models discussed above yield maximal neutron star mass above two solar mass which are all very close: DBHF (Bonn A) [231] gives  $M_{\max} = 2.26M_{\odot}$ , BHF + 3-BF  $M_{\max} = 2.3M_{\odot}$  [235] and the variational calculations with 3-BFs + boost correction gives  $M_{\max} = 2.21M_{\odot}$  [228]. A soft EOS comparable to the soft Skyrme force, i.e. a chiral relativistic mean field model with  $K=194$  MeV used in [14] yields  $M_{\max} = 2.0M_{\odot}$ .

Since strangeness is not conserved in weak interactions  $K^-$  condensation can occur in neutron stars at densities above  $3 \div 5\rho_0$  [12, 13, 14, 16, 66], depending on the strength of the  $K^-N$  interaction and the nuclear EOS. The  $K^-$  condensate introduces additional negative charge which enhances the proton fraction in the star and makes the EOS softer. Its influence depends therefore strongly on the high density behavior of the symmetry energy. It has been found that the maximal mass is reduced by about 20  $\div$  25% by a  $K^-$  condensate [13, 14] which would then rule out an EOS softer than  $K \lesssim 180$  MeV. Neutron stars constrain the isospin symmetric EOS from below.

Of particular interest is in this context the symmetry energy which characterizes the isospin dependence of the nuclear forces and determines the proton fraction inside a neutron star. In isospin asymmetric matter the binding energy is a functional of the proton and neutron densities. Asymmetric matter is characterized by the asymmetry parameter  $\beta = Y_n - Y_p$  which is the difference of the neutron and proton fraction  $Y_i = \rho_i/\rho$ ,  $i = n, p$ . The isospin dependence of the energy functional can be

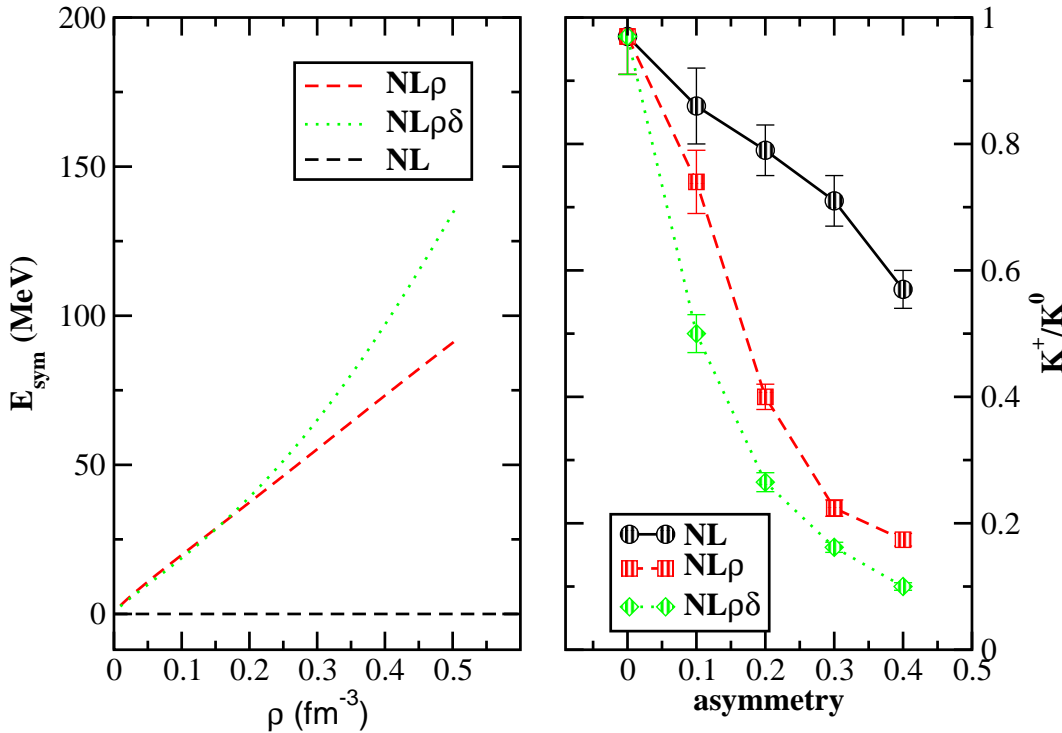


Figure 52: Left: symmetry energy of the various models as a function of density. Right:  $K^+/K^0$  ratio in nuclear matter at density  $2.5 \rho_0$  and temperature  $T = 60$  MeV as a function of the proton-neutron asymmetry  $\beta$  obtained from RBUU calculations with periodic boundary conditions. The results are taken from [199].

expanded in terms of  $\beta$

$$E(\rho, \beta) = E(\rho) + E_{\text{sym}}(\rho)\beta^2 + \mathcal{O}(\beta^4) + \dots \quad . \quad (116)$$

The high density behavior of the symmetry energy is at present largely unconstrained and kaons could again turn out to be a suitable tool to derive constraints from heavy ion collisions. In this case the  $K^+/K^0$  ratio has been suggested as a promising observable by the Catania group [199]. The isospin dependence of the elementary production cross sections reflects the asymmetry of the emitting source which is connected to the stiffness of symmetry energy and thus translated into the corresponding  $K^+$  and  $K^0$  yields. RBUU calculations with periodic boundary conditions for equilibrated nuclear matter at 2.5 times saturation density and a temperature of  $T = 60$  MeV, shown in Fig. 52, indicate a strong sensitivity on  $E_{\text{sym}}$  and the isospin dependence of the nuclear forces. The calculations are based on non-linear Walecka mean field including either the vector isovector  $\rho$ -meson ( $\text{NL}\rho$ ) or in addition the scalar isovector  $\delta$ -meson ( $\text{NL}\rho\delta$ ). The NL model contains only isoscalar  $\sigma$  and  $\omega$  mesons and has therefore  $E_{\text{sym}} = 0$ . The measurement of  $K^{+,0}$  mesons in symmetric and highly isospin asymmetric colliding systems might therefore provide experimental access to the isospin dependent part of the nuclear EOS.

## 7 Summary and outlook

Kaon and antikaon production in nucleus-nucleus collisions around threshold energies opens the possibility to attack a variety of physics questions which have important implications in nuclear physics, QCD and astrophysics. The present article tried to summarize the status of the field and to point out which problems could be settled and which questions are still open.

Theory predicts strong modifications of the kaon and antikaon properties in a dense hadronic environment. Mean field models as well as chiral perturbation theory predict a repulsive  $K^+$  potential of about  $V_{K^+} \simeq + (20 \div 30)$  MeV at nuclear saturation density. Such a value is in agreement with empirical kaon-nucleon scattering. The  $K^-$ -nucleon interaction, in contrast, is resonant around threshold and requires non-perturbative approaches. The strength of the  $K^-$  potential is still an open question. The depth of the attractive antikaon-nucleon potential ranges from  $V_{K^-} \simeq - (50 \div 100)$  MeV, obtained within chiral coupled channel dynamics, to  $V_{K^-} \simeq - (100 \div 200)$  MeV predicted by mean field approaches and the analysis of kaonic atoms. In contrast to the  $K^+$  mesons the  $K^-$  mesons develop complicated spectral properties in the medium.

In heavy ion collisions at intermediate energies, i.e. at energies around the threshold region, strangeness is generally produced in the early and high density phase of the reaction. However, the freeze-out conditions for kaons and antikaons are completely different. Due to strangeness conservation  $K^+$  mesons cannot be reabsorbed by the surrounding nucleons and their chemical freeze-out takes place early. Final state interactions, i.e. elastic scattering or charge exchange reactions and the influence of the optical kaon-nucleon potential change their dynamical pattern but not the abundances. This makes  $K^+$  mesons to a suitable 'penetrating' probe to study the dense fireball created in a heavy ion reaction. Antikaons, in contrast, are strongly coupled to the environment through strangeness exchange reactions. This leads to a late freeze-out and a loss of memory on the early reaction stages.

The link of the underlying physics to the heavy ion experiments must be provided by dynamical transport models. The precision of such models depends thereby crucially on the elementary input, i.e. the knowledge of the elementary reaction cross sections. This input is much better constrained by data for the  $K^+$  mesons than for  $K^-$ . In addition, the quasiparticle picture which underlies all types of semiclassical transport approaches, is much better justified for the kaons than for the antikaons. Hence state of the art transport calculations have reached a reasonable degree of consistency concerning  $K^+$  production and dynamics. The comparison to experiment concerning both, total yields as well as dynamical observables such as in-plane and out-of-plane flow pattern, supports the existence of a slightly repulsive in-medium potential as predicted by chiral dynamics. This picture is complemented by data from proton-nucleus reactions.

Concerning the antikaons the situation is less satisfactory, both from the experimental as well as from the theoretical side. To settle the question of a strongly attractive  $K^-$ -nucleon potential is one of the major challenges of this field in future. If the  $K^-$ -nucleon potential is strong enough, this can lead to deeply bound  $K^-$  states in nuclei [265] and even to light kaonic nuclear clusters [266]. Such states would be much stronger bound than the  $\pi^-$  states observed in pionic atoms [51]. Some calculations predict even a collapse of the nuclear wave functions to densities significantly above saturation density in  $K^-$ -nuclear clusters which would allow to access the nuclear forces at very short distances. The existence of such molecule states would thus open a completely new field in hadron physics with strong implications on nuclear structure. Heavy ion reactions as well as proton-nucleus reactions are the tools to clarify the preconditions for this hypothesis.

To draw firm conclusions on the in-medium antikaon properties will, however, require significant efforts to control their off-shell dynamics. The same holds for other hadrons, e.g. vector mesons, where dramatic changes of their spectral properties are expected. First attempts towards a quantum transport have been made but an exact treatment of the quantum evolution equations requires a better knowledge of off-shell transition elements and in-medium spectral functions of all the involved hadron species. To develop a consistent quantum transport is the major challenge of future theoretical heavy ion physics. The same holds for proton-nucleus reactions. Also there the quantitative understanding of high precision meson production data, e.g. from GSI, COSY or KEK, requires to control the off-shell dynamics of such processes.

Finally the kaons turned out to provide a suitable tool to attack another longstanding question, namely the stiffness of the nuclear equation-of-state. The high density behavior of the EOS has severe

astrophysical consequences since it determines e.g. the maximal mass and the radii of neutron stars. Although heavy ion reactions test mainly isospin symmetric matter they put constraints on theoretical models which are also applied to neutron stars. The systematic measurement of the  $K^+$  excitation function in heavy and light systems down to energies far below threshold can here be considered as a breakthrough. Extreme subthreshold energies exclude distortions from surface effects and ensure that the  $K^+$  mesons originate from supra-normal nuclear densities. To overcome the production thresholds requires a high degree of collectivity which, on the other hand, introduces the sensitivity on the compression achieved in the reaction. The comparison with data strongly supports an EOS which is 'soft' in a density regime between 1-3 times saturation density. Such a behavior is consistent with the predictions from microscopic many-body calculations and the constraints obtained from nucleon flow data in heavy ion reactions. Based on similar arguments the  $K^+/K^0$  ratio has recently been proposed as a tool to access the isospin dependence of the nuclear EOS and to constrain the symmetry energy. If this turns out to be true, subthreshold kaon production can probably be considered as the most successful observable to constrain nuclear forces at high densities.

### Acknowledgments:

The author would like to thank the following people for valuable discussions and/or for providing experimental data or results of theoretical calculations:

J. Aichelin, H.-W. Barz, E. Bratkovskaya, G. Burau, W. Cassing, L.-W. Chen, A. Faessler, T. Gaitanos, T. Gutsche, Ch. Hartnack, N. Herrmann, E. Kolomeitsev, C.M. Ko, A. Larionov, M. Lutz, V. Lyubowitzki, H. Oeschler, A. Ramos, P. Senger, C. Sturm, L. Tolos, K. Tsushima, Y.-M. Zheng

## References

- [1] J.W. Harris et al., Phys. Rev. Lett. 47 (1981) 229; S. Schnetzler et al., Phys. Rev. Lett. 49 (1982) 989;
- [2] D. Miskowiec et al. [KaoS Collaboration], Phys. Rev. Lett. 72 (1994) 3650.
- [3] J. Ritman et al. [FOPI Collaboration], Z. Phys. A 352 (1995) 355.
- [4] S. Okubo, Phys. Lett. B 5 (1963) 165; G. Zweig, CERN Report No.8419/TH, (1964) 412; I. Iizuka, Prog. Theor. Phys. Suppl. 37 & 38 (1966) 21.
- [5] V. Koch, Int. J. Mod. Phys. E6 (1997) 203.
- [6] J. Gasser and H. Leutwyler, Phys. Rep. 87 (1982) 77.
- [7] D.B. Kaplan and A.E. Nelson, Phys. Lett. B 175 (1986) 57;  
A.E. Nelson and D.B. Kaplan, Nucl. Phys. Lett. B 192 (1987) 193.
- [8] G.E. Brown and M. Rho, Phys. Rep. 269 (1996) 333.
- [9] S. Klimt, M. Lutz, W. Weise, Phys. Lett. B 249 (1990) 386.
- [10] T. Maruyama, K. Tsushima and A. Faessler, Nucl. Phys. A 535 (1991) 497; K. Tsushima, T. Maruyama and A. Faessler, Nucl. Phys. A 537 (1992) 303.
- [11] E. Friedmann, A. Gal and C.J. Batty, Nucl. Phys. A 579 (1994) 518.
- [12] G.E. Brown, C.-H. Lee, M. Rho, V.Thorsson, Nucl. Phys. A 567 (1994) 937.

- [13] V. Thorsson, M. Prakash, J.M. Lattimer, Nucl. Phys. A 572 (94) 693.
- [14] G.Q. Li, C.-H. Lee, G.E. Brown, Phys. Rev. Lett. 79 (1997) 5214.
- [15] G.E. Brown, H. Bethe, Astrophys. J. 423 (1994) 659.
- [16] F. Weber, Prog. Part. Nucl. Phys. 54 (2005) 193.
- [17] M. Lutz, A. Steiner, W. Weise, Nucl. Phys. A 574 (1994) 755.
- [18] C. Fuchs, T. Gaitanos, Nucl. Phys. A 714 (2003) 643.
- [19] P. Danielewicz, Ann. Phys. (N.Y.) 152 (1984) 239; Ann. Phys. (N.Y.) 152 (1984) 305.
- [20] W. Botermans, R. Malfliet, Phys. Rep. 198 (1990) 115.
- [21] G.F. Bertsch, S. Das Gupta, Phys. Rep. 160 (1988) 189.
- [22] W. Cassing, V. Metag, U. Mosel, K. Niita, Phys. Rep. 188 (1990) 363.
- [23] J. Aichelin, Phys. Rep. 202 (1991) 233.
- [24] S.A. Bass et al., Prog. Part. Nucl. Phys. 41 (1998) 255.
- [25] W. Cassing, E.L. Bratkovskaya, Phys. Rep. 308 (1999) 65.
- [26] K. Shekhter, C. Fuchs, A. Faessler, M.I. Krivoruchenko, B.V. Martemyanov, Phys. Rev. C 68 (2003) 014904.
- [27] V.S. Uma Maheswari, C. Fuchs, Amand Faessler, L. Sehn, D. Kosov, Z. Wang, Nucl. Phys. A 628 (1998) 669.
- [28] W. Cassing, S. Juchem, Nucl. Phys. A 665 (2000) 377; Nucl. Phys. A 677 (2000) 445.
- [29] G.E. Brown, K. Kubodera, M. Rho, V. Thorsson, Phys. Lett. B 291 (1992) 355;
- [30] N. Kaiser, P.B. Siegel, and W. Weise, Nucl. Phys. A 594 (1995) 325.
- [31] G.E. Brown and M. Rho, Nucl. Phys. A 596 (1996) 503.
- [32] T. Waas, N. Kaiser, and W. Weise, Phys. Lett. B 379 (1996) 34.
- [33] T. Waas, M. Rho, and W. Weise, Nucl. Phys. A 617 (1996) 449.
- [34] N. Kaiser, T. Waas, and W. Weise, Nucl. Phys. A 612 (1997) 297.
- [35] M. Lutz, Phys. Lett. B 426 (1998) 12.
- [36] G. Mao, P. Papazoglou, S. Hofmann, S. Schramm, H. Stöcker, W. Greiner Phys. Rev. C 59 (1999) 3381.
- [37] M.F.M. Lutz, C.L. Korpa, Nucl. Phys. A 700 (2002) 309.
- [38] M.F.M. Lutz and E.E. Kolomeitsev, Nucl. Phys A 700 (2002) 193.
- [39] G.Q. Li, C.M. Ko and B.A. Li, Phys. Rev. Lett. 74 (1995) 235; G.Q. Li, C.M. Ko, Nucl. Phys. A 594 (1995) 460.

- [40] S. Weinberg, Phys. Rev. 166 (1968) 1568.
- [41] M. Gell-Mann, R. Oakes, B. Renner, Phys. Rev. 175 (1968) 2195.
- [42] S.J. Dong, J.F. Lagae, K.F. Liu, Phys. Rev. D54 (1996) 5496.
- [43] B. Borasoy, R. Lewis, P.P. Ouimet, Phys. Rev. D65 (2002) 114023.
- [44] B. Borasoy, Eur. Phys. J. C 8 (1999) 121.
- [45] T. Inoue, V.E. Lyubovitskij, T. Gutsche, A. Faessler, Phys. Rev. C 69 (2004) 035207.
- [46] C. Fuchs, D. Kosov, Amand Faessler, Z.S. Wang and T. Waindzoch, Phys. Lett. B 434 (1998) 254.
- [47] B.D. Serot and J.D. Walecka, Adv. Nucl. Phys. 16 (1988) 1.
- [48] T.D. Cohen, R.J. Furnstahl, D.K. Griegel, Phys. Rev. C 45 (1992) 1881.
- [49] A.D. Martin, Nucl. Phys. B 179 (1981) 33.
- [50] T. Waas, R. Brockmann and W. Weise, Phys. Lett. B 405 (1997) 215.
- [51] P. Kienle and T. Yamazaki, Prog. Part. Nucl. Phys. 52 (2004) 85.
- [52] J. Delorme, M. Ericson, and T.E.O. Ericson, Phys. Lett. B 295 (1992) 379.
- [53] E. Friedman, A. Gal, Phys. Lett. B 578 (2004) 85.
- [54] C.J. Batty, E. Friedmann, A. Gal, Nucl. Rep. 287 (1997) 385.
- [55] K. Tsushima, K. Saito, A.W. Thomas, S.V. Wright, Phys. Lett. B 429 (1998) 239.
- [56] J. Schaffner, J. Bondorf, I. N. Mishustin, Nucl. Phys. A 625 (1997) 325.
- [57] P. Ring, Prog. Part. Nucl. Phys. 73 (1996) 193; Lect. Notes Phys. 641 (2004) 175.
- [58] M. Iwasaki et al., Phys. Rev. Lett. 78 (1997) 3067.
- [59] V. Bernard, N. Kaiser and U.-G. Meissner, Nucl. Phys. A 615 (1997) 483.
- [60] E.E. Kolomeitsev, D.N. Voskresensky, B. Kämpfer Nucl. Phys. A 588 (1995) 889.
- [61] A. Ramos, E. Oset, Nucl. Phys. A 671 (2000) 481.
- [62] L. Tolos, A. Ramos, A. Polls, T.T.S. Kuo, Nucl. Phys. A 690 (2001) 547.
- [63] L. Tolos, A. Ramos, A. Polls, Phys. Rev. C 65 (2002) 054907.
- [64] A. Müller-Groeling, K. Holinde, J. Speth, Nucl. Phys. A 513 (1990) 557.
- [65] V. Koch, Phys. Lett. B 337 (1994) 7.
- [66] E.E. Kolomeitsev, D.N. Voskresensky, Phys. Rev. C 68 (2003) 015803.
- [67] A. Sibirtsev, W. Cassing, Nucl. Phys. A 641 (1999) 476.
- [68] J. Schaffner-Bielich, V. Koch, M. Effenberger, Nucl. Phys. A 669 (2000) 153.

- [69] A. Baca, C. Garcia-Recio, J. Nieves, Nucl. Phys. A 673 (2000) 335.
- [70] M. Lutz, W. Florkowski, nucl-th/0004020.
- [71] A. Ramos, S. Hirenzaki, S.S. Kamalov, T.T.S. Kuo, Y. Okumura, E. Oset, A. Polls, H. Toki, L. Tolos, Nucl. Phys. A 691 (2001) 258.
- [72] C.L. Korpa, M.F.M. Lutz, Acta Phys. Hung. A 22 (2005) 21.
- [73] D. Lissauer, E.V. Shuryak, Phys. Lett. B 253 (1991) 15.
- [74] J.-P. Blaizot, R.M. Galain, Phys. Lett. B 271 (1991) 32.
- [75] B.V. Martemyanov, A. Faessler, C. Fuchs, M.I. Krivoruchenko, Phys. Rev. Lett. 93 (2004) 052301.
- [76] A.G. Nicola, J.R. Peláez, Phys. Rev. D 65 (2002) 054009.
- [77] N. Willis [NA50 Collaboration], Nucl. Phys. A 661 (1999) 534c.
- [78] C. Hoehne [NA49 Collaboration], Nucl. Phys. A 661 (1999) 485c.
- [79] J.L. Nagle [PHENIX Collaboration], Nucl. Phys. A 715 (2003) 252.
- [80] S.S. Adler et al. [PHENIX Collaboration], nucl-ex/0410012.
- [81] Subrata Pal, C.M. Ko, Zi-wei Lin, Nucl. Phys. A 707 (2002) 525.
- [82] G. Chanfray, M. Ericson, nucl-th/0406003; *ibid.* nucl-th/0402018.
- [83] W. Cassing et al., Z. Phys. A 349 (1994) 77; Phys. Lett. B 238 (1990) 25.
- [84] E.Ya. Paryev, Eur. J. A 5 (1999) 307; Eur. J. A 9 (2000) 521.
- [85] Z. Rudy, W. Cassing, L. Jarczyk, B. Kamys, P. Kulessa, Eur. Phys. J. A 15 (2002) 303; Z. Rudy, W. Cassing, L. Jarczyk, B. Kamys, A. Kowalczyk, P. Kulessa, Eur. Phys. J. A 23 (2005) 379.
- [86] J. Randrup and C.M. Ko, Nucl. Phys. A 343 (1980) 519; Nucl. Phys. A 411 (1983) 537.
- [87] J.T. Balewski et al. [COSY-11 Collaboration], Phys. Lett. B 338 (1996) 859; Phys. Lett. B 420 (1998) 211.
- [88] M. Büscher et al. [ANKE-Collaboration], Eur. Phys. J. A 22 (2004) 301.
- [89] L. Xiong, C.M. Ko and J.Q. Wu, Phys. Rev C 42 (1990) 2231.
- [90] S.W. Huang, A. Faessler, G.Q. Li, R.K. Puri, E. Lehmann, D.T. Khoa and M. A. Matin, Phys. Lett. B 298 (1993) 41.
- [91] Bao-An Li, Phys. Rev. C 50 (1994) 2144.
- [92] C. Hartnack, J. Jaenicke, L. Sehn, H. Stöcker, J. Aichelin, Nucl. Phys. A 580 (1994) 643.
- [93] T. Maruyama, W. Cassing, U. Mosel, S. Teis, K. Weber, Nucl. Phys. A 573 (1994) 653.
- [94] E. L. Bratkovskaya, W. Cassing, U. Mosel, Nucl. Phys. A 622 (1997) 593.
- [95] C.M. Ko, G.Q. Li, J. Phys. G 22 (1996) 405.

[96] Ch. Hartnack, J. Aichelin, *J. Phys. G* 28 (2002) 1649.

[97] A. Sibirtsev, *Phys. Lett. B* 359 (1995) 29.

[98] G.Q. Li, C.M. Ko, W.S. Chung, *Phys. Rev. C* 57 (1998) 434.

[99] G. Fäldt, C. Wilkin, *Z. Phys. A* 357 (1997) 241.

[100] K. Tsushima, A. Sibirtsev, A.W. Thomas, *Phys. Lett. B* 390 (1997) 29.

[101] A. Sibirtsev, K. Tsushima, A.W. Thomas, *Phys. Lett. B* 421 (1998) 59.

[102] K. Tsushima, A. Sibirtsev, A.W. Thomas, G.Q. Li, *Phys. Rev. C* 59 (1999) 369.

[103] B. Friman, H.J. Pirner, *Nucl. Phys. A* 617 (1997) 496.

[104] M. Post, U. Mosel, *Nucl. Phys. A* 688 (2001) 808.

[105] A.I. Titov, B. Kämpfer, *Eur. Phys. J. A* 12 (2001) 217.

[106] G. Penner, U. Mosel, *Phys. Rev. C* 66 (2002) 055211; *Phys. Rev. C* 66 (2002) 055212.

[107] C. Fuchs, M.I. Krivoruchenko, H. Yadav, A. Faessler, B.V. Martemyanov, K. Shekther, *Phys. Rev. C* 67 (2003) 025202.

[108] Amand Faessler, C. Fuchs, M.I. Krivoruchenko, B.V. Martemyanov, *Phys. Rev. C* 68 (2003) 068201.

[109] C. Fuchs, Z. Wang, L. Sehn, Amand Faessler, V.S. Uma Maheswari, D.S. Kosov, *Phys. Rev. C* 56 (1997) R606.

[110] K. Tsushima, S. W. Huang, A. Faessler, *Phys. Lett. B* 337 (1994) 245; *J. Phys. G* 21 (1995) 33.

[111] Subrata Pal, C.M. Ko, Zi-wei Lin, *Phys. Rev. C* 64 (2001) 042201.

[112] E.L. Bratkovskaya, W. Cassing, C. Greiner, M. Effenberger, U. Mosel, A. Sibirtsev, *Nucl. Phys. A* 675 (2000) 661.

[113] W. Zwermann, B. Schürmann, *Phys. Lett. B* 145 (1984) 315.

[114] C. Quentmeier et al. [COSY-11 Collaboration], *Phys. Lett. B* 515 (2001) 276.

[115] A. Sibirtsev, W. Cassing, C.M. Ko, *Z. Phys. A* 358 (1997) 101.

[116] W. Cassing, E.L. Bratkovskaya, U. Mosel, S. Teis, A. Sibirtsev, *Nucl. Phys. A* 614 (1997) 415.

[117] C.M. Ko, *Phys. Lett. B* 120 (1983) 294; *ibid. Phys. Lett. B* 138 (1984) 361.

[118] H.W. Barz, L. Naumann, *Phys. Rev. C* 68 (2003) 041901(R).

[119] J.S. Hyslop, R.A. Arndt, L.D. Roper, R.L. Workman, *Phys. Rev. D* 46 (1992) 961.

[120] Ch. Hartnack, H. Oeschler, J. Aichelin, *Phys. Rev. Lett.* 90 (2003) 102302; *Erratum Phys. Rev. Lett.* 93 (2004) 149903(E).

[121] W. Cassing, L. Tolos, E.L. Bratkovskaya, A. Ramos, *Nucl. Phys. A* 727 (2003) 59.

- [122] X. S. Fang, C.M. Ko, G.Q. Li, Y. M. Zheng, Phys. Rev. C 49 (1994) R608.
- [123] Z. Wang, Amand Faessler, C. Fuchs, V.S. Uma Maheswari, D.S. Kosov, Phys. Rev. Lett. 79 (1997) 4096.
- [124] Z.S. Wang, Amand Faessler, C. Fuchs, V.S. Uma Maheswari, T. Waindzoch, Phys. Rev. C 57 (1998) 3284.
- [125] Particle Data Group, Phys. Rev. D 66 (2002) 1; Eur. Phys. J. C 3 (1998) 1.
- [126] F. Balestra et al. [DISTO Collaboration], Phys. Rev. C 63 (2001) 024004.
- [127] W.S. Chung, G.Q. Li, C.M. Ko, Nucl. Phys. A 625 (1997) 347.
- [128] A.I. Titov, B. Kämpfer, B.L. Reznik, Phys. Rev. C 65 (2002) 065202.
- [129] K. Tsushima and K. Nakayama, Phys. Rev. C 68 (2003) 034612.
- [130] A. Mangiarotti et al. [FOPI Collaboration], nucl-ex/0209012.
- [131] H.W. Barz, M. Zetenyi, Gy. Wolf, B. Kämpfer, Nucl. Phys. A 705 (2002) 223.
- [132] J. Aichelin and C.M. Ko, Phys. Rev. Lett. 55 (1985) 2661.
- [133] G.Q. Li, C.M. Ko, Phys. Lett. B 349 (1995) 405.
- [134] P. Senger and H. Ströbele, J. Phys. G 25 (1999) R59.
- [135] D. Best et al. [FOPI Collaboration], Nucl. Phys. A 625 (1997) 307.
- [136] S.A. Bass, C. Hartnack, H. Stöcker and W. Greiner, Phys. Rev. C 51 (1995) 3343.
- [137] S. Teis, W. Cassing, M. Effenberger, A. Hombach, U. Mosel, and Gy. Wolf, Z. Phys. A 356 (1997) 421.
- [138] A. Wagner et al. [KaoS Collaboration], Phys. Lett. B 420 (1998) 20.
- [139] A. Wagner et al. [KaoS Collaboration], Phys. Rev. Lett. 85 (2000) 18.
- [140] F. Laue et al. [KaoS Collaboration], Eur. Phys. J. A 9 (2000) 397.
- [141] R. Barth et al. [KaoS Collaboration], Phys. Rev. Lett. 78 (1997) 4007.
- [142] C. Sturm et al. [KaoS Collaboration], Phys. Rev. Lett. 86 (2001) 39.
- [143] M. Büscher et al., Phys. Rev. C 65 (2002) 014603.
- [144] M. Debowski et al., Z. Phys. A 356 (1996) 313.
- [145] N.K. Abrosimov et al. J. Exp. Theor. Phys. 67 (1988) 2177.
- [146] V. Koptev, M. Büscher et al. [ANKE Collaboration], Phys. Rev. Lett. 87 (2001) 022301.
- [147] P. Koch, B. Müller, J. Rafelski, Phys. Rep. 142 (1986) 167.
- [148] P. Braun-Munzinger, K. Redlich, J. Stachel, nucl-th/0304013.
- [149] J. Cleymans, D. Elliott, A. Keranen, E. Suhonen, Phys. Rev. C 57 (1998) 3319.

- [150] J. Cleymans, H. Oeschler, K. Redlich, Phys. Rev. C 59 (1999) 1663.
- [151] J. Cleymans, H. Oeschler, K. Redlich, Phys. Lett. B 485 (2000) 27.
- [152] A. Förster, F. Uhlig et al. [KaoS Collaboration], Phys. Rev. Lett. 91 (2003) 152301.
- [153] A. Förster et al. [KaoS Collaboration], J. Phys. G 31 (2005) S693.
- [154] G.Q. Li, C.-H. Lee and G.E. Brown, Nucl. Phys. A 625 (1997) 372.
- [155] K. Wisniewski et al. [FOPI Collaboration], Eur. Phys. J. A9 (2000) 515.
- [156] G.E. Brown, M. Rho, C. Song Nucl. Phys. A 690 (2001) 184.
- [157] M. Menzel et al. [KaoS Collaboration], Phys. Lett. B 495 (2000) 26.
- [158] L. Tolos, A. Polls, A. Ramos, J. Schaffner-Bielich, Phys. Rev. C 68 (2003) 024903.
- [159] Z.S. Wang, Amand Faessler, C. Fuchs, V.S. Uma Maheswari and D. Kosov, Nucl. Phys. A 628 (1998) 151.
- [160] G.Q. Li, G.E. Brown, Nucl. Phys. A636 (1998) 487.
- [161] Y. Shin, et al. [KaoS Collaboration], Phys. Rev. Lett. 81 (1998) 1576.
- [162] P.C. Martin and J. Schwinger, Phys. Rev. 115 (1959) 1342.
- [163] L.P. Kadanoff, G. Baym, *Quantum Statistical Mechanics*, (Benjamin, New York, 1962).
- [164] S.R. de Groot, W.A. van Leeuwen, C.G. van Weert, *Relativistic Kinetic Theory*, (North Holland, Amsterdam, 1980).
- [165] P. Henning, Phys. Rep. 253 (1995) 235.
- [166] C. Greiner, S. Leupold, Ann. Phys. 270 (1998) 328.
- [167] R. Brockmann, R. Machleidt, Phys. Rev. C 42 (1990).
- [168] B. Blättel, V. Koch, U. Mosel, Rep. Prog. Phys. 56 (1993) 1.
- [169] H.S. Köhler, Phys. Rev. C 51 (1995) 3232.
- [170] O. Benhar, A. Fabrocini and S. Fantoni, Nucl. Phys. A 505 (1989) 267; Nucl. Phys. A 550 (1992) 201.
- [171] C. Ciofi degli Atti, E. Pace and G. Salme, Phys. Rev. C 43 (1991) 1153.
- [172] J. Lehr, M. Effenberger, H. Lenske, S. Leupold, U. Mosel, Phys. Lett. B 483 (2000) 324.
- [173] C. Fuchs, Amand Faessler, M. El-Shabshiry, Phys. Rev. C 64 (2001) 024003.
- [174] W. Cassing, S. Juchem, Nucl. Phys. A 672 (2000) 417.
- [175] G.F. Bertsch and S. Das Gupta, Phys. Rep. 160 (1988) 190.
- [176] A. Lang, W. Cassing, U. Mosel, K. Weber, Nucl. Phys. A 541 (1992) 507.
- [177] X.S. Fang, C.M. Ko and J.M. Zheng, Nucl. Phys. A 556 (1993) 499.

- [178] X. S. Fang, C.M. Ko, G.Q. Li, Y. M. Zheng, Nucl. Phys. A 575 (1994) 766.
- [179] Z.S. Wang, C. Fuchs, Amand Faessler, and T. Gross-Boelting, Eur. Phys. J. A 5 (1999) 275.
- [180] Z.S. Wang, Amand Faessler, C. Fuchs, T. Waindzoch, Nucl. Phys. A 645 (1998) 177; Erratum Nucl. Phys. A 648 (1999) 281.
- [181] C. Fuchs, Amand Faessler, E. Zabrodin, Y.M. Zheng, Phys. Rev. Lett. 86 (2001) 1974.
- [182] Y.M. Zheng, C. Fuchs, A. Faessler, K. Shekhter, Y.P. Yan, Ch. Kobdaj, Phys. Rev. C 69 (2004) 034907.
- [183] E.L. Bratkovskaya, W. Cassing and U. Mosel, Phys. Lett. B 424 (1998) 244.
- [184] C. David, C. Hartnack, J. Aichelin, Nucl. Phys. A 650 (1999) 358.
- [185] V. Flaminio et al., CERN-HERA 84-01.
- [186] J.J Jones et al., Phys. Rev. Lett. 26 (1971) 860; B. Nelson et al., Phys. Rev. Lett. 31 (1973) 901.
- [187] D. J. Candlin et al., Nucl. Phys. B 226 (1983) 1.
- [188] K. Watson, Phys. Rev. 88 (1952) 1163.
- [189] C. Hanhart, K. Nakayama, Phys. Lett. B 454 (1998) 176.
- [190] N.K. Glendenning, D. Von-Eiff, M. Haft, H. Lenske, M.K. Weigel, Phys. Rev. C 48 (1993) 889.
- [191] K. Tsushima, K. Saito, J. Haidenbauer, A.W. Thomas, Nucl. Phys. A 630 (1998) 691.
- [192] C.M. Keil, F. Hofmann, H. Lenske, Phys. Rev. C 61 (2000) 064309.
- [193] R. Elmer et al. [KaoS Collaboration], Phys. Rev. Lett. 77 (1996) 4884.
- [194] C. Sturm, PhD thesis, Darmstadt 2001.
- [195] R.W. Bland et al., Nucl. Phys. B 13 (1969) 595.
- [196] E.E. Kolomeitsev, C. Hartnack, H.W. Barz, M. Bleicher, E. Bratkovskaya, W. Cassing, L.W. Chen, P. Danielewicz, C. Fuchs, T. Gaitanos, C.M. Ko, A. Larionov, M. Reiter, Gy. Wolf, J. Aichelin, J. Phys. G 31 (2005) 741.
- [197] L.-W. Chen, C.-M. Ko, Y. Tzeng, Phys. Lett. B 584 (2004) 269.
- [198] P. Danielewicz, Nucl. Phys. A 673 (2000) 275.
- [199] G. Ferini, M. Colonna, T. Gaitanos, M. Di Toro, nucl-th/0504032.
- [200] A. Larionov, U. Mosel, Phys. Rev. C 72 (2005) 014901.
- [201] J. Aichelin and C. Hartnack, proceedings to the XXV Int. Workshop on Gross Properties of Nuclei and Nuclear Excitations, Hirschegg 1997, ed. by H. Feldmeier et al., Hirschegg, Austria, 1997.
- [202] P. Danielewicz and S. Pratt, Phys. Rev. C 53 (1996) 249.
- [203] Homework on *Transport Theories for Heavy Ion Reactions*, E. Kolomeitsev privat communication.

[204] A. Mishra, E.L. Bratkovskaya, J. Schaffner-Bielich, S. Schramm, H. Stöcker, Phys. Rev. C 70 (2004) 044904.

[205] F. Laue et al. [KaoS Collaboration], Phys. Rev. Lett. 82 (1999) 1640.

[206] G.Q. Li, G.E. Brown, Phys. Rev. C58 (1998) 1698.

[207] K. Tsushima, A. Sibirtsev, A. W. Thomas, Phys. Rev. C 62 (2000) 064904.

[208] H. Herrmann and the FOPI Collaboration, Prog. Part. Nucl. Phys. 42 (1999) 187.

[209] T. Gaitanos, C. Fuchs, H. H. Wolter, A. Faessler, Eur. Phys. J. A 12 (2001) 421.

[210] A. Hombach, W. Cassing, S. Teis, U. Mosel, Eur. Phys. J. A5 (1999) 157.

[211] C. Fuchs, T. Gaitanos, H. H. Wolter, Phys. Lett. B 381 (1996) 23; T. Gaitanos, C. Fuchs, H. H. Wolter, Nucl. Phys. A 650 (1999) 97.

[212] P. Crochet et al. [FOPI collaboration], Phys. Lett. B 486 (2000) 6.

[213] E.L. Bratkovskaya et al, in preparation.

[214] F. Uhlig, A. Förster et al. [KaoS Collaboration], nucl-ex/0411021

[215] D. Brill et al. [KaoS Collaboration], Phys. Rev. Lett. 71 (1993) 336.

[216] L.B. Venema et al. [TAPS Collaboration], Phys. Rev. Lett. 71 (1993) 835.

[217] G.Q. Li, C.M. Ko and G.E. Brown, Phys. Lett. B 381 (1996) 17.

[218] [KaoS Collaboration], privat. comm.

[219] M. Nekipelov et al. [ANKE-Collaboration], Phys. Lett. B 540 (2002) 207.

[220] GSI Conceptual Design Report, <http://www.gsi.de/GSI-Future>

[221] H.A. Gustafsson et al., Phys. Rev. Lett. 52 (1984) 1590.

[222] P.-G. Reinhard, M. Bender, Lect. Notes Phys. 641 (2004) 249 (and references therein).

[223] B.D. Serot, J.D. Walecka, Int. J. Mod. Phys. E 6 (1997) 515 (and references therein).

[224] R.J. Furnstahl, Lect. Notes Phys. 641 (2004) 1.

[225] M. Lutz, B. Friman, Ch. Appel, Phys. Lett. B 474 (2000) 7.

[226] P. Finelli, N. Kaiser, D. Vretenar, W. Weise, Eur. Phys. J. A 17 (2003) 573; Nucl. Phys. A 735 (2004) 449.

[227] V.R. Pandharipande and R.B. Wiringa, Rev. Mod. Phys. 51 (1979) 821.

[228] A. Akmal, V.R. Pandharipande, D.G. Ravenhall, Phys. Rev. C 58 (1998) 1804.

[229] T. Gross-Boelting, C. Fuchs, and A. Faessler, Nucl. Phys. A 648 (1999) 105.

[230] C. Fuchs, Lect. Notes Phys. 641 (2004) 119 (and references therein).

[231] E. van Dalen, C. Fuchs, A. Faessler, Nucl. Phys. A 744 (2004) 227.

- [232] H. Müther, A. Polls, *Prog. Part. Nucl. Phys.* 45 (2000) 243.
- [233] R. Machleidt, *Advances in Nuclear Physics* 19, 189, eds. J.W. Negele, E. Vogt, Plenum, N.Y., 1986
- [234] W. Zuo, A. Lejeune, U. Lombardo, J.F. Mathiot, *Nucl. Phys. A* 706 (2002) 418.
- [235] X.R. Zhou, G.F. Burgio, U. Lombardo, H.-J. Schulze, W. Zuo, *Phys. Rev. C* 69 (2004) 018801.
- [236] U. van Klock, *Phys. Rev. C* 49 (1994) 2932.
- [237] R. Machleidt, *Int. J. Mod. Phys. B* 15 (2001) 1535 [[arXiv:nucl-th/9911059](https://arxiv.org/abs/nucl-th/9911059)]
- [238] J. Aichelin, H. Stöcker, *Phys. Lett. B* 176 (1986) 14.
- [239] R. Stock, *Phys. Rep.* 135 (1986) 259.
- [240] M.R. Stockmeier et al., [FOPI Collaboration], *GSI Scientific Report* (2001) 35.
- [241] C. Fuchs, L. Sehn, E. Lehmann, J. Zipprich and Amand Faessler, *Phys. Rev. C* 55 (1997) 411.
- [242] A.B. Larionov, M. Effenberger, S. Leupold, U. Mosel, *Phys. Rev. C* 66 (2002) 054604.
- [243] J. Helgesson and J. Randrup, *Ann. Phys. (N.Y.)* 244 (1995) 12.
- [244] J. Helgesson and J. Randrup, *Phys. Lett. B* 439 (1998) 243.
- [245] P. Danielewicz and S. Pratt, *Phys. Rev. C* 53 (1996) 249.
- [246] K. Morawetz, V. Spicka, P. Lipavsky, G. Kortemeyer, Ch. Kurts, R. Nebauer, *Phys. Rev. Lett.* 82 (1999) 3767; K. Morawetz, P. Lipavsky, V. Spicka, N.-H. Kwong, *Phys. Rev. C* 59 (1999) 3052.
- [247] J.W. Harris et al., *Phys. Lett. B* 153 (1987) 463; *Phys. Rev. Lett.* 58 (1987) 463.
- [248] F.D. Berg et al., [TAPS Collaboration], *Phys. Rev. Lett.* 72 (1994) 977.
- [249] O. Schwalb et al., [TAPS Collaboration], *Phys. Lett. B* 321 (1994) 20.
- [250] R. Averbeck et al., [TAPS Collaboration], *Z. Phys. A* 359 (1997) 65.
- [251] A. Wagner et al., [KaoS Collaboration], *Phys. Lett. B* 420 (1998) 20.
- [252] D. Pelte et al., [FOPI colloboration], *Z. Phys. A* 357 (1997) 215; *Z. Phys. A* 359 (1997) 55.
- [253] C. Fuchs, A. Faessler, S. El-Basaouny, E. Zabrodin, *J. Phys. G* 28 (2002) 1615.
- [254] C. Fuchs, *Prog. Part. Nucl. Phys.* 51 (2004) 113.
- [255] A. Schmah et al., [KaoS Collaboration], C. Fuchs, A. Faessler, H. Mansour, (2005) *Phys. Rev. C* in press.
- [256] Ch. Hartnack, habilitation thesis, Nantes 2005, [[nucl-th/0507002](https://arxiv.org/abs/nucl-th/0507002)].
- [257] P. Danielewicz, R. Lacey, W.G. Lynch, *Science* 298 (2002) 1592.
- [258] N. Herrmann, J.P. Wessels, T. Wienold, *Ann. Phys.* 49 (1999) 581.
- [259] A.B. Larionov, W. Cassing, C. Greiner, U. Mosel, *Phys. Rev. C* 62 (2000) 064611.

- [260] P. Danielewicz, Roy A. Lacey et al., Phys. Rev. Lett. 81 (1998) 2438; C. Pinkenburg et al., Phys. Rev. Lett. 83 (1999) 1295.
- [261] P.K. Sahu, W. Cassing, U. Mosel, A. Ohnishi Nucl. Phys. A 672 (2000) 376; P.K. Sahu, W. Cassing; Nucl. Phys. A 712 (2002) 357.
- [262] A. Andronic et al. [FOPI Collaboration], Nucl. Phys. A 661 (1999) 333c; Phys. Rev. C 64 (2001) 041604; Phys. Rev. C 67 (2003) 034907.
- [263] D. Brill et al. [KaoS Collaboration], Zeit. f. Phys. A 355 (1996) 61.
- [264] T. Gaitanos, C. Fuchs, H.H. Wolter, Nucl. Phys. A 741 (2004) 287.
- [265] J. Yamagata, H. Nagahiro, Y. Okumura, S. Hirenzaki, nucl-th/0501037.
- [266] Y. Akaishi, A. Dote, T. Yamazaki, nucl-th/0501040.

